



Review

Electrocatalysis at Electrodes for Vanadium Redox Flow Batteries [†]

Yuping Wu ¹ and Rudolf Holze ^{2,3,*} ¹ State Key Laboratory of Materials-oriented Chemical Engineering, and School of Energy Science and Engineering, Nanjing Tech University, Nanjing 211816, China; wuyp@njtech.edu.cn² AG Elektrochemie, Institut für Chemie, Technische Universität Chemnitz, D-09107 Chemnitz, Germany³ Institute of Chemistry, Saint Petersburg State University, St. Petersburg 199034, Russia

* Correspondence: rudolf.holze@chemie.tu-chemnitz.de; Tel.: +49-371-5313-1509

† Reports being available on or before 20 August 2018, have been inspected for this report.

Received: 30 July 2018; Accepted: 23 August 2018; Published: 13 September 2018

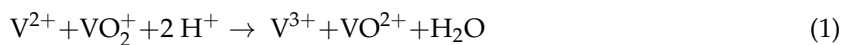


Abstract: Flow batteries (also: redox batteries or redox flow batteries RFB) are briefly introduced as systems for conversion and storage of electrical energy into chemical energy and back. Their place in the wide range of systems and processes for energy conversion and storage is outlined. Acceleration of electrochemical charge transfer for vanadium-based redox systems desired for improved performance efficiency of these systems is reviewed in detail; relevant data pertaining to other redox systems are added when possibly meriting attention. An attempt is made to separate effects simply caused by enlarged electrochemically active surface area and true (specific) electrocatalytic activity. Because this requires proper definition of the experimental setup and careful examination of experimental results, electrochemical methods employed in the reviewed studies are described first.

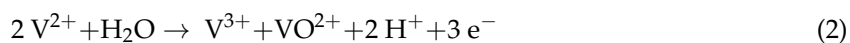
Keywords: electrocatalysis; surface activation; carbon felt; graphite felt; underpotential deposition

1. Introduction

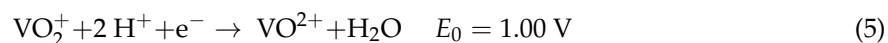
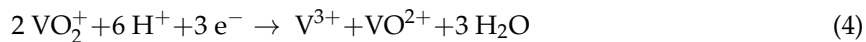
Two chemical compounds may undergo a chemical reaction when mixed according to



The free enthalpy (Gibb's energy) produced by this reaction is just released as heat. When the reaction is localized at two electrodes the chemical energy can be recovered as electric energy:



and



In reactions (2) and (3) V^{2+} species are converted into V^{3+} or into V^{3+} and $\text{V}(\text{IV})$ species and the reaction happening at an inert electrode is an oxidation reaction. Under this condition, the electrode is named an anode. When recharging the battery the reaction is reversed and is now called a cathode. In reactions (4) and (5) $\text{V}(\text{V})$ -species are converted into $\text{V}(\text{IV})$ or V^{3+} - and $\text{V}(\text{IV})$ species. These are reduction reactions and the electrode is called cathode. Again the name changes upon recharging. Because of the mixture of V^{3+} - and $\text{V}(\text{IV})$ species in the case of reaction (4), this solution is often referred

to as a $V^{3.5+}$ -electrolyte. To avoid the quite obviously expected confusion the electrode where reactions (2) and (3) happen is called the negative electrode, while the other one is the positive electrode in the following text.

In a patent granted in 1949, the operating principle of a flow battery was described for the first time [1], (see also [2]). Elsewhere a first proposal of a redox battery was reported in 1974 [3] (see also [4]). Because the reactants are practically always redox systems these devices are sometimes also named redox batteries. To increase electrode currents, forced convection is applied to enhance mass transport by circulating the electrolyte solution between a tank and the cell(s) by pumping. The device is now called a redox flow battery RFB. Further details of a system can be integrated into the designation when naming it e.g., VRB or VRFB. This is an all-vanadium redox flow battery that was first patented in 1986 [5], as in the initial example. The basic layout and the operating principle can be visualized in the following picture (Figure 1), commercially device is shown in Figure 2.

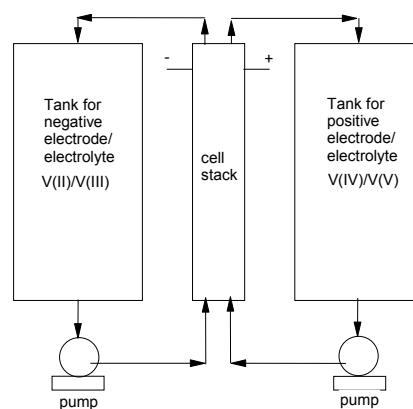


Figure 1. Scheme of a redox flow battery.

The power generation capability of a redox battery is given by the cell stack: Larger electrode areas provide higher current, more cells connected in series generate higher voltage output. The size of the tanks controls the energy storage capacity. Actually the amount of redox-active materials in the stored electrolyte solution determines the storage capacity. Accordingly highly soluble redox-active materials are preferable. The RFB offers the unique option to scale an electrochemical energy storage device with respect to both characteristic properties separately according to the user's requirement. For large scale storage in terms of energy, larger tanks will be required. This scale-up, required in particular for load-leveling and for seasonal storage, comes particularly cheap.



Figure 2. VRFB, 8 kW maximum power, 10 kW maximum power uptake, storage capability 16 kWh, Yinfeng New Energy, Yangzhou, China.

For early general overviews on RFBs see [6,7], for recent reviews see [8–33]. Comparisons between various RFBs are available, for example in [34]. Reviews dealing with specific aspects e.g., regarding membranes needed as separator between the two half cells [35–40] or the use of organic redox species [41–43] are also available. A comparative study of some redox electrolyte systems with respect to their suitability as test systems for the evaluation of cell designs has been reported [44]. The use of RFBs in a changing energy landscape including growing use of renewable energy sources from the grid level down to localized applications, including details like CO₂-footprint has been highlighted [45–64]. Availability of raw materials for RFBs has been addressed [65]. Further details and technical features such as operating temperature, flowfield design etc. [66–79], modeling [80,81] as well as economical aspects of RFBs, in particular of all-vanadium RFBs [82–87], will be treated elsewhere in this volume. This will include topics like attempts to increase energy density that is currently limited by solubility of redox salt components (e.g., Vanadium solid-salt battery VSSB) [88,89]. RFBs using organic (nonaqueous) solvents have been considered and kinetic data as well as suggestions for electrode materials etc. have been reported [90,91]. Kinetic data for $[V(acac)_3]^{0+/+/-}$ at carbon paper and bucky paper have been reported [92] as has the use of nitrogen-doped CNTs decorated on nickel foam as an electrode in non-aqueous RFBs [93].

For successful implementation of RFBs of various chemistries and operating principles, further developments resulting in substantial improvements are required. Which property needs such improvement most urgently, certainly depends on the perspective of the researcher and engineer. From an economic perspective the expensive ion exchange membrane has been an on-going challenge, from the application engineer's perspective, solubilities and higher concentrations demand attention, but from the electrochemist's point of view the capabilities of the electrodes in terms of higher sustained currents at decreased overpotentials seems to be most important. Further overpotentials caused by slow transport (diffusion overpotentials) or by low conductivity of the electrolyte solution or the membrane are relatively minor, as was nicely illustrated in a typical publication [94]. From a simple three-electrode measurement enabling separation of the cell voltage into electrode potentials the vast part of cell overvoltage under load could be assigned to the negative electrode overpotential. Further impedance measurements providing details of these electrode overpotentials demonstrated that the major part of the negative electrode overpotential was due to some kinetic process (presumably transport including diffusion, forced convection etc.), charge transfer directly related to electrocatalytic properties of the electrode provided a smaller but nevertheless considerable contribution [94,95]. Measurements were done at slow, natural flow driven by gravity, however, so this would be the cause for the sluggish mass transport observed in this study.

The following review starts with an overview of experimental methods applied in studies of VRFBs and their electrodes. The following chapter deals with materials as used in VRFBs in particular as electrodes. The major part that follows, is devoted to electrocatalysis of redox processes involving vanadium ion at these materials before and after catalytically relevant modifications and treatments.

2. Methods

Experimental electrochemical methods used to determine kinetic parameters of electrode reactions (exchange current density j_0 , standard exchange current density j_{00} or rate constant k_0) have been collected comprehensively elsewhere [96]. To compare data necessary e.g., to judge the catalytic (accelerating or impeding) effect of an electrode modification, specific data related to a defined electrode surface area are needed. Mostly current densities including exchange current densities j_0 etc. are stated with respect to the geometric surface area A_{geom} . In the case of smooth electrodes like polished glassy carbon or pyrolytic graphite, this is presumably acceptable because the difference between the geometric surface area and the true electrochemically active surface area EASA [97] as determined by double layer capacity measurements, hydrogen or carbon monoxide adsorption/desorption measurements or other techniques is small (for an overview of methods see [98–100], for selected methods and applications see [101–105]). The relationship between both is frequently expressed as roughness factor R .

$$R = \frac{\text{EASA}}{A_{\text{geom}}} \quad (6)$$

At small roughness factors the EASA being only slightly larger than A_{geom} does not act as a truly larger surface area that provides more sites for the electrode reaction to take place. Because many electrode reactions tend to be diffusion-limited this observation can be rationalized when considering the thickness of the diffusion layer that is usually much larger than the thickness of any surface roughness features. A comprehensive examination that attempts to find the critical roughness where further increasing roughness will actually provide added EASA which should be considered when calculating j_0 , is currently under way in the author's laboratory [106]. Actual correction of the value of j_{00} initially recorded with respect to A_{geom} and corrected by the roughness factor has been applied infrequently only [107,108]. For an attempt regarding various RFBs see [109].

In the case of porous materials, a further surface area of the material merits attention: the surface area as determined with e.g., nitrogen adsorption (BET-method [110–112]). As has been pointed out earlier [113] EASA may be only a small fraction of the BET-surface area, and the surface area actually contributing to current generation—different from the EASA as determined by e.g., C_{DL} -measurements—may be even smaller than EASA as determined by e.g., impedance measurements [113] or by cyclic voltammetry. Carbon materials offer in comparison to metallic electrode materials one further complication. Because of the pronounced anisotropy of graphite (and many other carbon-based materials, too) surfaces vary widely in structure and reactivity [114,115]. This can be easily verified with highly oriented pyrolytic graphite. Its basal plane shows hardly any electrochemical reactivity whereas its edge planes are highly reactive. In a study of graphite powders of various particle sizes with different fractions of edge-planes attached to a highly oriented pyrolytic graphite (HOPG) electrode this topic has been investigated further [116]. The activity of the obtained catalyst for the positive VFB electrode reaction layer increased with decreasing particle size. This is attributed to larger EASA and more exposed edge-planes. An attempt to apply these considerations to felt electrodes has been reported [117]. With HOPG and partially masked graphite foil this observation was verified for both VRFB electrode reactions. The differences were particularly striking at low vanadium species concentrations [118]. Dioxygen chemisorption probes preferentially edge-area (i.e., in activated surface area ASA measurements) whereas BET surface area includes all kinds of area, i.e., also the basal plane area (which dominates in many cases of carbon felt for example). Electrochemical measurements (CV and impedance) enable a distinction between these types of surfaces, so a deconvolution of BET surface area into edge- and basal plane fractions is possible without performing dioxygen chemisorption experiments. This might be of practical relevance because electrochemical processes proceed preferably at edge sites.

The strong correlation between charging current and BET surface area as observed by Jow et al. [119] is a purely empirical relation without a well-defined cause-effect relationship. It does not provide any information on EASA and its relation to BET surface area. Consideration of C_{DL} -values would have been a major advantage possibly providing deeper insight.

Different from most materials as listed in ref. [96], electrode materials employed in the VRB are not flat and smooth, but have highly developed structures like graphite felt, metal foams or other porous matter. Consequently most of the methods listed in ref. [96] cannot be applied. Even the most basic technique of cyclic voltammetry (CV) may suffer from electrode potential drops along the porous structure. Chronoamperometry has been suggested also [108]. Measurements of the electrode impedance [120–122] elsewhere used as a standard technique to elucidate kinetic data has been used frequently (e.g., [94,95]), unfortunately often in a rather superficial way. Nevertheless based on impedance measurements, Fink et al. claimed that the actual reaction rates at the positive and the negative electrode in a VRFB are of the same order of magnitude, and that rate constants depend on chemical composition of the material. Oxygen-containing surface groups increase the wettability and catalyze the $\text{V}^{2+}/\text{V}^{3+}$ reaction whereas they slow down the $\text{V(IV)}/\text{V(V)}$ reaction [123]. A further complication arises when measurements are performed with a flowing electrolyte solution.

Depending on the type of pump used, fluctuations of flow caused by the pump may occur and seriously affect impedance measurements in particular at low frequencies [124]. According to the experimental setup for impedance measurements, electrode impedances (this requires a three-electrode setup) or cell impedances are obtained. The latter approach may be based on a full-cell arrangement with both positive and negative electrodes in place or on a double half-cell DHC arrangement as suggested elsewhere [94,125] and subsequently employed by Pezeshki et al. [124] with two identical electrodes and only one electrolyte solution. This setup may be considered as a further development of the single electrode or half-setup described by Aaron et al. [126]. In this approach the electrolyte solution is fed either in a parallel arrangement into both half-cells simultaneously (see e.g., in [127]) or in series through both cells (e.g., in [124]) (see Figure 3). In both setups the chemical composition during measurements at both open circuit potential and under current flow, stays constant because electrochemical transformations in both cells compensate each other exactly.

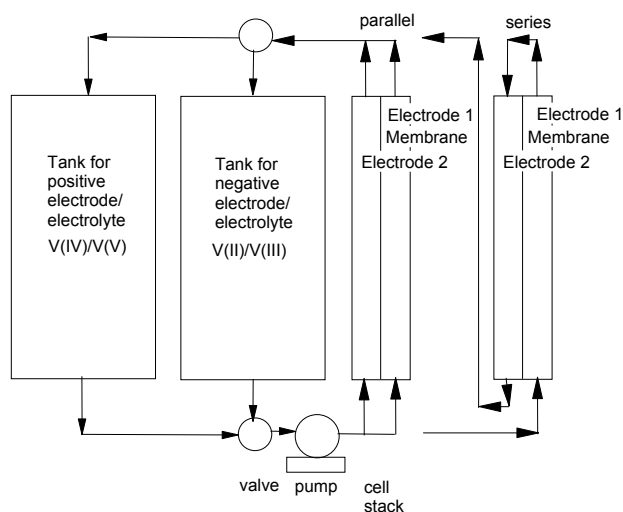


Figure 3. Scheme of the double half-cell setup.

The three-electrode setup will provide information related to the electrode under study and to the steps of the electrode reaction proceeding there. The latter approach will contain convoluted data pertaining to both electrodes, the respective electrode reactions and the cell including e.g., membrane, and electrolyte solution between electrodes and membrane in the case of the full-cell approach. In the case of the completely symmetric half-cell setup, the mostly ohmic contributions of the membrane and the electrolyte solution can be easily removed from the overall impedance. The remaining impedance can just be divided by 2 yielding the identical electrode impedance [94,124,125]. When measurements are done at the spontaneously established rest potential (or rest cell voltage/open circuit voltage), the electrolyte solution represents a composition of 50% state of charge (i.e., concentrations of both redox constituents are equal), both electrode reactions and their impedances are identical and with respect to the applied sinusoidal voltage perturbation mirror-symmetrical. This approach has also been suggested elsewhere in an attempt to resolve the frequently observed confusion between electrode and cell impedances in lithium ion battery studies [128]. A specific cell setup suitable for RFB with felt electrodes has been proposed [129] and a simplified design for smaller electrodes requiring a less powerful potentiostat is currently under development in the author's laboratory [130].

Attention should be paid to well-defined and reproducible electrode compression [131]. The correlation between carbon felt compression and cell performance has been studied and careful optimization is recommended [132]. An experimental approach to measure polarization curves combined with monitoring current density distributions has been described [133]. Microfluidic cells have been described [134,135] and porous carbon electrodes for this kind of cell have been examined [136]. Voltage step coulometry has been suggested as a method to characterize materials for VRFBs [137]. A thermo-electrochemical method of investigation of kinetic, mechanistic and thermodynamic aspects

has been proposed and applied to the positive VRFB reaction [138]. Critical reviews of all method used in studies of RFBs are available [139–141]. Modeling has been applied to both electrodes [142].

Consequently most reported studies on electrode kinetics address catalytic properties of the electrode material only in qualitative and relative terms by stating, for example, differences in available currents at given electrode potentials (or recorded electrode potentials at fixed currents) or increased voltage or energy efficiency as indicators of improved catalytic activity after application of chemical or thermal treatment, surface modification etc. Because efficiency data depend on applied current density and the applied current densities vary widely, these data are quoted only reluctantly in this report.

3. Materials

By far the most frequently used electrode material is carbon in numerous different forms [31,143,144]. Its popularity derives from its low price and its considerable chemical stability. This applies also to other RFB chemistries beyond VRFB sometimes utilizing chemically aggressive redox constituents. Stability of materials and systems is addressed only infrequently. When done, results are mostly reported as energy efficiency of a device as a function of charge/discharge cycles. In addition however, capacity retention should also be displayed because a rapidly declining storage capability, even at high efficiency, is less welcome. More detailed investigations appear to be needed in order to identify causes of deterioration and finally failure, and to find either more stable materials or to enhance stability of already identified materials. This also applies to degradation of auxiliary materials like bipolar and current collector plates by corrosion [145], bulk aging [146], chemical attack [147], or overcharge [148,149]. For overviews on bipolar plates and related components see [150–155]. Online mass spectroscopy showed that CO₂ and CO are major corrosion products at a graphite positive electrode [156], and only at very positive electrode potentials oxygen evolution dominates. A bipolar electrode design going beyond the bipolar plate design has been proposed [157]. Carbon nanotube- and graphite-filled polymer bipolar plates have been proposed [158].

Derr et al. have studied chemical [159] and electrochemical [160] ageing of carbon felt in a VRFB. Effects of temperature and vanadium concentration were noted. Accordingly in the case of chemical ageing, a joint chemical attack of the sulfuric acid and the vanadium ions was concluded. XPS data indicate an increase of oxygen-containing functional groups. The negative electrode was affected more strongly. Ageing under load (charge/discharge) also caused significant increase of the number of functional groups. Scanning electron microscopy revealed peeling off from the fibers presumably due to ion intercalation resulting in loss of EASA. Impedance measurements showed major increases of the charge transfer resistance, unfortunately double layer capacities were not explored with respect to the claimed loss of EASA. Overpotentials at the positive electrode were minor in comparison to those at the negative electrode. In particular the reduction reaction V³⁺ → V²⁺ seems to be very slow. This becomes even more pronounced during ageing. The effect of cut-off voltages (1.65 and 1.8 V) on performance losses has been examined with carbon felt electrodes [161]. Among many details it was observed that catalytic activity towards V(III)-reduction decreased to the same extent as hydrogen evolution. Accordingly a degraded electrode will not provide more parasitic hydrogen evolution. Nibel et al. examined stability and degradation aspects more thoroughly with carbon paper and carbon felt without/with heat treatment [162]. Carbon felt turned out to be more stable. Improvements by heat treatment were found mostly at the negative electrode; exposure to very negative electrode potentials during charging appeared to be particularly critical.

Beyond solid graphite (OPG), stress-annealed pyrolytic graphite (SAPG), HOPG, and glassy carbon (GC), materials containing binders are also employed [163]. These materials are compact solids. They do not provide extended surface area for electrode reactions and are used in fundamental studies. In flow cells they are used as current collectors and mechanical support.

The following Table 1 provides an overview of further electrode materials; it includes also materials used for other RFB chemistries.

Table 1. Studied carbon-based materials.

Trade Name	Manufacturer	Generic Designation *	Properties	Studied Redox Reactions	Ref.
ATJ	Le Carbone-Lorraine	porous bulk graphite		Fe ²⁺ / ³⁺	[164]
BW-309	Toyobo Co., Ltd.	carbon fiber		V ⁴⁺ / ⁵⁺ , V ³⁺ / ⁴⁺	[165]
GRC	-	graphite reinforcement carbon		V ⁴⁺ / ⁵⁺ , V ³⁺ / ⁴⁺	[165]
GF-20	Nippon Carbon Co., Ltd.	carbon fiber		V ⁴⁺ / ⁵⁺ , V ³⁺ / ⁴⁺	[165]
JP845	Le Carbone-Lorraine	non-porous bulk graphite		Fe ²⁺ / ³⁺	[164]
NG	-	natural graphite		V ⁴⁺ / ⁵⁺	[166]
PG60	Le Carbone-Lorraine	porous bulk graphite		Fe ²⁺ / ³⁺	[164]
RVC-45PPI	Electrosynthesis Corp.	reticulated vitreous carbon		Fe ²⁺ / ³⁺	[164]
RVC-60PPI	Electrosynthesis Corp.	reticulated vitreous carbon		Fe ²⁺ / ³⁺	[164]
SGF	Stackpole	graphite felt		Fe ²⁺ / ³⁺	[164]
-	-	plastic-bonded natural graphite flake		Cr ²⁺ / ³⁺	[164]
-	-	Electrographite		Cr ²⁺ / ³⁺ , Fe ²⁺ / ³⁺	[167]
-	-	natural graphite		Cr ²⁺ / ³⁺ , Fe ²⁺ / ³⁺	[166]
Electrode graphite EH	Sigri	-		Fe ²⁺ / ³⁺	[163,168]
OPG	Ringsdorff	ordinary pyrolytic graphite		Fe ²⁺ / ³⁺	[163,169]
GC	Sigri, Metrohm	glassy carbon		Fe ²⁺ / ³⁺	[163,169]
Diabon N	Sigri	graphitized, polymer-bonded material		Fe ²⁺ / ³⁺	[163,169]
Ridurid V1017	Ringsdorff	non-porous material bonded with phenolic resin		Fe ²⁺ / ³⁺	[163,169]
WCA cloth	Union Carbide	porous graphite		Cr ²⁺ / ³⁺	[169]
ELAT carbon cloth	Fuel Cells Etc			V ²⁺ / ³⁺ , V ⁴⁺ / ⁵⁺	[170]
SGL 10AA	SGL Technologies	carbon paper		V ²⁺ / ³⁺ , V ⁴⁺ / ⁵⁺	[171]
TORAY carbon paper	Toray	carbon paper		V ²⁺ / ³⁺ , V ⁴⁺ / ⁵⁺	[126,162]
Donacarbo paper, S-251	Osaka Gas Chemicals	carbon paper		V ⁴⁺ / ⁵⁺	[172]
Felt	Union Carbide	carbon paper		Cr ²⁺ / ³⁺	[169]
GF-20-3 graphite felt	Nippon carbon	porous graphite		V ⁴⁺ / ⁵⁺	[173]
PAN GF-3F carbon felt	Nippon carbon			V ²⁺ / ³⁺ , V ⁴⁺ / ⁵⁺	[174]
GFA6 carbon felt	SGL Carbon, Germany			V ²⁺ / ³⁺ , V ⁴⁺ / ⁵⁺	[159]
Carbon felt +	SGL Carbon			V ²⁺ / ³⁺ , V ⁴⁺ / ⁵⁺	[127]
Carbon felt	Baofeng Jinshi New Materials Co.			V ⁴⁺ / ⁵⁺	[175]
Fiber graphite felt	Material Inc.			V ²⁺ / ³⁺ , V ⁴⁺ / ⁵⁺	[176]
Graphite felt	Beijing Great Wall	PAN [?] -based		V ⁴⁺ / ⁵⁺	[177]
Graphite felt	Shanghai Qijie Limited Co.	PAN-based		V ⁴⁺ / ⁵⁺	[178]
Graphite felt	SGL Carbon			V ²⁺ / ³⁺ , V ⁴⁺ / ⁵⁺	[127]
Graphite felt RVG-2000	Société Carbon-Lorraine	Rayon [#] -based		V ⁴⁺ / ⁵⁺	[179]
Graphite felt	Carbone Lorraine	Rayon-based		V ⁴⁺ / ⁵⁺	[180]
G 2225 cloth	Hitco	porous graphite		Cr ²⁺ / ³⁺	[169]
FMI	Fibre Materials Inc.	Rayon-based		V ²⁺ / ³⁺ , V ⁴⁺ / ⁵⁺	[181]
GFD 2	Sigri	PAN-based		V ²⁺ / ³⁺ , V ⁴⁺ / ⁵⁺	[181]

* Designation, names of manufacturers etc. as stated in the original reports; [†] The term carbon felt appears to be generally used for a felt carbonized but not graphitized at further elevated temperature. The use of carbon felt as a general term for all carbon-based felts connected with the terminology carbonized felt seems to be confusing only and is not pursued here; the use of the terms carbon felt and graphite felt in one sentence to designate the same material is discouraged; [?] PAN: Polyacrylonitrile; [#] Rayon: Synthetic cellulose-based fiber.

Physicochemical data on some participating vanadium ions have been reported [182]. The rate of the positive electrode reaction has been found to depend on concentration of the reactants and the supporting electrolyte [183]. At low concentrations of sulfuric acid used as supporting electrolyte slow kinetics (called low reversibility) were observed. At concentrations above 2 M the reaction became diffusion controlled and more reversible, while at even higher concentration above 3 M the increasing viscosity slowed down the reaction. Methanesulfonic acid has been proposed as a supporting electrolyte instead of sulfuric acid because of improved mass transport and electrode kinetics [184] as verified with a glassy carbon electrode.

For practical applications materials with sufficiently large specific surface areas are required to compensate for the sluggish kinetics. The most frequently used material is carbon-based felt in various forms, carbonized (carbon felt), graphitized (graphite felt), heat-treated, chemically modified etc. [185, 186]. Carbon cloth and paper have also been examined. Some of these materials show barely any electrochemical activity when exposed to an electrolyte solution for the first time. Pretreatment with e.g., nitric acid or electrochemical activation is recommended. The observed changes in electrochemical behavior evident in CVs by decreasing peak separation, can be assigned rather conclusively to true catalytic effects (peak separation yielding changed values of j_0) and increased surface area resulting in larger current peaks. In particular at large currents, IR-drop should be kept in mind. Some modifications and treatments (e.g., graphene deposition or nitrogen doping) might result in significant enhancement of the electronic conductivity. This will decrease ohmic overpotential. It will also result in peak shifts and finally decreased peak separation. Thus catalytic effects may be mixed up with ohmic effects. An overview of activation of some of these materials is available [31,187]. For intimate contact between electrolyte solution and electrode material, complete wettability is required. Surface treatments enhancing wettability have been reported, some examples are discussed below. The importance of wettability has been discussed elsewhere taking oxidative treatments of carbon paper used as the negative electrode as an example [188]. Improved electrode performance could be completely assigned to enhanced wetting, not to true catalytic effects of e.g., surface functional groups.

In addition to physical or chemical treatment of a given material inducing enhanced electrocatalytic activity, deposition of catalytically active materials on less active supports and formation of composites [189]. Of materials listed above with some more active component(s) have been suggested. These materials are presented below following a brief overview on catalysis. An early overview has been presented elsewhere [190].

4. Catalysis, Catalysts and Electrode Materials

In its broadest meaning, catalysis is acceleration (or less frequently inhibition) of a chemical reaction by an additional component which participates in the reaction but which is left unchanged after the reaction. Sometimes the term catalysis is used also in the discussion of chemical degradation of electrode materials in RFB, in particular when oxidative destruction of carbon-based materials in RFB happens. Indeed electrolyte solution components may act as catalysts in these undesirable reactions; nevertheless these processes are not treated here. Obviously the untreated electrode material is the point of reference. Accordingly the rate of both wanted as well as unwanted reactions obtained with the untreated material are assumed to be non-catalyzed—whether this is correct or not with respect to another material even less electrochemically active. This general concept is valid for both homogeneous and heterogeneous reactions. In the case of RFB, catalysis is mostly applied—if at all—to inhibit unwanted side reactions like parasitic hydrogen evolution at the negative electrode and/or to accelerate the intended redox reactions, in the latter case of a given redox reaction both directions may be affected. Dioxygen or carbon dioxide evolution at the positive electrode appears to be a minor problem. Because it might result in oxidation of the carbon material rapid loss of EASA and thus electrode performance must be expected if this undesirable side reaction occurs. A first-principle study of the adsorption/desorption kinetics of $V^{2+/3+}$ -ions on graphite been reported [191]. Results suggest formation or presence of ketonic functional groups at edge sites serving as active sites for redox ion adsorption. On basal planes such sites are absent;

this explains striking differences in reactivity observed elsewhere repeatedly. Reaction mechanisms suggested for a particular material, taking into consideration possible outcomes of surface treatments and modifications, will be presented and discussed below. In more fundamental studies electrode reactions at VRFB electrodes have been studied also on electrode materials of rather small practical interest like glassy carbon or bulk graphite. Results are also collected below. DFT-assisted calculations were employed in the understanding of the particular electrocatalytic effect of carbon nitride modified graphite felt [192]. The design was apparently contrary to the reports title not based on these theoretical tools. In similar attempts for boron-doped graphite felt, increased stability of the material was estimated theoretically before preparation [193].

Both cases of catalysis—accelerating and inhibiting—require surface treatment or some other modification of the electrode material. A separation between treatment (implying milder conditions) and modification in terms of different classes of materials as suggested elsewhere [194] is not pursued here because it will hardly be helpful in organizing the rather diverse reports. Instead—as detailed below—another classification, wherein suppression of hydrogen development is desired, in all reported cases, chemical modification by foreign metal deposition seems to be required. Without such modification hydrogen evolution varies with carbon material, accordingly optimization even without foreign metals may be possible [195]. Suppression is important to reduce losses by unwanted gas evolution at the negative electrode in particular at high currents in the charging mode. In addition it has been noted that hydrogen evolution at the negative graphite electrode changes surface morphology and introduces defect sites. Finally activity towards the V^{3+}/V^{2+} redox couple is diminished [196]. The suppression can be induced by deposition of metals with large hydrogen overpotential like bismuth or lead [197–200]. For acceleration of the redox reactions at carbon-based electrodes chemical surface treatment, e.g., exposure of the electrode material to a stream of an inert or slightly reactive gas (e.g., nitrogen, but also dioxygen) at elevated temperatures, treatment in water at elevated temperatures (hydrothermal procedure), soaking in aqueous nitric acid or deposition of substances like metals on the surface by chemical or electrochemical deposition processes may be applied.

Subsequently catalysis will be discussed with particular reference to those electrode materials which are currently considered for technical application.

In a more fundamental study Liu et al. have used a carbon black Vulcan XC-72 with Nafion® as a binder deposited on glassy carbon to study all conceivable vanadium ion redox reactions [201]. Rate constants were determined from CVs using numerical simulations and the procedure suggested by Nicholson [202]. They were $1.5 \pm 0.4 \times 10^{-3} \text{ cm} \cdot \text{s}^{-1}$ for the V(IV)/(V) couple and $2.0 \pm 0.4 \times 10^{-3} \text{ cm} \cdot \text{s}^{-1}$ for the $\text{V}^{2+/3+}$ couple. Somewhat remarkably the authors concluded that this carbon material meets the requirements for use in a VRFB. Various kinetic parameters of participating vanadium species with a glassy carbon electrode have been reported [203]. A study of the V^{3+} -ion reduction at a platinum electrode using a rotating disc electrode and impedance measurements yielded no conclusive results [204]. The V(III)/V(IV) redox couple has been studied at a glassy carbon with respect to its importance during initial pre-charging of electrolytes in a VRFB [205]. The surprisingly low apparent symmetry factor at large overpotentials for the V(V) reduction has been examined in detail [206]. A model involving electron transfer through a layer of adsorbed vanadium accounting for this observation has been proposed. The effect of various mechanical as well as chemical surface treatment methods on the electroreduction of V(V) ions has been examined [207]. No correlation between oxygen content and catalytic activity was found. Structural disorder correlated with electrocatalytic activity up to a certain optimum level.

Practically all RFB concepts proposed and studied so far including VRFBs, have employed preferably carbon-based (graphitic or similar) materials as electrodes because of the extreme oxidizing capability of this ion in its higher state of oxidation. Only cerium-containing systems have been an exception. There are several reasons for the dominating use of graphite and similar carbon-based materials [194]. These materials are

- cheap and abundantly available
- easily manufactured into particular shapes and forms

- chemically stable against practically all reactant solutions encountered in RFB
- mechanically stable during operation
- impermeable for electrolyte solution
- show reasonable electrocatalytic activities for many redox reactions in their pristine state

There are nevertheless some redox reactions that are slow at several electrode materials including carbon-based ones [96]. Because of the highly efficient artificially enhanced mass transfer resulting in very small concentration/diffusion overpotentials ($\eta_{\text{conc}} = \eta_{\text{diff}} + \eta_{\text{react}}$), these limitations have become a substantial obstacle requiring improvement of electrocatalytic properties of these materials.

Many carbon-based materials have been studied so far. A complete overview of materials, including data of characteristic properties, is not available so far. The list provided above is only a very first attempt. A comparison of morphologically different carbon materials for use as the positive VRFB electrode has been reported [208]. Content of sp^2 -carbon on the surface was found to significantly affect catalytic activity.

Most authors provide no or only insufficient technical data of their samples, sometimes even the source of the material is given incompletely or incorrectly. Investigations of the relationship between precursor materials and the obtained graphite materials, e.g., felts, are rare. In a typical study, felts made from polyacrylonitrile and Rayon have been compared taking a VRFB [181] and a Fe/Cr redox flow battery [209]. For comparison see also [127]. Differences in electronic conductivity (important in particular for power performance) and surface area were recorded. Rayon-based materials react more easily with oxygen yielding C=O-surface groups, but no significant differences in performance were observed. Effects of surface properties and graphitization of PAN-based graphite felt (It remains unclear why the authors call a material obtained by graphitization a carbon felt.) on the negative electrode reaction as a function of treatment temperatures have been studied [210]. Larger numbers of edge sites and oxygen-containing surface functional groups were found to be beneficial for higher electrochemical activity. The latter decreases with higher graphitization temperature. The relatively low electronic conductance of graphite felt as compared to carbon paper has been reported as a significant contributor to internal electrode resistance [124]. Surface modification by attached particles of various materials initially intended to enhance catalytic activity has turned out to be an option resulting also in decreased electronic resistance. For an example see [211].

The following reports on studied materials are arranged starting with carbon-based ones. A distinction is made between surface modifications by deposition of further carbon in one of its numerous modifications. Next, materials that are surface modified by treatments which change the surface of the starting material without adding further material (this may be considered surface-treatment in its most original sense) are reviewed. In two further sections, catalysis by metal and metal oxide deposits is discussed. Composite materials and non-carbon materials are treated. Some final remarks deal with the distinction between catalytic and surface enhancement effects.

4.1. Modified Carbons and Graphites

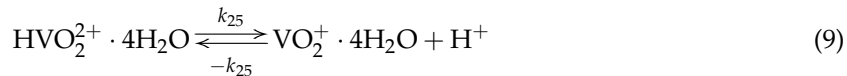
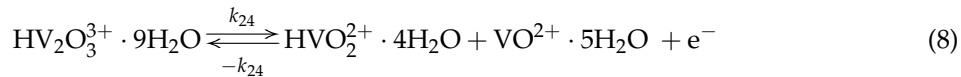
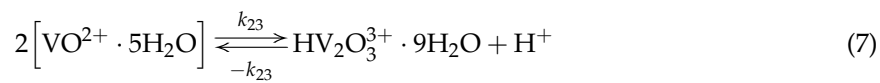
Carbon-based electrocatalyst materials utilized in RFB can be assigned mainly to four major approaches:

1. Structural modification of carbon (e.g., by carbon fiber or graphene deposition on graphite)
2. Mechanical or chemical surface treatment (e.g., by nitrogen doping of graphite felt)
3. Foreign metal deposits
4. Metal oxide deposits

4.1.1. Structural Modification of Carbon

As already indicated with the brief characterization (when available) of the carbon-based materials in the table above, most solid (i.e., non-porous) materials are either used in the form they are produced (e.g., plates, with mechanical structure providing flow fields and slightly increased true surface

area) or in polymer-bonded form when produced from powder or flakes. As a function of the process parameters used, porous or non-porous materials are obtained. Porous materials are quite obviously not suitable and desirable except for applications such as electrolysis, where the whole sample/electrode is exposed to the electrolyte solution. Data obtained in fundamental studies have been reported [15]. The exchange current density of the positive electrode reaction varied from $j_0 = 1.26$ to $6.33 \times 10^{-4} \text{ mA}\cdot\text{cm}^{-2}$ depending on the electrolyte concentration, while for the negative electrode, data ranging from $j_0 = 1.00$ to $1.76 \times 10^{-3} \text{ mA}\cdot\text{cm}^{-2}$ were reported. Lower overpotentials were found at the positive electrode; this observation has been confirmed in later studies. The reported symmetry factors (transfer coefficients) α and the Tafel-evaluation, implied that relatively higher overpotentials were to be expected during discharge than during charge. The suitability of spectral graphite as electrode material in the VRFB has been examined [212]. The material shows a roughness factor of 4 and was considered to be suitable for use as a positive electrode. Kinetics of the negative VRFB electrode reaction (according to the title) have been studied with a rotating disc electrode with a disk electrode of unspecified graphite [213]. In the report the positive electrode reaction was also studied, different from the title of the report. Rate constants for V(IV) oxidation from 7.89×10^{-14} to $4.38 \times 10^{-7} \text{ cm}\cdot\text{s}^{-1}$ and for the V(II) oxidation from 5.52×10^{-3} to $2.81 \times 10^1 \text{ cm}\cdot\text{s}^{-1}$ depending on the reactant concentration were reported. A sudden change of Tafel slope and R_{ct} during reduction of V(V) ions on a plain graphite electrode at large overpotentials has been observed [214]; participation of $\text{V}_2\text{O}_3^{3-}$ species has been suggested as an explanation. Similar observations have been reported elsewhere [215]; a complex chemical-electrochemical-chemical reaction sequence at low overpotentials changing into an electrochemical-chemical-chemical one was invoked as possible explanation. The unusually high Tafel slopes could not be explained. The oxidation of VO^{2+} at a rotating graphite disc electrode in acidic electrolyte solution has been studied at various acid and vanadium ion concentrations [216]. Based on obtained reaction orders compared with theoretical and published ones, a new CEC mechanism with two intermediates has been proposed.



Kinetics of vanadium species and corresponding neptunium species reactions have been reported; the generally faster kinetics of the former were explained in terms of the respective homogeneous rate constants [217]. For more extensive listings see [96]. Carbon fiber electrodes obtained by extracting fibers from carbon felts were studied for both VRFB electrode reactions [218] but obtained conclusions are rather diffuse.

Maruyama et al. have studied the electrochemical reduction of the dioxovanadium(5+) ion at a glassy carbon electrode electrochemically enriched by oxidative treatment with oxygen-containing functional groups [219]. Inspection of obtained electrochemical data suggests the pivotal role of OH-groups in the reduction mechanism. A kinetic study of both electrode reactions using 10 AA carbon paper in a full cell configuration confirmed the possibility of separating positive and negative electrode overpotentials when using an independent reference electrode [171]. Overpotentials at the negative electrode were significantly larger than those at the positive one; this was confirmed with double half-cell studies in this work. Wu et al. studied both electrode reactions at OPG, GC and carbon paper electrodes [220]. Rate constants were determined to be $k_0 = 1.0 \times 10^{-3} \text{ cm}\cdot\text{s}^{-1}$ for the positive and $k_0 = 1.1 \times 10^{-3} \text{ cm}\cdot\text{s}^{-1}$ for the negative electrode. They were two orders of magnitude larger than found with the smooth OPG and GC electrodes. The difference (the term “acceleration” in the title of the report appears to be misleading) was attributed to the vastly increased surface area of carbon paper. A dual porosity (dual-scale porosity) electrode was obtained by treating carbon paper with KOH [221].

Large pores ($\sim 10 \mu\text{m}$) established between the carbon fibers were maintained during the activation, small pores ($\sim 5 \text{ nm}$) were formed on the fiber surfaces during the activation. The latter caused the major growth of the BET-surface area by a factor of sixteen while keeping the hydraulic liquid permeation properties of the paper unaffected. Increases of energy efficiency in comparison to untreated paper from 82% to 88% at current densities $200 < j < 400 \text{ mA}\cdot\text{cm}^{-2}$ were measured. A similar approach has been reported by Zhang et al. [222]. Etching with KOH at 800°C created additional micropores and oxygen-containing functional groups. A reaction mechanism involving formation of metallic potassium was proposed. Improved wetting was noted, while enhanced electrochemical activity was observed in CVs and impedance measurements. An energy efficiency around 70% at $j = 150 \text{ mA}\cdot\text{cm}^{-2}$ was stable for at least 200 cycles. Carbon paper has been activated by a modified Hummer's method [223] and increased surface area and improved wettability were noticed. Improved performance as the positive VRFB electrode was also attributed to created functional groups. Application of this treatment to graphite felt also resulted in improved performance [224]. Increased hydrophilicity due to additional $-\text{OH}$ -groups was identified as a major reason of the improved performance.

The effect of the acid concentration on kinetics of the positive and negative electrode at various carbon materials has been explored by Kaneko et al. [165]. Apparent rate constants k_s ranging from 0.91×10^{-3} to $9.7 \times 10^{-3} \text{ cm}\cdot\text{s}^{-1}$ with graphite reinforced carbon depending on sulfuric acid concentration were reported. Effects of concentration of sulfuric acid and of V(V) ions has also been examined elsewhere [225] and an optimum acid concentration of 5 M was identified. By sucrose pyrolysis, activated charcoal on graphite felt was prepared by Yang et al. [226]. Increased surface area ($13.8 \text{ m}^2\cdot\text{g}^{-1}$) compared with unmodified graphite felt ($6.3 \text{ m}^2\cdot\text{g}^{-1}$) as well as increased oxygen content were found. At the positive VRFB electrode lower overpotentials and decreased peak separation were measured resulting in increased energy efficiency.

Lee et al. synthesized a macroporous graphitic nanoweb of three-dimensionally entangled nanoribbons [227]. A large surface area and pore volume were found. Decreased peak potential separations in CVs at both electrodes of a VRFB and an energy efficiency of 85.8% were reported, significantly better than 73.4% found with commercial carbon felts. Mesoporous carbon was deposited by a sol-gel process on PAN-based carbon felt and annealed at 1100°C [228]. The significant increase of peak currents of the positive electrode reaction was attributed to the enlarged surface area cause by the deposited mesoporous material. The increased peak potential was assigned to a decreased electronic conductivity of the material. Surface graphitization at 1100°C and higher reduces this negative effect. Mesoporous/mesocellular carbon foam without and with platinum modification attached to graphite felt has been suggested as positive electrode for a VRFB [229]. The electrochemical performance of electrode and cell was ascribed to the particular porosity and the large density of OH-functional groups on the carbon surface. Cell performance (80% energy efficiency over 10 cycles) in comparison to a cell with Vulcan XC-72-modified graphite felt also platinum-catalyzed, was significantly improved even when the amount of platinized XC-72 was doubled. Platinized Vulcan XC-72 (the term platinum-based seems to be rather inappropriate) loaded onto either glassy carbon or graphite felt (the rather confuse text seems to suggest this) using Nafion[®] as a binder has been suggested for use as a positive electrode [230]. Displayed CVs and discussion in the report apparently do not match. Energy efficiency of about 72% was stable for 10 cycles.

Holey-engineering [231] was applied to graphite felt by Liu et al. to obtain a porous graphite felt material [232]. The obtained product showed enhanced wettability and largely increase surface area resulting in improved performance of both electrodes up to current densities of $300 \text{ mA}\cdot\text{cm}^{-2}$ during up to 3000 cycles.

Recently numerous new forms of carbon such as carbon nanotubes, graphene etc. have been prepared and have attracted large interest in both fundamental and applied research [233–236]. Graphite and other solid (bulk) materials for fundamental studies as well as carbon and graphite felt, cloth etc. for applied studies have been modified by deposition of graphene, graphene oxide etc. The use of nanostructured materials in positive electrodes of batteries has been reviewed elsewhere [237].

Carbon dots were prepared on graphite felt by a one-pot solvothermal method by Zhou et al. [238]. Improved wettability and enhanced catalytic activity when compared with pristine graphite felt were observed for the positive electrode reaction as was evident from reduced peak separation in CVs and from wettability tests. An increased peak current as a likely consequence of enhanced wetting was not found. Catalytic effects of graphene quantum dots evidenced with CV have been reported [239].

Commercial graphene nanoplatelets were studied by Sankar et al. [240] for the positive electrode reaction. Both rotating disc electrode studies with the nanoplatelets attached to a glassy carbon electrode and attached to a graphite plate as used in a fuel cell by layer-by-layer assembly showed significantly increase exchange currents (two orders of magnitude large than with platinized carbon). A 5% increase in overall efficiency was recorded. Edge-halogenated graphene nanoplatelets were prepared by ball-milling nanoplatelets with halogen gas [241]. With Nafion® as a binder, a catalyst ink was prepared and deposited onto carbon felt. Best results were obtained with the brominated material. By plasma-enhanced chemical vapor deposition vertically aligned graphene nanosheet arrays were grown by Zhang et al. [242] and improved energy efficiency was reported. Graphene-like materials obtained by reduction of graphite oxide have been studied as electrode materials for the positive VRFB electrode [243]. High catalytic activity evidenced from CVs and improved electronic conductance beneficial to a lower cell resistance, were attributed to more restoration of sp^2 -domains by the processing. Nitrogen-doped graphene nanosheets were prepared by a simple hydrothermal reaction of graphene oxide with urea as a nitrogen source and coated onto a glassy carbon electrode for use as a positive electrode material [244]. The amount of nitrogen, in particular the type of nitrogen (quaternary nitrogen) turned out to be influential on observed electrode performance.

Han et al. prepared graphene oxide nanoplatelets by a modified Hummer's method. They applied vacuum drying at temperatures between 50 and 120 °C for 24 h, and subsequently deposited them onto a glassy carbon surface [245]. Oxygen-containing functional groups as well as hydroxylation were found on this electrode material. The material showed an increase of BET-surface area by a factor of 4 to 6 accompanied by a very large decrease in electronic conductivity. XPS showed a major increase in oxygen content. The sample dried at 50 °C was most active for both electrode reactions of the VRFB. This improvement was attributed to the increased oxygen content, i.e., the increased number of oxygen-containing surface functional groups. The oxygen content did not vary significantly between samples dried at different temperatures; the same applies to the electronic conductivity. BET surface area was actually larger after drying at higher temperatures. An explanation for this was not given. At higher currents the samples dried at higher temperatures showed lower ohmic overpotentials as expected. Reaction mechanisms were proposed for both reactions (see Figure 4) based on an earlier suggestion [246].

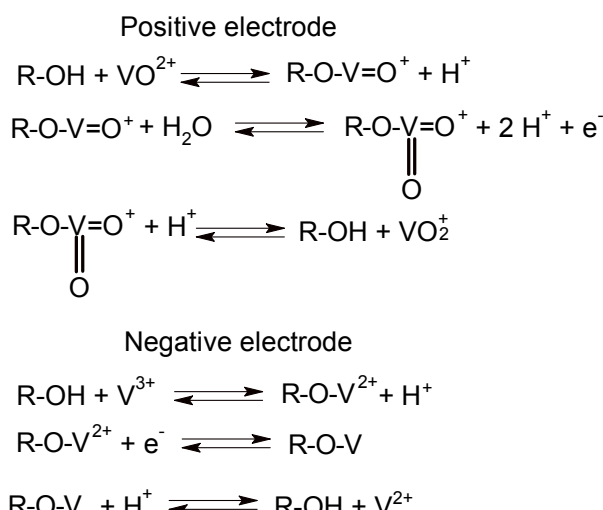


Figure 4. Proposed reaction mechanisms for positive (top) and negative (bottom) electrode reactions in a VRFB with graphene oxide nanoplatelets as electrocatalysts [245,246].

Moghim et al. modified carbon felt with reduced graphene oxide (rGO) by a simple deposition from a solution of the rGO [175]. Depending on the concentration of rGO in the deposition solution and thus presumably the more or less significant loading of the carbon felt with rGO, beyond a significant increase of current, the decrease in oxidation overpotential is remarkable, whereas the peak assigned to the reduction shows a much smaller shift. The decrease of peak separation may indicate a catalytic effect, but the significant asymmetry of the redox peaks indicates a striking irreversibility. A catalytic effect can also be deduced tentatively from the significantly reduced charge transfer resistance R_{ct} obtained from impedance measurements. Another beneficial effect of the deposition of rGO is the improved wetting observed with contact angle measurements. Unfortunately no values of double layer capacity accessible via the impedance measurements have been reported, it would have been interesting to see whether improved wetting results in increased EASA.

rGO was deposited electrophoretically on carbon paper for use as a positive VRFB electrode [247]. An increase of surface area by 24% was claimed but not substantiated in the report. A decrease of R_{ct} may imply some increase of EASA. Li et al. obtained rGO by electrochemical reduction and studied its activity for both positive and negative VRFB electrode reactions [248]. rGO was prepared on graphite felt by a hydrothermal method as reported by Deng et al. [249]. The number of oxygen-containing functional groups was vastly increased; the electronic conductivity as well as the stability (more than 500 cycles with almost no efficiency loss) were improved also. The material showed high activity for both the negative and the positive electrode reactions. An energy efficiency higher by 20%, improved performance at high currents and a discharge capacity greater by 300% were reported.

Gonzalez et al. deposited graphene oxide GO by an electrophoretic procedure from a suspension of GO in water on graphite felt [179]. Based on elemental analysis, XPS and SEM, the presence of a hybrid material with an increased number of oxygen-containing functional groups on the surface, was seen to increase wettability and presumably EASA. No further data supporting this were provided, but an increased capacitive current found in a displayed CV supports this assumption. The assumption that graphene-like sheets of GO (which apparently became partially reduced during the thermal treatment) might increase electronic conductance has been demonstrated elsewhere as being correct [211]. Electrochemical studies of the positive electrode reaction showed a significant peak shift of the oxidation electrode potential suggesting either increased catalytic activity and/or lower ohmic overpotential. The cathodic peak shifted toward higher electrode potentials and grew in magnitude implying in addition higher reversibility [250] of the electrode reaction. Higher energy efficiency was finally found. Di Blasi et al. treated graphene oxide in a reducing atmosphere at various temperatures between 100 and 300 °C and deposited the obtained material by wet impregnation from an alcoholic solution on carbon felt [251]. CVs covering both the positive and the negative redox electrode couple potentials showed some catalytic effect attributed in a rather general way to oxygen-containing surface functional groups. Higher treatment temperature resulted in a decrease even of this effect and this was attributed to decreasing wettability. Maruyama et al. prepared a network of reduced graphite oxide using carbon paper as a scaffold followed by heat-treatment resulting in partial reduction of the oxide [172]. Further studies of the positive electrode $V^{4+/5+}$ reaction showed significant decreases of electrode overpotential, smaller peak separation and increased peak current most pronounced for samples treated at 1000 °C. This material had shown the finest structure suggesting a large surface area (no BET or EASA data were provided) and smooth ion transport. To enhance wettability graphene oxide deposited on carbon felt was covalently functionalized with phosphonic acid groups [252]. CVs recorded for both VRFB cell reactions showed slightly diminished overpotentials but highly asymmetric currents. Accordingly energy efficiencies around 80% were recorded stable over 180 cycles. Reduced graphite and graphene oxide have been prepared and examined, these materials were considered particularly economically attractive [253]. The graphene obtained via reduction of graphene oxide turned out to be electrochemically more suitable than graphene obtained via other routes. This was attributed to increased restoration of 2D graphitic structures in the obtained platelets which in turn show higher electronic conductivity and more reactive edges. Graphene prepared by thermal exfoliation at 1000 °C from different graphene oxide samples have been examined as positive

VRFB electrodes [254]. Significant differences in electrochemical activity of prepared electrodes containing 70 wt.% graphene and 30 wt.% PVDF binder were found and attributed to a higher degree of restoration of 2D graphitic structures and subsequently enhanced electronic conductivity. How this can increase heterogeneous electron transfer rate was not explained. Onion-like carbon without any doping or further surface treatment has been prepared and tested as the positive VRFB electrode material [255]. Its performance when placed on a glassy carbon electrode using Nafion® as a binder was claimed to be comparable to that of the best modified carbon materials described elsewhere.

Carbon nanofibers CNF treated with KOH were mechanically deposited on graphite felt for use as a positive electrode [256]. Added oxygen-containing surface groups were identified with XPS. Enhanced wetting and mass transfer were noticed and attributed to the chemical etching. Energy efficiency increased by 4.4% to 85.7% and was reported to be stable over 50 cycles. On the surface of graphite felt CNFs were grown by chemical vapor deposition (CVD) for use as the positive electrode [257]. Compared with pristine graphite felt, increased peak currents and smaller peak separation were found in CVs. This was ascribed to increased surface area and more active reaction sites. A reaction mechanism involving C=C-bonds on the carbon surface was proposed.

CNTs in materials for the positive electrode were examined in more detail by Lv et al. [258]. Although the title suggests a study of the influence of the layer number in the nanotubes, the report actually focuses more on the effect of various amounts of oxygen-containing functional groups on the CNT surface. In agreement with many other studies discussed here, an increasing number correlates with increased catalytic activity. Highest activity in terms of peak separation in CVs and charge transfer resistance in impedance measurements was found with CNTs with smallest diameter and thinnest walls, surprisingly also with lowest numbers of functional groups. Nitrogen-doped CNTs were grown on graphite felt by a chemical vapor deposition procedure [259]. The substantially improved performance was attributed to various features of these catalysts: changes of the electronic structure of the CNTs by embedded nitrogen should influence favorably adsorption characteristics for vanadium-species; the doping causes generation of defect sites which are frequently more active catalytically; and the amount of surface oxygen species, which in many studies has been identified as being critically involved in the redox reactions, is increased; the doping makes the CNTs more accessible, i.e., the electrochemically active surface is increased probably because of a more hydrophilic surface. Nitrogen-doped CNTs were prepared using metal phthalocyanines as precursors on graphite felt [260]. Best results in terms of high nitrogen concentration, improved wettability and electronic conductivity were obtained with iron phthalocyanine, yielding an increase of energy efficiency of 20% compared with a VRFB using pristine graphite felt. Performance was stable for 30 cycles.

High purity CNTs modified with various amounts of oxygen-containing functional groups were examined as the positive electrode by Steimecke et al. [261]. (For experimental details see [262]) No significant influence was found. On the contrary the redox reaction at the negative electrode was strongly affected. Results obtained with scanning electrochemical microscopy indicate some higher activity with more functional groups also for the positive electrode. This apparent contradiction was rationalized invoking the suggestion that more functional groups do not provide additional reaction sites but increase wetting. By chemical vapor deposition nitrogen-doped CNTs have been prepared on carbon felt with ferrocene as a catalyst using melamine as a nitrogen source for use as a positive electrode [263]. Catalytic effects at the negative electrode were rather limited, but as the positive electrode the modified carbon felt showed significantly enhanced current in part due to the enlarged surface area and a reduced peak separation. Energy efficiency around 75% for 50 cycles was reported.

Bamboo-like CNTs were directly grown on graphite felt by CVD for use in both VRFB electrodes [264,265]. With added NH₃ during the CVD nitrogen-doping was afforded. Tests of the material as a positive electrode showed significantly enhanced peak currents and reduced peak separation in CVs. Energy efficiency increased to 81% for 70 cycles in comparison to 86.3% for untreated felt and 76.1% for thermally activated felt. A composite of CNTs and macroporous carbon was prepared starting with polystyrene beads as template and polypyrrole as a starting material [266].

A large increase of EASA evidence by measurement of C_{DL} was found. Experiments with the positive electrolyte solution showed a five-fold increase of current with a thin electrode layer as compared to a non-macroporous material.

Using a hydrothermal procedure Fu et al. obtained a composite of nitrogen-doped reduced graphene oxide and multiwalled carbon nanotubes MWCNTs which was deposited for testing on a GC electrode with Nafion® as a binder [267]. Large surface area verified by C_{DL} measurements, nitrogen-doping and sufficient electronic conductivity, were stated to provide high electrochemical activity of the positive electrode. Yang et al. prepared MWCNTs on graphite felt by controlled pyrolysis of sucrose [268]. (Elsewhere just porous carbon (i.e., activated charcoal) was obtained [226]) Reliable attachment of the MWCNTs on the felt was achieved by further pyrolysis products. Increased surface area (5-fold BET area), reduced overpotentials, charge transfer resistance and finally increased energy efficiency were claimed as benefits.

Li et al. examined pristine MWCNT and hydroxylated as well as carboxylated MWCNT with and without oxidative treatment in a boiling solution of $H_2SO_4 + HNO_3$. These were subsequently supported on GC and carbon felts for the positive VRFB electrode [269]. The improved performance of the functionalized MWCNT, in particular of the carboxylated one, was attributed to participation of the oxygen-containing surface groups in the redox reaction. Both positive and negative electrode reactions of the VRFB showed increased peak currents but no peak potential shift. Based on this evidence a truly catalytic effect or just a result of the increased surface area may be concluded. For the positive electrode a decrease of the charge transfer resistance was observed with the oxidatively treated material indicating a catalytic effect of oxygen functionalities on the surface. For the negative electrode, untreated SWCNT performed better. The largest peak current increase in CVs was observed with the carboxylated form. The rather minor increase of BET surface area during oxidative treatment suggests catalytic effects. In a following study these authors attributed the enhanced performance in addition to enlarged surface area and number of surface defects [270].

Short carboxylated MWCNTs were grafted onto graphite felt by Wei et al. [271]. Improvements of electrode kinetics for both VRRFB electrodes yielding an energy efficiency of 82% were observed. A MWCNT (called MWNT in this report) mix with graphite was described by Huang et al. [272]. Best performance for the positive electrode in terms of peak separation in CVs and smallest charge transfer resistance in impedance measurements was observed at 15%wt. of MWCNT. Cell performance was also best at this composition. Energy efficiencies up to 84% were found. Mixtures of graphite powder and MWCNTs at various mass ratios with a large fraction of PTFE as a binder were attached to graphite paper for use as a positive electrode [273]. A large increase of surface area was attributed to the MWCNT fraction. Improved electrochemical performance was ascribed to this increased surface and improved electronic conductance. Using a vacuum filtration method, freestanding bucky paper electrodes were prepared from MWCNTs and tested for both VRFB electrodes [274]. Preparation parameters such as amount of surfactant and sonication time were varied. Although a decrease of electronic conductivity with increasing amount of surfactant was expected, electrochemical activity increased, implying that electron transfer was current limiting, not electronic conductivity. Energy efficiencies around 60% were reported during the initial 50 cycles.

The influence of impurities on the electrochemical activity of MWCNTs has been studied extensively [275]. Pure MWCNTs obtained from commercial MWCNTs by extensive purification treatment and processed into bucky paper sheets show low electrochemical activity because their surface is mostly composed of inactive basal planes. With various surface-activating treatments modified bucky paper (i.e., MWCNTs) were obtained. In addition carbon black and c60 (presumably fullerene) (both additives were designated as carbonaceous impurities) were added in variable amounts. Creation of oxygen-containing surface functional groups increased the electrochemical activity of the MWCNTs. In the presence of said additives the effects of this surface treatment was lower because these impurities coated the MWCNTs surface as some sort of debris.

Fundamental advantages of carbon cloth over carbon paper, in particular greater durability, have been highlighted by Tenny et al. [276]. Further increase of surface area by MWCNT grown on the cloth was noticed. Collected data imply an improved performance with the positive electrode reaction. Acid-treated MWCNTs were deposited in carbon felt for use as positive and as negative electrode in a VRFB [277] and improvements were observed. In a comparative study the effects of nitrogen- and oxygen doping on properties of MWCNT and their activity in the positive electrode reaction have been examined [278]. Although the oxygen-doped ones did not have the largest BET surface and the largest number of heteroatoms, this material was most active in terms of results from CV and impedance measurements. This was attributed to their largest content of sp^2 carbon causing highest electronic conductivity.

Friedl et al. noted a decrease of catalytic activity of MWCNT for the positive electrode reaction with an increasing amount of oxygen-containing functional groups in their study, taking into account the true interfacial surface area when calculating exchange current densities [109]. A mixture of cross-linked MWCNT and graphene oxide nanosheets was prepared in an elaborate procedure by Han et al. [279] and subsequently tested using a glassy carbon electrode support. Compared with both constituent materials improved electrocatalytic activity for the positive electrode was reported. Few layered graphene oxide nanosheets were attached with a binder (PVDF, poly(ether ether ketone) PEEK etc.) to a graphite plane for examination as an electrode in various RFBs including the positive and negative VRFB electrodes [280]. The best performance was observed when using PEEK as a binder.

A mixed deposit of carbon nanofibers and nanotubes on carbon felt was prepared via thermal decomposition of acetylene on a nickel catalyst deposited before (adsorption from an aqueous $NiNO_3$ solution followed by calcination) on the felt by Park et al. [281]. The catalyst showed significant activity for both the positive and the negative electrode. An improvement of energy efficiency up to ~64% was found. CVs showed the best performance of catalysts prepared at 700 °C. Mixtures of graphite particles and CNT at various ratios with polyvinylidene fluoride PVDF as a binder were prepared and coated onto platinum by Zhu et al. [282]. With graphite only, low peak separation put small peak currents were found for both VRFB electrode reactions. A small addition (5 wt.%) of CNT caused major gains. Mild heat treatment of the CNT before mixing improved catalytic effects further.

MWCNTs were heat-treated and chemically activated in a 1:1 mixture of $H_2SO_4:HNO_3$ [283]. Significant changes of the MWCNT and enhanced electrocatalytic activities for both VRFB electrodes were reported. Various properties affected by the treatment were invoked as explanation, including increase surface oxygen content, improved electronic conductivity and increased surface area. Carboxylated CNFs of various lengths were attached to carbon felt using Nafion® as a binder by Wei et al. [271]. Improved activity (as compared to the pristine carbon felt) was observed for both the negative and the positive electrode. The material was stable for 50 cycles. Substantial improvements in terms of higher coulombic and energy efficiency of 82% as well as higher reversibility (i.e., rate of electrode reaction) of the redox processes were attributed to the CNTs, in particular to the catalytic properties of carboxylic surface functional groups on the CNT and the large electronic conductivity of the latter. Various methods to grow carbon nanofibers by vapor growth (VGCF) followed by impregnation with various metal ions have been examined by Yang et al. [284]; application of nickel and cobalt coatings was evaluated. Beyond increased production costs of the electrode only general efficiency improvements were stated. Conclusive results were not reported. Graphene-nanowalls on graphite felt electrodes were prepared via a microwave plasma-enhanced chemical vapor deposition route by Li et al. [285]. Graphene nanowalls were found to be wrapped vertically around the felt fibers providing increased EASA, in particular graphene edges with enhanced catalytic activity for the positive electrode. A three-fold increased rate of the electrode reaction and 11% increase of energy efficiency and highly stable performance were obtained. Carbon nanowalls deposited on gold substrates using a radiofrequency plasma enhanced procedure at varied experimental conditions (varied flow of argon) for use as the positive electrode have been described [286]. Medium flow rate yielded the best performing material.

To study the location of active sites, in particular of oxygen functionalities, for both electrodes of the VRFB edge-functionalized graphene nanoplatelets and—for comparison—reduced graphene oxide were examined by Park et al. [287,288]. Improved activity of edge-functionalized nano platelets was attributed to their higher crystallinity and oxygen defects at edge sites. When MWCNT are in turn modified with metal deposits they will be discussed in detail below (Section 3). For modifications of the surface structure in a topographic sense see also following Section 4.1.2.

He et al. have studied CNTs sulfonated (i.e., attachment of sulfonic functional groups) in a hydrothermal treatment in chlorosulfonic acid and subsequently attached to glassy carbon for the negative VRFB electrode [289]. Increased wettability observed in contact angle measurements indicating larger EASA (also found as increased C_{DL} in impedance measurements), agreeing with increased peak currents found in CV at practically unchanged electrode potentials. This does not seem to support enhanced catalytic activity. The markedly decreased charge transfer resistance seems to suggest increased activity, but given the markedly changed EASA this might just be a surface effect (see also below). CNTs modified by covalently attached hydroxamic acid have been examined by Noh et al. [290] for use at both electrodes. Larger improvement at the positive electrode was attributed to the larger number of atoms in the redox ions. Taking into account Z- and E-configuration of the hydroxamic acid this could be further supported.

Carbon nanospheres with a significant content of nitrogen deposited on graphite felt were prepared by a thermal procedure starting with dopamine [291]. Using XPS pyridinic, pyrrolic and graphitic nitrogen were identified. The graphitic nitrogen (elsewhere called quarternary) was assumed to be responsible for the increased catalytic activity for both the negative and the positive electrode because of its capability to interact with positively charged vanadium species via its excess electron in the ionized state. In addition increased wettability was observed, increasing EASA. Results indicating this increased activity from CVs were supported by data from impedance measurements. Energy efficiency stayed constant up to 350 cycles, while capacity loss up to the 343rd cycle was much smaller than with plain graphite felt electrodes. Carbon microspheres codoped with nitrogen and phosphorous loaded onto a glassy carbon electrode and graphite felt have been examined as materials for positive VRFB electrodes [292]. Codoped material was more active than the only N-doped one. Energy efficiency increased by 5.1% compared with pristine, undoped material and was stable at around 80% for 50 cycles.

Boron-doped carbon deposited on carbon felt was obtained by chemical reduction of carbon dioxide with NaBH_4 [293]. Significant reductions of peak separation in CVs and charge transfer resistance of the positive electrode, as well as improved energy efficiency were reported. Boron-doped graphite felt has been suggested as electrode material for both VRFB electrodes [193]. Compared to simple thermal treatment boron-doping caused a further decrease of peak separation in the CV recorded for the positive electrode reaction. The doping increased stability considerably and an energy efficiency of about 80% was found even after 2000 cycles at $j = 240 \text{ mA} \cdot \text{cm}^{-2}$, accompanied by about 60% capacity loss.

Sulfur-doped graphene on pencil graphite electrodes has been reported by Gursu et al. [294]. Increased peak currents of the positive electrode reaction possibly due to the quite obviously increased EASA and significantly increased peak separation were observed. The great activity claimed by the authors is not apparent. B_4C has been studied with first principles calculations [295]. The central carbon atom was predicted as being a highly reactive site for redox processes primarily because of the unpaired electrons in its environment. Experimental verification for both VRFB electrodes with B_4C supported on graphite felt reinforced this claim, resulting in the designation of this material as being “bifunctional”. An energy efficiency of 88.9% at $80 \text{ mA} \cdot \text{cm}^{-2}$ was found.

Carbon nanorods were prepared by a chemical etching procedure with cobalt catalyst on carbon felt by Abbas et al. [296]. Etching time and temperature were optimized. Reaction of Co_3O_4 formed from the cobalt precursor on the felt with carbon yielded CO and CoO, the latter was subsequently reoxidized with air during the thermal treatment. Other metals turned out to be less efficient. Major improvements of wettability and doubling of surface area were found. For the positive electrode some

increase of peak current and decrease of overpotential were found, effects at the negative electrode were more pronounced. The energy efficiency of about 87% was stable over 100 cycles.

Addition of a small amount of graphite oxide to graphite powder subsequently mixed with PTFE as a binder yielded superior electrodes with the improved performance attributed to the added oxygen functional groups offered by the graphite oxide [297].

Carbon materials from natural sources (biomass) have received growing attention for many applications in electrochemistry including their use as electrode material or electrode constituents in batteries, supercapacitors etc. In addition to economic and ecological aspects biomass-derived materials frequently have suitable pore size distribution, doping by natural constituents like nitrogen or oxygen as advantage. Liu et al. have used shaddock peel as a source for preparation of a porous carbon material [298]. It showed a sufficiently large BET-surface area of $882.7 \text{ m}^2 \cdot \text{g}^{-1}$; because of its biological origin it contained significant amounts of nitrogen and phosphorous as well as oxygen-containing surface groups. Graphite felts as well as a smooth glassy carbon modified with this material showed significantly improved behavior in terms of increased peak currents and lower overpotentials in CVs. This finding is supported with results of impedance measurements. An energy efficiency of about 80% was reported. Activated carbon derived from orange peels have been examined as electrode materials [299]. With PVDF as a binder the obtained material was coated onto a graphite plate. In the VRFB cell a graphite felt was used in addition, and accordingly cells with pristine graphite and coated graphite bipolar plates were compared. CVs showed for both electrode reactions without and with coating, large asymmetries of current peaks. Impedance data for the negative electrode indicate a reduced charge transfer resistance with the coated plate. Performance degradation within the first 100 cycles was insignificant with 93.1% (instead of 91% for uncoated plates) at $20 \text{ mA} \cdot \text{cm}^{-2}$. Porous carbon from orange peel waste codoped with boron and nitrogen at various reasons with incorporated Ketjenblack particles as electrode material finally placed on carbon felt for both VRFB electrodes was prepared by Ryu et al. [300]. Nitrogen was already contained in the organic raw material and boron was added in the subsequent handling. According to displayed CVs the effect of added boron for the positive electrode reaction was rather small; the claim of synergistic effects particularly pronounced at a boron/nitrogen ratio 0.65 was support to a peak current maximum found in CVs.

Preparation of coconut-derived mesoporous carbon has been reported [301]. With PVDF binder the material was coated onto Toray paper. Using this material as positive and as negative electrode an energy efficiency of 50% was reported for the 100th cycle. A coating of carbon black nanoparticles with graphitic layers of nitrogen-containing layers derived from self-assembled corn proteins [302] was prepared and its activity for both VRFB electrodes was reported. Attachment of the obtained materials to a carbon felt electrode was afforded by applying a catalyst ink with Nafion® as a binder. Increased peak currents and diminished peak separation were observed in CVs. Larger number of oxygen-containing functional groups and nitrogen defects were suggested as reasons for the improved activity. Performance was stable for 100 cycles. Carbon nanoparticles treated first with nitric acid were attached to graphite felt using Nafion® as a binder [303]. Thin electrodes enabled the use of a simple flow field in a flow-by instead of the commonly used flow-through arrangement. The reduced ohmic losses (because of the thinner electrode) and a still sufficiently large surface area (because of the attached nanoparticles) provided an energy efficiency of 84.8% at $j = 100 \text{ mA} \cdot \text{cm}^{-2}$ stable over 30 cycles. An electrode for the positive side of the VRFB prepared by carbonizing cotton pads was compared with thermally treated carbon paper [304]. Smaller peak separation in CVs and better high rate performance were found in this comparison.

Nitrogen-doped carbon was prepared by a hydrothermal process starting with glucose and ethylenediamine as nitrogen source [305]. With Nafion® as a binder this material was attached to a glassy carbon rotating disk electrode. Enhanced catalytic activity for the positive electrode was noticed.

Graphitization at lower temperatures catalyzed by added iron ions followed by embedding further carbon using a salt-template procedures has been reported [306]. At the lower graphitization temperature higher nitrogen contents could be retained; energy costs can be reduced. The added

carbon provided large surface area increases. Improved performance at both VRFB electrodes was demonstrated with CVs showing lower electrode overpotentials, diminished peak separation and increased peak currents.

4.1.2. Mechanical, Thermal or Chemical Surface Treatment

Simple thermal treatment (i.e., heat-treatment) may be considered as the simplest kind of treatment and was first reported for the VRFB by Sun and Skyllas-Kazacos in the mid-1990s [176]. The optimal thermal treatment conditions for the graphite felt were found to be 400 °C for 30 h. The improved performance was attributed to the increased number of surface oxygen functional groups that increased the hydrophilicity of the graphite felt while providing active sites for the vanadium redox couple reactions. Other examples of thermal treatment have been mentioned above and some experimental details have been previously reviewed [307]. Heat-treatment of carbon felt under airless conditions for use as positive and negative electrode material has been examined [308]. The number of oxygen-containing surface groups was found to be larger than with untreated carbon felt or carbon felt partially oxygenated, but the BET-surface area increased by only 149%. For the positive electrode reaction, peak current increase and peak separation decrease were found, indicating true catalytic and possible surface effects. R_{ct} values from impedance measurements confirmed this. No results were reported for the negative electrode. Carbon paper heat-treated at 345 °C for 10 h showed an increase of the number of carboxylic groups on the surface and a growth of surface area, consequently improved performance was noticed [309].

Depending on the chemical environment present during such treatment thermal treatment in most case will be equivalent to some chemical surface treatment. In a typical example microwave treatment applied by Cho et al. turned out to be heat-treatment in a mixed argon/oxygen atmosphere [310]. Accordingly results showed increased surface area and more oxygen-containing functional groups. When this material was used as the positive electrode cell performance data were improved accordingly. Microwave treatment of graphite felt under atmospheric conditions with a recorded sample temperature of 400 °C yielded similar results [311]. Various treatment durations were applied. When used as the positive electrode best results in terms of peak current and separation in CVs and R_{ct} in impedance measurements were found after 15 min treatment. Energy efficiency of 73% at $j = 50 \text{ mA} \cdot \text{cm}^{-2}$ was found during 50 cycles.

Surface oxidation of carbon and carbon-based materials yielding acidic and oxygen-containing surface functionalities had been reported earlier already in general terms [312]. In a comparative study of several graphite-based electrodes without and with chemical and electrochemical activation treatments an optimal oxygen content of 5% was identified, higher oxygen contents caused decreasing electronic conductance of the materials and of R_{ct} [313]. A comparative study of the effects of various surface treatment procedures on both electrode reactions was reported by Kim et al. [314]. The connection between various oxidative treatments of carbon paper, wettability and performance as negative and positive electrode has been studied [188] and the major influence of increased wettability was stressed. Positive effects of increased surface area and added surface functional groups were concluded. Zeng et al. addressed the specifically the question, whether improved electrode performance is due to increased surface area or to functional groups, i.e., to true catalysis [315]. This question has been discussed in general terms above already. Using a hydrothermal process to introduce controlled numbers of oxygen-containing surface functional groups Zeng et al. studied both the negative and the positive VRFB electrodes. Improving effects of these groups were only minute at the positive electrode but larger at the negative electrode. The initially asked question was not answered.

Selective etching of graphitic carbon paper assisted by various metal catalysts has been employed by Maruyama et al. [316]. Enhanced exposure of edge planes of graphite known to be of higher electrocatalytic activity than basal planes was found. The influence of treatment temperature and metal catalyst was studied and improvements were observed at both VRFB electrodes. Holes with diameters between 171 and 421 μm diameter were generated by laser in carbon paper with a hole density ranging from 96.8 to 649.8 holes per cm^2 [317]. Improvement of cell performance in terms of

enhanced mass transport was observed. Some catalytic effect was ascribed to thermal activation of carbon around the holes. Excessive hole density was detrimental because active surface area decreased too much. Ultrasound-assisted etching of carbon paper with chlorosulfonic acid resulted in surface functionalization with sulfonic acid groups and in enhanced wetting when the material was used as a positive VRFB electrode [318]. R_{CT} was significantly decreased; this might have been due to enlarged EASA caused by enhanced wetting or to enhanced catalytic activity. Energy efficiency grew by 5.1% to 80.8% for a cell with modified carbon paper.

Electrochemical treatment, i.e., activation, has been reported for various carbon materials. In case of supercapacitor electrode studies, repetitive electrode potential cycling resulted in swelling of the topmost part of, for example glassy carbon, associated with significantly enlarged values of C_{DL} [319,320]. The negative VRFB electrode reaction was remarkably accelerated at pyrolytic graphite by electrochemical treatment in 1 M H_2SO_4 at $E_{Ag/AgCl} = 2.1$ V for one minute [321]. Oxygen surface groups were verified by infrared spectroscopy. The fraction of parasitic hydrogen evolution decreased from 12% to 0.1%. Activation by anodic polarization of a graphite electrode in an electrolyte solution containing $VOSO_4$ and H_2SO_4 at various electrode potentials was applied [322]. Increasing activation electrode potential correlated with increasing electrochemical reaction rate constant of the positive VRFB electrode reaction. The improvement was attributed to enhanced wetting and an increased amount of surface oxides.

Roughness effects afforded by sandpaper and surface functionalization by electrochemical activation of glassy carbon were studied by Cao et al. [323]. Increased surface roughness was found to be beneficial, presumably because of increased EASA, whereas oxygen-containing functional groups caused by electrochemical pretreatment were found to be detrimental to the positive electrode reactions. Bourke et al. have studied glassy carbon, carbon paper, carbon xerogel and fibers from graphite felt after anodic and cathodic electrochemical treatment (i.e., activation) for both the negative and the positive electrode reactions [324] and basically the same observations were reported for a carbon fiber microelectrode [325]. After briefly reviewing the rather divergent kinetic data obtained with carbon-based materials, they applied anodic treatment at $E_{sat.Hg_2SO_4} = 1.5$ V or cathodic treatment at $E_{sat.Hg_2SO_4} = -2$ V for studies with the negative redox electrode $E_{sat.Hg_2SO_4} = -0.9$ V for studies of the positive electrode couple. The treatment was called normalization treatment and further details had been reported before [326]. The positive electrode kinetics are always accelerated by cathodic and slowed down by anodic treatment, with the opposite effects observed for the negative electrode kinetics. Rate constants of the positive electrode reaction are always larger. Because the operating potentials of both electrodes differ substantial the actual state of oxidation or reduction of the material may vary. The role of oxidized surface functional groups and their changes as a function of pretreatment and actual operating electrode potential are invoked as causes for the observed catalytic effects. With glassy carbon the detrimental effects of pretreatment at positive electrode potentials for VO^{2+} reduction was examined [327]. Reactivation was possible by sufficiently negative potential excursions. The deactivation depended on the applied potential value, not on the duration of its application. This supports the assumption that just creation and subsequent reductive removal of oxygen containing surface groups are relevant and no other surface modification is possibly slower in happening. Anodic polarization of solid graphite at $E_{SCE} = 1.8$ V in 2 M H_2SO_4 has been applied [328]. Improved behavior for both VRFB electrode reactions in terms of peak separation and peak current in CVs as well as reduced R_{CT} were attributed to oxygen-containing functional groups created by electrochemical activation. Disagreement with other reports is noticeable. The shape of some displayed CVs implies significant enlargement of EASA and this might be convoluted with true catalytic effects. Zhang et al. [178] performed anodic activation of graphite felt in aqueous 1 M H_2SO_4 solution. Results showed a significant increase of the anodic peak of the positive electrode redox couple, the actual amount correlated with the amount of anodic charge passed in the activation procedure with a maximum at $560\text{ mA}\cdot\text{g}^{-1}$ passed. A corresponding decrease of the charge transfer resistance was deduced from impedance measurements and XPS data indicated an increase of the

number of oxygen-containing functional groups presumably responsible for the enhanced catalytic activity. Electrochemical activation of graphite felt in diluted 1 M sulfuric acid yielded a material with increased surface area (measured with BET method) and more carboxylic group (found with XPS) [329]. Optimum electrochemical performance was noticed after passing 3000 C·g⁻¹ during electrochemical treatment. The effect of the extent of electrochemical activation (i.e., oxidation) of graphite felt has been studied [330]. More extensive activation expressed in terms of passed oxidation charge resulted in a lower values of R_{ct} up to a passed charge of 6000 C·g⁻¹; beyond this value R_{ct} grew again. The enhanced electrocatalytic activity was ascribed to carboxylic groups on the surface. In studies of electrode materials for the VRFB electrochemical activation has been applied with graphite felt exposed to a positive electrode potential. Exact numbers were not reported as only a voltage was applied between two pieces of felt in a solution of sulphuric acid [179]. The catalytic effect on the positive electrode was remarkably close to that of modification with graphene oxide. The effect of applied current density during electrochemical activation of graphite felt in aqueous 1 M H₂SO₄ was reported [331]. Roughening was evident from SEM; XPS indicated increased density of oxygen-containing surface functional groups. Decreased charge transfer resistance from impedance measurements and increased peak currents in CV indicated enhanced catalytic activity. Activation at 50 mA·cm⁻² showed the best effects and an improved energy efficiency of 77% was found. Anodic treatment of carbon felt in weak acids like citric or oxalic acid resulted in enhancement of catalytic activity for the positive electrode reaction attributed to increased density of surface functional groups containing oxygen [332]. Energy efficiency grew from 81.4% to 85.4% after treatment with ethylene diamine tetra acetic acid. Application of a square wave electrode potential program to graphite felt in an alkaline electrolyte solution of 2 M NaOH resulted in an increased number of oxygen-containing functional group and added nano-scale porosity [333]. Enhanced wettability and accelerated electrode kinetics for both electrodes of a VRFB were observed. An energy efficiency of 87.5 was found, this being 4.2% larger than with pristine felt. Taking four different carbon materials the effect of electrochemical activation has been studied in detail by Buckley et al. [334]. Treatment at negative potentials enhances the kinetics of the V(IV)/V(V) couple and slows down those of the V(II)/V(III) couple. Treatment at positive potentials has the opposite effects. In conclusion periodic interchange of the electrolyte solutions and electrode polarities were suggested.

Simple chemical treatment of graphite felt in boiling concentrated sulfuric acid for five hours has yielded dramatic improvements in performance of a VRFB [246] as expressed in decreased overall cell resistance and increased energy efficiency (up to 91%). Use of nitric acid or a mixture of nitric and sulfuric acids resulted surprisingly in increases of cell resistance. The increased number of C-O and C=O groups on the felt surface evidenced by XPS was invoked as possible reason of the improved performance of the sulphuric acid treated felts for both the negative and positive electrodes of the VRFB. A reaction mechanism as depicted in Figure 5 was suggested.

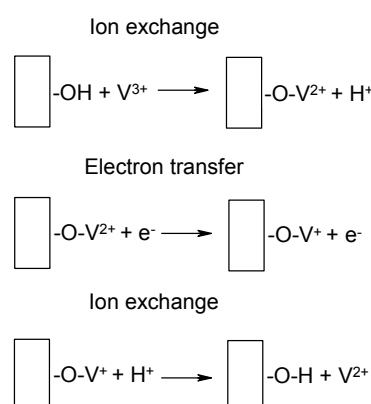


Figure 5. Proposed reaction mechanism of the positive electrode at chemically activated graphite felt [246].

For the mechanism at the positive electrode an earlier suggestion was invoked [335]. Treatment of PAN-based graphite felt in 98% sulfuric acid followed by heat-treatment at 450 °C was explored [336]. An increased number of carboxylic surface groups were found. Surface erosion resulted in an increased value of BET-surface area. Improved performance of this material when used as a positive electrode in a VRFB was observed. Carbon paper treated in highly concentrated sulfuric acid showed some improvement of performance when used as the positive electrode [337]. This was ascribed to carboxylic functional groups created by this treatment, possibly erosion of the material created additional surface area. PAN-based carbon paper was hydroxylated in a mixture of H₂SO₄/HNO₃ (V/V: 3/1) and used for both electrodes in a VRFB [338]. Significantly increased electrochemical activity in terms of decreased peak separation and increased peak current in CVs as well as reduced values of R_{ct} in impedance measurements results was noticed. An optimum treatment time was identified (8 h) and improved energy efficiency, rather stable during 100 cycles, was observed.

Carbon felt was afforded with oxygen-rich phosphate groups by treatment with ammonium hexafluorophosphate by Kim et al. [339]. Wettability was improved; significantly enhanced catalytic activity at the negative electrode of a VRFB (k increased from 0.007×10^{-3} to $2.227 \times 10^{-3} \text{ m}\cdot\text{s}^{-1}$) also resulted in diminished hydrogen evolution resulting in improved energy efficiency. The value of 87.6% decreased to 86% after 100 cycles.

Thermal treatment in air or a dioxygen-containing atmosphere has been applied to improve catalytic activity of Rayon- and PAN-based carbon and graphite felts [127]. Positive effects were found for the negative electrode; these improvements resulted in major performance gains of the full cell. Because graphitization resulted in significant decreases of BET area and EASA catalytic and surface area effects (see also below) are hard to separate. Subsequent thermal activation in turn resulted in surface area increases again. When exchange current densities j_0 initially calculated based on the geometric surface area of the electrode were normalized with respect to a “total carbon surface area” (which in turn seems to be equivalent to the total surface area and the BET surface area) changes of j_0 were much less pronounced. In an earlier study of thermal activation of graphite felt for different times and at different temperatures in air well-defined optimum conditions (400 °C and 30 h) were identified [176]. Energy efficiency increased from 78% to 88%. Improved performance was attributed to enhance wetting an increased density of oxygen-containing functional groups on the surface as concluded from XPS. For the positive electrode a reaction mechanism was proposed (Figure 6):

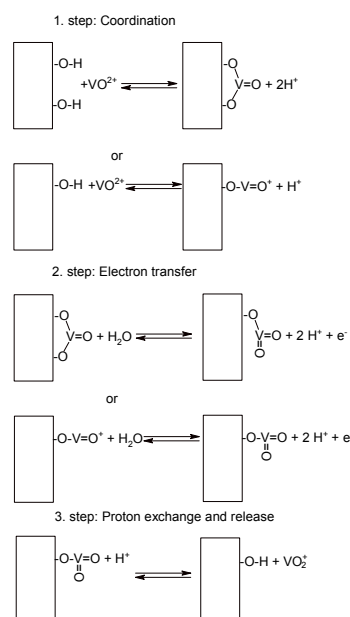


Figure 6. Proposed reaction mechanism steps for the positive electrode reaction in a VRFB with thermally treated graphite felt [176].

Kil et al. treated graphite felts in an atmosphere of ozone for only 8 min at 180 °C, for comparison treatment in air for 5 h at 500 °C was performed [340]. Ozone treatment resulted in more oxygen functionalities and higher BET surface area despite the lower process temperature and the shorter exposure. For both VRFB electrodes significantly increased currents and reduced peak separations were observed, energy efficiency increased from 82.6% with pristine felt to 90.7% for the ozone-treated one. The effect of dioxygen plasma treatment on Rayon- and PAN-based carbon felt for both VRFB electrodes has been examined [341]. No increase of BET surface area was observed. Both electrodes were claimed to show increased activity for the negative redox couple reactions. It was assigned to the oxygen-containing functional groups created by said treatment. The activity of the treated PAN-based felt for the positive electrode had decreased. Displayed CVs indicate that Rayon-based felt showed the best performance as the negative electrode with heat-treatment only, but no plasma-treatment, at the positive electrode performance was best after heat-treatment only. PAN-based felt was best for both electrodes after heat- and plasma-treatment. Treatment of graphite felt in oxygen plasma followed by treatment with H₂O₂ left numerous oxygen functional surface groups [342]. Beneficial effects were found at both electrodes of a VRFB; cell energy efficiency at $j = 150 \text{ mA} \cdot \text{cm}^{-2}$ is improved by 8.2% without obvious decay for 55 cycles. By varying the oxidation techniques, amounts and identity of the functional groups could be controlled. O-C=O groups were found to be effective whereas C-O and C=O were found to be detrimental for performance. A combination of corona discharge and H₂O₂ was proposed by Kim et al. for activation of carbon felt [343]. Increased density of oxygen-containing functional groups and improved wetting were stated. Increased peak currents and decreased peak separation were found for both VRFB electrodes in CVs. Hydrothermal treatment with H₂O₂ and sulfuric acid also resulted in enhanced wetting [344]. Addition of oxygen-containing functionalities was verified by infrared spectroscopy, while increased electrocatalytic activity was evidence in CVs that showed lower peak separation and higher peak currents, and in decrease R_{ct} -values in impedance measurements. Energy efficiencies up to 80% were recorded. The influence of surface oxygen groups on glassy carbon activated by various oxidative chemical and electrochemical procedures at the negative electrode has been studied [345]. Higher oxygen contents determined by XPS were found to correspond to lower charge transfer resistances and higher reactivities.

An atmospheric pressure nitrogen plasma jet was used for activation of graphite felt [346]. Deep penetration into the felt was claimed as a particular advantage. Increased wetting and additional nitrogen- and oxygen-containing functional groups were found as benefits, resulting in an increase of energy efficiency from 62% to 76%. The source of the oxygen in the newly created functional groups evidence with XPS was not specified. Short treatment of graphite felt in an atmosphere of CO₂ resulted in a highly active material [347]. Improvements even better than after treatment in nitrogen atmosphere, as evidenced by increased peak currents in CVs and decreased charge transfer resistance in impedance measurements, were attributed to enlarged surface area (10 fold BET), enhanced wettability, and increased number of oxygen-containing functional groups. Decreased cell resistance and increased energy efficiency 84% were reported. Heat-treatment of carbon paper in a mixture of 42% O₂/58% N₂ (somewhat confusingly this was called oxygen-enriched) resulted in an improvement in energy efficiency from 63% (without treatment) to 76% at $j = 200 \text{ mA} \cdot \text{cm}^{-2}$. A considerable increase of EASA from 0.24 to 51.22 m²·g⁻¹ was identified as the major reason of the improved performance, however the noticed decrease in activation overpotential at practically relevant current densities could not be clearly related to catalytic effects because no CVs were reported.

CNTs were codoped with nitrogen and sulfur by a heat-treatment in the presence of thiourea [348]. Graphite felt modified with the doped CNTs showed enhanced activity in terms of reduced overpotentials, i.e., reduced peak separation and increased peak currents in CVs and diminished R_{ct} in impedance measurements, for the positive electrode reactions. Energy efficiency was stable over 40 cycles, but capacity decreased significantly over this time.

A pencil graphite electrode (frequently called graphene coated electrode in title and text), was chlorine-doped by electrochemical treatment in perchloric acid with various electrode potentials being

applied [349]. Presumably the extensive electrochemical treatment in various inorganic solutions was assumed to generate graphene on the surface. Tests as a positive electrode in a VRFB showed a significant peak current increase in CVs and a significant increase in peak potential separation. Hardly any improvement of electrocatalytic activity can be noticed, so the increased peak implies increased EASA. The great electrochemical activity remains mysterious as do many other details.

Etching of graphite felt with HF followed by hydrothermal treatment with H_2O_2 to yield a material for the positive electrode was proposed by He et al. [350]. Reduced peak separation and increased peak currents were observed in CVs, while in impedance measurements a smaller charge transfer resistance was found. Energy efficiency stayed around 75% for 50 cycles, but significant capacity losses were observed during the test. Etching of graphite felt utilizing a NiO/Ni-redox process resulted in a highly porous material with features indicative of the presence of graphenated graphite [351]. Its suitability as positive and negative electrode was examined. Increased surface area (according to BET increased by a factor of three) and numerous oxygen-functionalities contributed to improved electrode and cell performance. Stable operation over 200 cycles even at high currents was claimed. Energy efficiency stayed 87% at $j = 50 \text{ mA} \cdot \text{cm}^{-2}$ for 50 cycles according to displayed data.

Carbon cloth was first heat-treated at 500 °C for 6 h under air, subsequently mixed with KOH-slurries in different weight ratios and heat-treated at 800 °C for 1.5 h by Zhou et al. [170]. The KOH-activation resulted in considerable BET surface area gains. At an intermediate carbon/KOH-ratio the increase in the number of oxygen functionalities passed a maximum. The high porosity provided good electrolyte solution utilization, while the increased surface area and density of oxygen-containing functionalities resulted in improved performance in terms of energy efficiency of 80% stable over 200 cycles at $j = 400 \text{ mA} \cdot \text{cm}^{-2}$.

Rather unspecific earlier reports on “activated carbon fiber electrodes” [352] apparently confirmed the general and much older experience, that carbon-based electrodes treated at elevated temperatures in e.g., a nitrogen-containing gas atmosphere provided significantly enhanced electrocatalytic activity [353]. Catalytic effects for numerous electrode reactions of interest have been observed [354]. Carbon paper heat-treated in NH_3 at 600 and 900 °C showed increased nitrogen content and enhanced wetting without morphology changes possibly affecting mechanical stability [355]. Peak currents of the positive electrode reactions were increased significantly while energy efficiency was marginally improved by 2.6%.

Mesoporous carbon was prepared using a soft-template approach. It was subsequently doped with nitrogen in a stream of NH_3 and attached to a glassy carbon disk electrode [356]. Compared with untreated mesoporous carbon (which showed barely any activity) and with graphite (not further specified) increased activity for the V^{4+}/V^+ redox couple was found. The catalytic mechanism influenced by the nitrogen-doping was not elucidated. The doping also causes changes in the porous structure enabling diffusion of redox species. Nitrogen-doped mesoporous carbon has been prepared by Liu et al. and tested as a positive electrode reaction material when attached to a glassy carbon disc using Nafion® as a binder [357]. Catalytic effects of the nitrogen doping for the positive electrode reaction and enhanced transport attributed to the mesoporous structure for both reactions were observed. Significant hydrogen evolution at the negative electrode prohibits the use of this material as a negative electrode in a VRFB however. The rate constant of the positive electrode reaction is $k_0 = 7.0 \pm 0.9 \times 10^{-3} \text{ cm} \cdot \text{s}^{-1}$.

Kim et al. heat-treated graphite felt in a stream of NH_3 to achieve direct nitridation [358]. Wettability was not affected, but improved energy efficiency after an optimum treatment temperature of 850 °C was found for the initial 50 cycles. Thermal oxidation of graphene felt in air followed by annealing with melamine as a nitrogen source yielded an activated electrode material for the positive VRFB-electrode [359]. Introduction of oxygen before nitrogen was found to be beneficial for the activity. Presumably the oxygen functionalities assist the introduction of nitrogen in its various forms (i.e., binding geometries). BET data indicate an increase of surface area. Increasing peak currents, in particular of the negative-going peak, and diminished peak-splitting attest to the improved

activity at the positive electrode. This was supported by impedance data. Full-cell experiments with a nitrogen-free negative electrode indicate stable performance during 130 cycles at 75.6% energy efficiency. The slightly lower value of 71.2% with a nitrogen-containing electrode is presumably due to more hydrogen evolution at the negative side. Heat-treatment of graphite felt at 600 and 900 °C resulted in modified felts [360] with excellent activity of the latter one at both VRFB electrodes. This was attributed to increased electronic conductivity and more active sites as well as improved wettability (no data were provided, no evidence given however). Various methods for co-doping of graphite felt with oxygen and nitrogen were compared with respect to use of the obtained material as positive VRFB electrode [361]. Combining ammonia and oxygen yielded particularly active material because of the high density of created oxygen- and nitrogen containing functional groups.

As an alternative to thermal treatment of graphite felt in a nitrogen gas-containing atmosphere, procedures employing aqueous solutions of ammonia have been proposed [362]. Improvements in coulombic and voltage efficiency were attributed to the enhanced electrocatalysis of the treated graphite felt, in particular to the nitrogenous surface groups. Carbon cloth subjected to hydrothermal treatment in ammonia has been proposed for the positive electrode [363]. No change of surface appearance was effected but the number of nitrogen-containing functional groups increased 5 times according to XPS. The rate constant of the electrode reaction increased from $1.47 \times 10^{-4} \text{ cm}\cdot\text{s}^{-1}$ to $2.27 \times 10^{-4} \text{ cm}\cdot\text{s}^{-1}$. Energy efficiency grew by 4.3% and stayed stable for 50 cycles.

Carbon paper showed increased nitrogen content and improved wetting after hydrothermal treatment in an aqueous ammonia solution [364]. Enhanced electrocatalytic activity, as evidenced by reduced peak separation and increased peak currents in CVs of the positive electrode, was best at a treatment temperature of 220 °C, and was assigned to an increased number of nitrogen reaction sites. Surface smoothness of carbon fibers was not affected by the treatment. Intentional nitrogen-doping has recently attracted attention for electrodes to be used in RFBs [259]. Jin et al. prepared nitrogen-doped graphene sheets by annealing graphite oxide with urea at 700–1050 °C as the positive electrode material of a VRFB [365]. Variation of the annealing temperature was expected to provide different nitrogen contents and variation of the relative fraction of different nitrogen bonding geometries. Detailed studies revealed that instead of the amount of incorporated nitrogen, the actual type of nitrogen (pyridinic-N, pyrrolic-N, quaternary nitrogen, and oxidic-N) as determined ex situ by XP spectroscopy was crucial. Quaternary nitrogen was identified as the active center for the $\text{VO}^{2+}/\text{VO}_2^+$ redox reaction. A specific nitrogen-vanadium interaction taking into account the bonding state of the quaternary nitrogen, its electronic environment and the charge of the reactant ions was proposed as the pivotal step of the catalyzed reaction. Huang et al. achieved codoping of carbon felt with nitrogen and oxygen in a plasma [366]. Reduced charge transfer hindrance of the $\text{VO}^{2+}/\text{VO}_2^+$ redox reaction could be deduced from the CVs and this was corroborated with impedance data. Accordingly energy efficiency improved. In addition stability of cell performance was markedly better. Codoping with nitrogen and oxygen by ammonoxidation (NH_3 and O_2) of graphite felt has been examined for both VRFB electrodes [367]. This is also called co-functionalization; actually a more precise term because doping suggests incorporation of heteroatoms into a lattice and not as a functional group on the surface. Improved cell performance was observed. Lee and Kim produced N-doped graphite felt by coating the pristine felt with polydopamine followed by heat-treatment in an argon atmosphere [368]. The considerably improved performance of this material used as a positive electrode was attributed to additional nitrogen-containing surface groups and increased EASA related to improved wetting. The slight increase of peak currents seems to be due to increased EASA, while enhanced catalytic activity caused the reduced peak separation in CVs. Both effects may have contributed to a reduced R_{ct} in impedance measurements. Less pronounced improvements were observed at the negative electrode. Energy efficiency was stable at 83.5% for 50 cycles.

Results of thermal treatment of graphite felt in an atmosphere of NH_3/O_2 (1:1) used subsequently as the positive electrode in a VRFB have been reported by Flox et al. [177,369]. A significant growth of both nitrogen and oxygen content in the fiber was found. Best results in terms of decreased redox peak

separation and increase of peak current were obtained with treatment at 773 K for 24 h. Application of the Randles-Ševčík-equation provided values of EASA and the largest increase was found with said treatment. Apparently both surface increase and true catalytic effects may have been operative. Impedance data support the assumed catalytic effect based on reduced charge transfer resistance values. Running 50 CV cycles did cause only minor changes indicating some stability. It may be noted that practical tests of VRFBs easily run into many hundred cycles.

A coating of polyprrole on graphite felt prepared by chemical oxidation of pyrrole served as nitrogen source in the subsequent thermal treatment at 900 °C [173]. Further modification with cobalt ions was achieved by soaking the polymer-coated felt in a solution of cobalt nitrate before the heat-treatment. These cobalt ions were leached out with sulfuric acid after this treatment, the ions served only as promoters of increased nitrogen content during heat-treatment. Enhanced catalytic effect in comparison to pristine graphite was evident from increased peak current and decreased peak separation in CVs as well as from reduced charge transfer resistance in impedance measurements. A substantial increase in energy efficiency by 34% was found when compared with a cell employing only pristine graphite.

Treatment of graphite felt at 700 °C for 5 min only with added water vapor resulted in an electrode material showing enhanced performance for the positive electrode reaction in terms of energy efficiency that increased up to 83.1%. This was attributed to an increase of the amount of oxygen-containing surface functional groups [370].

Both treatments (nitrogen-doping and surface oxidation) can possibly change the wettability of the surface in addition to creating functional groups and defects. Enhanced wettability may be desirable in numerous electrochemical applications as it may help to increase EASA. It has been noted that electronic conductivity of for example graphene, may be negatively affect by introduction of otherwise desirable surface functionalities [365]. Because most studies pertained to electrocatalysis of dioxygen reduction in fuel cell and related electrolytic applications [371,372] the applicability of these results for RFB needed experimental reappraisal. Hollax and Cheng have studied the kinetics of the Cr^{2+/-3+} and Fe^{2+/-3+} redox couples at HOPG after oxidative treatment in air at 600 °C [373]. Conceivable synergistic effects of oxygen and nitrogen functionalities on carbon felt for the negative electrode were studied by Lee et al. [374]. By a simple dip-coating in aqueous solutions of sucrose (Oxygen groups), melamine (Nitrogen groups) and regenerated silk fibroin (both groups) and subsequent heat-treatment, modified carbon felt was obtained. The simultaneous presence of both types of functional groups showed in CVs the highest increase of catalytic activity both in terms of peak separation and peak current. This was assigned to the formation of pyridonic structures on the carbon surface with both oxygen and nitrogen interacting with vanadium ions.

Although thermal treatments applied so far mostly are simple they tend to be expensive from an energetic point of view. Fenton's reagent (Fenton's reagent is an aqueous solution of Fe(II)-salts with hydrogen peroxide. It has a very high oxidation capability (see relevant standard potentials [96]) based presumably on the formation of hydroxyl radicals according to $\text{H}_2\text{O}_2 + \text{Fe}^{2+} \rightarrow \text{Fe}^{3+} + \text{OH}^- + \text{OH}^*$ [375]. The conversion of Fe(II) into Fe(III) causes the need for either supply of further Fe(II) in order to keep the reaction going or regeneration of Fe(II) from Fe(III) by reduction. This can be simply performed electrochemically, accordingly the name of the reagent is now Electro-Fenton's reagent [376]). Ref. [96,375,376] is a very effective oxidant and has been proposed as an alternative way to create catalytically active hydroxylated surfaces [377]. Closer investigation of the influence of growing concentration of H_2O_2 showed that etching of the graphite felt became more extensive and the intensity of the peak assigned to surface OH-groups increased. Data from CVs and impedance measurements indicated enhanced electrochemical activity for the positive electrode. An intermediate amount of addition turned out to be best and excessive treatment was no more beneficial. Energy efficiency grew from 67.9% for a cell with untreated felt to 74.2% for a cell with treated one.

Hydrothermal sulfonation of CNTs was suggested by He et al. [378]. Enhanced wettability but unchanged morphology were observed. When used as the negative electrode, reduced peak separation

and increased peak currents were found in CVs. Apparently some, possibly minor, catalytic effect beyond increase of EASA was operative. For the positive electrode the attached functional groups were named as causes of improved electrode and cell performance. Decreased charge transfer resistance but almost unchanged peak separation makes assessment of a catalytic effect difficult. Unquestionably a major peak growth was observed. Codoping of graphite felt with phosphorus and fluorine proposed by Huang et al. [379] yielded more hydrophilic electrodes with significantly improved rate performance that was stable over about 1000 cycles in an actual VRFB. Performance of the positive electrode was improved in particular. CoP particles physically adsorbed on graphite felt showed only rather moderate effects and an increase of energy efficiency by 5.4% during 50 cycles when compared with pristine graphite felt [380].

Iron phthalocyanine FePc and cup-stack carbon nanotubes were mixed in a weight ratio 1:10 and heat-treated at 800 °C [381]. Increased peak currents were observed for the positive VRFB electrode. In a further report the optimization of the physical properties was described [382]. Although the same procedure of catalyst preparation was employed as in the previous report [381] now a coating presumably of FePc is discussed. A higher fraction of FePc resulted in larger surface area and surface concentration of iron. The average pore size decreases with growing fraction. Optimum performance in terms of CV data was observed with 0.06 g FePc mixed with 0.1 g MWCNT. Rate constants of several vanadium ion redox reactions are listed. In a further study, optimization of the catalyst layer formed on a glassy carbon electrode was attempted by varying the amount of Nafion® used as a binder with inclusion of magnesium oxide as a pore-forming agent [383]. Apparently the binder is used to attach the catalyst material to a glassy carbon electrode used in further studies. Lower binder content allowed for a thinner coating on the catalyst that is beneficial for mass transfer. Too small binder fraction caused insufficient dispersion of the catalyst in the layer causing lower activity. The pores generated by adding MgO turned out to be beneficial.

Improved wettability of graphite felt was afforded by impregnation with Nafion® ionomer [384]. Results and their explanation are slightly diffuse however. Presumably OGF means untreated graphite felt. The wider electrochemical window claimed as a benefit shown in a CV clearly indicates larger peak separation, hardly implying improved performance. Increased peak currents indicate the effect of enhanced wetting. Energy efficiencies declining from 73.08% in the first cycle to 70.76% in the 30th are better than respective values obtained with pristine graphite felt.

Ion etching and sand-blasting of both natural graphite and electrographite yielded favorable electrocatalytic effects for both Cr^{2+/3+} and Fe^{2+/3+} redox reactions with the plain graphite showing slightly better results [167,168]. These effects could not be explained alone by invoking increased surface roughness and wettability. Authors suggested participation of acidic surface oxides in the redox reaction by enhanced adsorption of the redox ions at these functions. The lower durability of this effect in case of the Cr^{2+/3+} system was attributed to the fact, that during reduction of Cr³⁺-ions the electrode potential is negative enough to cause reduction of these oxide groups. Effects of thermal oxidation in air of graphite felt on the Fe^{2+/3+}-redox couple have been described [385]. An optimized burn-off resulting in three-fold enhancement of cell performance was found and surface oxide chemistry was mentioned to explain the effect, with a minimal amount of quinoid groups being desirable.

4.1.3. Foreign Metal Deposits

Foreign metal deposits that act as highly efficient electrocatalysts in electrochemical reactions have received considerable attention since the discovery of underpotential metal deposition [386–388] and the associated greatly enhanced electrocatalytic activity of these modified surfaces in for example electrooxidation of alcohols at fuel cell electrodes. Creation of foreign metal deposits on metallic substrates at electrode potentials positive to the calculated Nernst-potentials involving obviously strong interactions beyond simple metal deposition, i.e., crystallization, has been the subject of a long debate, but quite obviously the effect appeared initially to be limited to metal electrodes. Large catalytic effects were also observed nevertheless when traces of metal ions were added to electrolyte solutions in

systems, where carbon-based electrodes were employed (e.g., in the electroreduction of dichloroacetic acid [389–391]). Acceleration of the V(IV)/V(V)-redox reaction by cobalt- and manganese-modification of a PTFE-bonded carbon/graphite mix has been reported [392] with insufficient experimental details and without conclusive results.

In subsequent studies metal deposition and catalytic activity were investigated more systematically on various solid graphite-based materials [168]. First kinetic and further electrochemical data of the graphite or graphitic material (for details see preceding section, Table 1) itself were recorded as a benchmark for comparison. The studied metal ions were Ag^+ (upd), Bi^{3+} (upd), Cd^{2+} (upd), Co^{2+} (upd), Cu^{2+} (upd), Ni^{2+} (upd), Pb^{2+} (upd), Pd^{2+} (upd), Pt^{2+} (upd), Sn^{2+} (upd), Tl^{2+} (upd), and Zn^{2+} (upd), where upd indicates underpotential deposition and upd indicates metal deposition at electrode potentials negative to the Nernst potential. In all cases numerically submonolayer coverages were found. Scanning electron micrographs show particle deposits. Pyrolytic materials show lowest electrocatalytic activity measured as exchange current density j_0 . Enlargement of EASA due to the metal deposits is mostly small. A factor of 2–3 can be deduced from measurements of the double layer capacitance. Changes of j_0 were substantially higher, with palladium increases by a factor of 22–170 reported in some cases. Obviously these enhanced activities are no simple surface enlargement effect (for a further discussion of this aspect see Section 4.4). In several cases metal deposits resulted in lower j_0 . The investigated redox system $\text{Fe}^{2+/3+}$ is considered to be an outer-sphere reaction where—at least according to general assumptions—specific adsorption of the reactants on the electrode surface is insignificant. Accordingly the identity of the metal should be of no particular importance. Although kinetic data for a broader discussion of this topic taking into account the metals used here for surface modifications are scant [96], it appears likely, that metal-specific interactions either directly between metal deposit and redox ion or indirectly via the water molecules or other loosely coordinated species may be operative. In the case studied here the redox system was $(\text{NH}_4)_2\text{Fe}(\text{SO}_4)_2/(\text{NH}_4)\text{Fe}(\text{SO}_4)_2$ with either water or sulfate ions forming the inner ligand sphere of the iron ions.

As an alternative procedure metal impregnation has been proposed [393]. Electrocatalytic activity of plain platinum metal was observed for the positive electrode and the highest activity was found with an iridium-impregnated electrode. Good results were also observed for Mn-, Te-, and In- impregnation.

Tin deposited from SnCl_2 added to the electrolyte solution was found to be effective at the negative electrode, but at the positive electrode acceleration of the oxidation reaction was barely noticed [394]. An energy efficiency of 89.3% was reported. Indium-modified carbon paper used as the positive electrode was examined by Xiang and Daoud [395]. Indium particle deposits were found with enhanced wetting, reduced peak separation, increased peak currents and improved stability during 100 CV cycles (compared with unmodified carbon paper) attributed to these deposits. Electrodeposited bismuth on graphite has been studied as the electrode for the negative electrode reaction [396]. As evidenced with CV, some improvement of electrocatalytic activity was observed. A reaction mechanism involving initial formation of BiH_x which in turn reduced V^{3+} was suggested. This also helps to inhibit the unwanted hydrogen formation. Bismuth was deposited on carbon and graphite felt using a high temperature hydrogen reduction method [397]. The higher activity of carbon felt was ascribed to C-OH and quaternary nitrogen groups. Bismuth nanoparticles improved the electroactivity of the negative electrode. Cell performance did not improve because of the higher ohmic polarization found with carbon felt.

In addition to electrodeposition of metallic materials, further deposition procedures and electrode systems have been reported. Gonzalez et al. soaked untreated graphite felt in a solution saturated with Bi_2O_3 in 0.01 M HCl [180]. The felt was heat-treated at 450 °C in air yielding a material with elemental bismuth nanoparticles (size~35–50 nm) at 1.04 at.% content. The measured BET surface area increased from $0.92 \text{ m}^2 \cdot \text{g}^{-1}$ for thermally treated graphite felt to $3.36 \text{ m}^2 \cdot \text{g}^{-1}$ for the bismuth-containing material. CVs showed a significant increase of current and decrease of peak-separation. The latter observation is indicative of enhanced catalytic activity. Metallic bismuth nanoparticles were deposited on graphite felt as the negative electrode in a VRFB by simply adding a small amount of BiCl_3 (10

mM) to the electrolyte solution [398]. Changes in CVs were found only for the negative electrode. This is expected since a bismuth deposit will be stable only at sufficiently negative electrode potentials. Peak separation decreased indicating some acceleration of the electrode reaction. The enormous asymmetry—the cathodic charge was a multiple of the anodic one—indicates parasitic reduction reactions (presumably hydrogen evolution, but no blank scan was run and reported) in the negative going scan. Somewhat surprisingly this striking fact was not addressed in the report. The effect of bismuth addition to carbon felt electrodes by chemical reduction of adsorbed BiCl_3 for both VRFB electrodes has been systematically studied. At the positive electrode bismuth was dissolved into Bi^{3+} and stayed in this form in solution without having any effect; at the negative electrode bismuth was deposited and showed significant effects in terms of increased peak currents and reduced peak separation in CVs and reduced charge transfer resistance in impedance measurements [399]. At 2 wt.% the effect was at its maximum with an energy efficiency of 79% at $j = 160 \text{ mA}\cdot\text{cm}^{-2}$ for over 300 cycles. Carbon felt has been etched with KOH first before deposition of bismuth nanoparticles for use as a negative VRFB electrode [400]. The etching caused additional micropores and oxygen-containing surface group subsequently promoting bismuth deposition. In CVs peak separation was decreased, while in impedance measurements R_{ct} was found to be smaller. Energy efficiency was found to be 79.3% at $j = 160 \text{ mA}\cdot\text{cm}^{-2}$, 36.2% higher than with a cell having a pristine carbon felt electrode. Antimony was deposited at the negative VRFB electrode from Sb^{3+} -ions added to the electrolyte solution [401]. Increase of apparent vanadium ion diffusion coefficients and decrease of R_{ct} were observed. Energy efficiency increased from 57.5% at $j = 120 \text{ mA}\cdot\text{cm}^{-2}$ to 67.1% after addition of 5 mM Sb^{3+} -ions. Improvements are attributed to antimony nanoparticles deposited on the graphite felt.

Cubic nano-Pt and nano-CuPt₃ have been deposited on graphene oxide and in turn inkjet-printed or drop cast on a support [369,402]. The obtained catalyst was suitable for the $\text{VO}^{2+}/\text{VO}_2^+$ redox couple. The bimetallic system was more active than the platinum system and both were superior to the metal-free graphene. Only surface enlargement effects (with the monometallic material providing 105% surface increase and an even higher one with the bimetallic system) were suggested to explain the improved performance. Copper nanoparticles on graphite felt as a negative electrode were prepared in situ by adding a small concentration of CuSO_4 to the negative electrolyte solution [403]. CVs showed a small increase of peak current and no change of peak separation. The impedance data supported the assumption of a surface, but no catalytic effect of the copper deposits. Somewhat surprisingly cell data showed major performance improvements with an energy efficiency of 85% stable over 50 cycles.

Han et al. modified rGO with mixed ruthenium/selenium deposits by a chemical procedure using ethylene glycol as a reactant [404]. With Nafion® as a binder the catalysts (without/with Ru/Se) were applied to a glassy carbon disc electrode. The positive electrode reaction $\text{VO}^{2+}/\text{VO}_2^+$ was significantly accelerated when compared to the same system without Ru/Se, as evidenced from lowered peak potential separation, increased peak currents and decreased charge transfer resistance obtained from impedance measurements. The increase of the constant phase element used in the impedance evaluation by two orders of magnitude suggests that an increased EASA may be responsible in part for the increased peak currents.

Huang et al. [405] have described a modification of graphite felt with platinum-loaded MWCNTs to be applied in a VRFB as the positive electrode. No kinetic data allowing an estimate of catalytic effects were reported, but the authors assigned the substantial improvement of system efficiency to the improved catalysis of both vanadium half-cell reactions. The effects of various amounts of platinum added by chemical reduction of hexachloroplatinic acid with methanol has been studied with platinum-modified Vulcan XC-72 attached with Nafion® as a binder to glassy carbon or onto carbon felt on the positive electrode reaction [406]. According to rotating ring disc electrode measurements, the reaction rate constant increased by a factor of two with increased platinum loading, and somewhat surprisingly the exchange current density increased by a factor of five. Energy efficiency grew from 51.8% to 72.3%. The highest platinum content of 15 wt.% on XC-72 yielded best data. Iridium-decorated graphene prepared via a coreduction strategy starting with IrCl_3 and graphene oxide with NaBH_4 as

reductant finally deposited on a platinum slice has been identified as a particularly active electrode material for the positive electrode of an all-vanadium RFB [407]. The iridium deposits caused an increase of EASA. No explanation of this effect is given, but it may be increased wettability or inhibition of graphene agglomeration, which are both surface area-enlargement effects. Higher affinity to oxygen-containing species [408] was however assumed to be the cause for more $\text{VO}^{2+}/\text{VO}_2^+$ -species to participate in redox reactions. Iridium modification of graphite felt used as positive electrode in a VRFB has been examined [409]. Enhanced electronic conductance of the felt, and accordingly reduced cell resistance were noticed. Increased electrochemical activity was obvious in CVs and impedance data.

Nickel-plated carbon felt has been prepared by electroless plating and has been characterized extensively [410]. A major improvement of ASR has been stated without even defining this uncommon acronym. No electrochemical data were reported.

4.1.4. Metal Oxide Deposits

Following numerous observations of electrocatalytic activity of various manganese oxides in several electrode reactions using carbon felt as a matrix and utilizing its electronic conductivity for current collection, a composite material with MnO_2 for use as the positive electrode in a VRFB has been prepared by Ma et al. [411] by applying a simple hydrothermal procedure. Samples prepared with an acidic reaction solution showed an even and fine dispersion of MnO_2 . The Raman spectra indicate a slightly higher number of defects as deduced from the intensity ratio of D- and G-band and a significantly larger overall intensity. This in turn may imply a surface area increase which would be not unusual given the fact that graphite acted as reductant in the hydrothermal reaction. This might cause surface roughening not addressed by the authors. Impedance data show a significant decrease of the charge transfer reaction by more than an order of magnitude in comparison with pristine graphite felt. This is certainly due to the catalytic effect of the MnO_2 but might also be due to increased surface area. Improved rate performance and energy efficiency were reported. Within 120 charge/discharge cycles no decrease of energy efficiency (approx. 80%) was observed. Kim et al. deposited Mn_3O_4 on carbon felt in a hydrothermal procedure, with subsequent heat-treatment at 500 °C for 5 h being necessary to keep the deposit in place during flow cell operation [174]. Increased electrocatalytic activity for the negative and the positive electrode were found. Improved adherence was verified with scanning electron microscopy and analysis of the electrolyte solution for dissolved manganese. Various reasons including enhanced wettability and lower charge transfer overpotential were invoked as explanation. Mn_3O_4 anchored on MWCNTs prepared by a solvothermal method and deposited on a graphite plate/graphite felt has been proposed as material for the positive VRFB electrode [412]. CVs obtained with the coated graphite plate showed increased peak currents but no significant change of peak separation. The improved performance was assigned to improved electronic conductance and improved mass transport. Energy efficiency of 84.7%, better by 3.7% as compared to a cell with pristine graphite felt and stable over 50 cycles was reported. A nitrogen-doped graphene Mn_3O_4 catalyst to be used as the positive electrode was prepared by Ejigu et al. by coreduction of graphene oxide and KMnO_4 in the presence of NH_3 and subsequent deposition on a glassy carbon electrode [413]. As described above in detail four types of nitrogen were found with XPS, graphitic nitrogen being present in considerable amount, was identified as the most relevant form. The catalyst with all components (nitrogen in the graphene lattice and the manganese oxide) was markedly better than comparison samples with either nitrogen or manganese oxide alone, as evident from significantly increased peak currents and decreased peak separation as well as from a diminished charge transfer resistance found in impedance measurements.

PbO_2 was plated on graphite felt by a pulse electrodeposition method for use as a positive electrode [414]. CVs showed a major increase of peak current presumably caused by the increased surface area evidence in microscope pictures also shown. Decrease of peak separation was barely visible; the deposited lead dioxide did not show obvious catalytic activity. The observed decrease of

R_{ct} can be explained easily with the increased surface area. Energy efficiency reached 89% and was stable during 30 cycles. PbO_2 deposited on spectral graphite was found to be unstable when used as a positive VRFB electrode [212].

Yao et al. prepared WO_3 on superactivated carbon by deposition from a water/alcohol mixture containing $(\text{NH}_4)_6\text{W}_7\text{O}_{24} \cdot 6\text{H}_2\text{O}$ [415]. The product was dispersed in alcohol with added Nafion® as a binder; the dispersion was spray-coated on carbon paper. Expected catalytic effects at the positive and the negative electrode of a VRFB were examined. At the positive electrode, reduction of electrode overpotential and large peak current increase were found. For the negative electrode the peak current increase was dominant. Using this electrode in both sides of the cell, an energy efficiency of 80.5% was found. A catalytic mechanism as displayed schematically in Figure 7 was suggested.

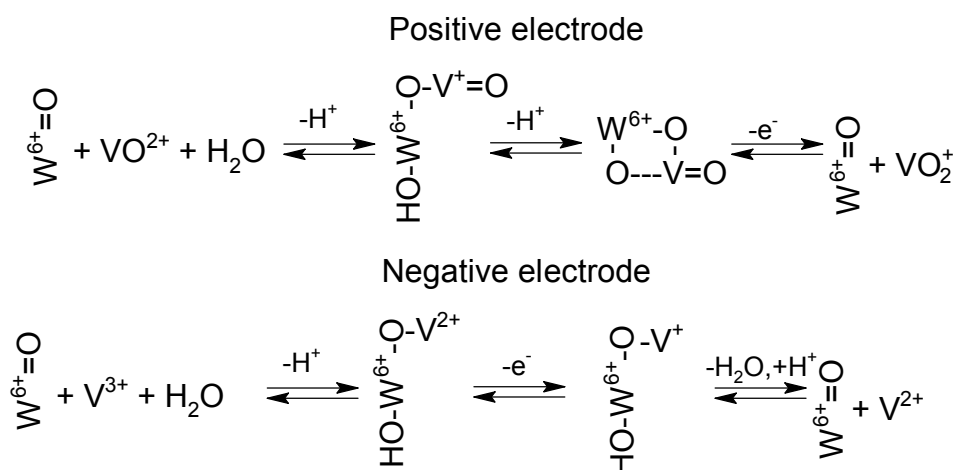


Figure 7. Proposed reaction mechanism of WO_3 deposited on superactivated carbon on carbon paper [415].

Interlaced $\text{WO}_3/\text{MWCNTs}$ were deposited by electroreduction of functionalized MWCNTs and wolframate ions on bulk graphite [416]. Improved kinetics of the positive electrode reaction were evidence from CVs, impedance measurements and chronoamperometry when comparing the results obtained with those of graphite modified with MWCNTs or WO_3 only. Using a hydrothermal method WO_3 was deposited on graphite felt for use as a positive VRFB electrode [417]. At a loading of $1.1 \text{ mg} \cdot \text{cm}^{-2}$ WO_3 at $j = 70 \text{ mA} \cdot \text{cm}^{-2}$ an efficiency of 87.87% was during 20 cycles found. A slightly increased overpotential of the vanadium oxidation seems to be slightly at odds with this conclusion. Zhou et al. deposited ZrO_2 -nanoparticles on graphite felt at various concentrations via an immersion-precipitation procedure [418]. For both the positive and the negative electrode improved accessibility and more active sites were found as evident from slightly increased peak currents and somewhat decreased peak separation. This resulted in an energy efficiency of 67. 4% as compared to 53.8% for the plain graphite felt. Niobium-doped WO_3 nanowires were prepared on graphite felt by a hydrothermal procedure for use as the positive electrode [419]. Highest activity in terms of reduced peak separation and increased peak currents in CV and reduced R_{ct} in impedance measurements was found at a Nb/W ratio of 0.03. Improved energy efficiency, stable over 30 cycles, was reported. Carbon felt decorated with WO_3 and nitrogen has been proposed as a positive electrode [420]. In CVs decreased peak separation implied enhanced electrocatalytic activity and increased peak currents may also be due to increased EASA (not reported). Decrease of R_{ct} support this interpretation. Stability data were not provided.

Cao et al. prepared MoO_3 deposits on carbon paper and examined the activity of this electrode material for both the positive $\text{VO}^{2+}/\text{VO}_2^+$ and the negative $\text{V}^{2+}/\text{V}^{3+}$ electrode reactions [421]; as an alternative approach, the effects of added MoO_4^{2-} in the electrolyte solutions was examined. Smaller peak potential separations were found. At the positive electrode the flakes caused a greater reduction,

while at the negative electrode the solution additive was more effective. VRFBs with both flakes on both electrodes and solution additives showed enhanced power density. MoO₂ nanocrystals interconnected on mesocellular carbon foam have been proposed for the positive electrode [422]. Improved performance was observed.

Hydrogen-treated rutile TiO₂ was grown on a core of graphite felt fibers and tested as negative electrode [423]. Strongly increased peak currents and much lowered overpotential suggested increased catalytic activity. This in turn resulted in improved efficiency stable for 100 cycles, although parasitic hydrogen evolution was also noticed. Anatase TiO₂ added with 20 wt.% to Vulcan XC-72 carbon black has been proposed as an electrode material for the negative VRFB electrode coated with Nafion® binder presumably on a carbon felt [424]. Enhanced wetting and increased currents in CVs were found. Accordingly improved cell performance was observed. Similar observations were reported by these authors for carbon felt coated with a TiO₂/carbon black composite [425]. This study replicated the previously quoted one. Electrospun carbon nanofibers with embedded TiO₂ were suggested as negative electrode [426]. And the improved cell performance was attributed to the high electronic conductivity of the CNF network combined with the electrocatalytic properties of TiO₂.

Ta₂O₅ nanoparticles were deposited on graphite felt by Bayeh et al. [427]. Optimum performance evidence by separated peak separation in CVs and diminished charge transfer resistance in impedance measurements were observed at 0.75 wt.% of Ta₂O₅. No deterioration was found with VRFBs after 100 cycles.

Neodymium oxide Nd₂O₃ nanoparticles have been deposited onto carbon felt by a precipitation method at different loadings for use as both positive and negative VRFB electrode [428]. High dispersion of the particles was observed. Higher energy efficiency and more stable performance were also observed in comparison to a cell with carbon felt with heat-treatment only. Nb₂O₃ was deposited on graphite felt using a hydrothermal procedure [429]. The basically poorly conducting material showed high electrocatalytic activity at both VRFB electrodes provided that nanosize and even distribution were achieved. Further addition of tungsten afforded by adding water-soluble tungsten compounds to the electrolyte solutions helped to establish this. Energy efficiency was improved by about 11% at $j = 150 \text{ mA} \cdot \text{cm}^{-2}$ for at least 50 charge/discharge cycles. Nanostructured niobium oxides in electrochemical energy and storage devices have been reviewed [430].

RuO₂ deposited electrochemically on MWCNT attached with a binder (PVC) to a stainless steel mesh has been proposed as a positive electrode in a VRFB [431]. Corrosion rate of the steel was considered to be acceptable. Smaller peak separation and increased peak currents were observed for the modified electrode in CVs.

Various amounts of CeO₂ (0.1–0.5 wt.%) were deposited by a precipitation process on graphite felts [432]. Used as positive electrode this modification resulted in improvements observed in wetting studies, CVs and somewhat poorly defined impedance measurements. Best results were found at 0.2 wt.% CeO₂.

4.2. Composite Materials

Because the vast majority of reports discussed here deal with highly porous electrodes, the term composite may be hardly applicable. Although electrodes even for technical applications could be made of purely graphitic materials like OPG, SAPG or HOPG (see also: [433,434]) most commercially used solid materials are composites of carbon and polymeric binders yielding both compact, non-porous, as well as porous materials. The use of some polymer-carbon composites in VRFB had been reviewed [435,436]. Mixtures of graphite and acetylene black with PVDF as a binder have been examined for use in VRFB [437]. Pure graphite yielded highly reversible CVs for both electrodes at small currents only. Addition of acetylene black resulted in increased currents. An optimum mass ratio of $m_{\text{AB}}:m_{\text{G}} = 15:85$ for the positive and 4:96 for the negative electrode were reported. Kim has prepared a mix of various graphites and carbon black for improved conductivity with PTFE as a binder which were subsequently attached to dimensionally stable positive electrodes (dimensionally stable

anode DSA) [166]. The higher activity of graphite was accredited to the greater surface concentration of functional groups. The latter was tentatively attributed to the added conductive carbon black. Furthermore depending on the formation process reticulated, foam-like materials, cloth-like or felt-like products as well as glassy materials can be obtained. Addition of a binder serves mostly an improved processability. Fibrous structures help in providing large surface areas with electrolyte solution flooding and also provide highly turbulent flow. These structural-morphological details became most obvious in a comparative study of carbon felt and polymer-bonded activated carbon as electrode materials with cobalt impregnations. Graphene-modified graphite with PVDF as a binder was prepared by Tsai et al. [438] and deposited on a platinum support. An optimum content of 3 wt.% yielding significant peak current increases of the positive electrode was found.

A composite of polydopamine and Mn_3O_4 at different mass ratios was deposited on graphite felt by Li et al. [439] and tested for the positive electrode reaction. A synergistic effect, i.e., results better than the expected summed effect of the single components, was found. Decreased peak separation and increased peak currents were observed in CVs, impedance measurements showed decreased charge transfer resistances.

A composite material of WO_3 nanowires and graphene nanosheets formed into a foam was synthesized by Kaptamu et al. [440] via a multistep process. The material enabled an energy efficiency of 83.73% and no degradation after 50 cycles. Evidence of covalent attachment of the tungsten oxide to the graphene sheets was obtained. A composite of rGO and $TiNb_2O_7$ has been proposed as material for both electrodes in a VRFB [441]. Increased electrocatalytic activity for both reactions was found in terms of decreased CV peak separation corroborated by decrease R_{ct} values from impedance measurements. Energy efficiency was stable at 80% for 200 cycles at $j = 120 \text{ mA} \cdot \text{cm}^{-2}$ and the discharged capacity stayed at 90% of its initial value during these cycles.

Electrospinning of materials has developed into a frequently applied technique for preparing felt-like electrode materials [442], for a typical example see e.g., [443]. Obtained fibers are sometimes called electrospun carbon nanofibers ECNFs. Using electrospinning a flexible material having a particularly large EASA with respect to its volume has been reported [444]. With respect to electrode volume high current densities were recorded of the positive electrode reaction implying a large EASA per electrode volume offered by the ECNFs. The influence of graphitization on electrochemical activity and performance of ECNFs for the positive VRFB electrode has been studied [445]. Increasing graphitization temperature and increasing amount of used iron catalyst Fe(III)acetyl acetonate resulted in higher degree of graphitization. An intermediate degree of graphitization was found to be most suitable. No unambiguous optimum preparation parameter set was provided.

ECNFs modified with phosphotungstic acid have been suggested as material for both VRFB electrodes [446]. Displayed CVs showed large irreversibility in terms of charge under current peaks obtained with GC as a support. Decreased peak separation and R_{ct} in impedance measurements indicate enhanced electrocatalytic activity. Energy efficiency amounted to 83% at $j = 20 \text{ mA} \cdot \text{cm}^{-2}$ for 180 cycles.

To improve hydrophilicity of PAN-based ECNFs embedding CeO_2 has been suggested [447]. This addition caused minor morphological changes and an increase of EASA by a factor of four. Peak separation in CVs for both the negative and the positive electrode were barely different with incorporated CeO_2 whereas peak currents grew significantly. Decrease of R_{ct} can also be explained with increased EASA. Energy efficiency increased accordingly stable over 50 cycles. A very thin and freestanding carbon nanofiber net was obtained by electrospinning [448]. Attention was paid to the effect of the temperature during the thermal treatment following spinning. Highest activity for the negative electrode reaction was found at 1100 °C, higher temperatures decreased the activity. For the positive electrode this trend was not observed. Accordingly the role of surface functional groups at the negative electrode was considered to be high whereas at the positive electrode this role is negligible. Material obtained at this temperature also showed highest electronic conductance. A slightly different optimum temperature of 1000 °C has been reported elsewhere [449]. Higher relative electrochemical

activity for the positive VRFB electrode reaction in comparison to conventional carbon felt electrodes has been found when examining both materials attached to a glassy carbon electrode. Relationships between structure and surface characteristics relevant when electrospun and heat-treated carbon fibers are used as positive electrodes have been investigated with CVs and impedance measurements [450]. Poorest performance was observed with a carbonization temperature of 1300 °C. As an explanation it was suggested that with growing temperature up to 1300 °C surface composition plays a dominant role for catalytic activity whereas at higher temperatures edge planes of formed graphite crystallites become dominant. Between 1000 and 1300 °C reduction of catalytically relevant oxygen-containing groups happens diminishing catalytic activity, at higher temperatures more graphite crystallites more active again are formed. The influence of heat-treatment temperature on electrode performance of electrospun PAN-based nonwoven web (Apparently a nonwoven web is the same as a felt in the given context.) has been studied [451]. Increase of treatment duration facilitated unwanted hydrogen evolution. Energy efficiency of 85% at $j = 50 \text{ mA} \cdot \text{cm}^{-2}$ for 90 cycles was reported.

ECNFs codoped with boron and nitrogen have been examined for the positive VRFB electrode [452]. When compared with single-doped CNFs prepared in the same way a beneficial effect of the codoping in terms of decreased peak separation and increased peak current in CVs and reduced R_{ct} in impedance measurements was found. Particularly important are the heat-treatment temperature and the way doping is performed. Catalytic mechanisms were proposed.

Carbon nanofibers obtained by electrospinning of PAN were modified with graphite nanopowders [71]. Increased content of nanopowder yielded at mass ratio 1:50 best electrochemical performance at both electrodes. With mixtures of e.g., a dissolved a polymer and a metal oxide precursor composite fibers can be obtained which turn into composite materials after heat-treatment. Busacca et al. used polyvinylpyrrolidone and vanadium(V)oxytriisopropoxide as starting materials and prepared a CNF/V₂O₃ composite [453]. CV and impedance measurements of the positive electrode reaction showed significant improvements of electrode kinetics provided by the added metal oxide in terms of diminished peak separation and charge transfer resistance. A rather graphitic structure of the carbon component and the 3D V-V-framework provided sufficient electronic conductance. Addition of manganese acetate to the solution of PAN yielded after heat-treatment of the electrospun fibers a blend containing 20 wt.% of Mn₃O₄ [454]. Used as electrodes in a VRFB this material showed activity for both electrodes evidenced in CVs and impedance measurements. An energy efficiency of 81% was achieved.

PAN-based ECNFs with embedded CNTs and bismuth nitrate have been prepared [455]. Those modified with CNT were best as positive electrodes, bismuth-modified ECNFs were best as negative electrodes. A major advantage of the latter was suppression of parasitic hydrogen evolution. Actual effects in CVs regarding catalytic effects at both electrodes were minor; only suppression of the hydrogen evolution was very significant.

4.3. Non-Carbon Materials and Miscellaneous Concepts

Metal-based electrodes—actually metal foils or sheets—have been studied only rarely. Iridium-oxide coated dimensionally stable electrodes have been evaluated as positive electrode in a VRFB [190]; no specific catalytic effects were reported. Han et al. prepared nanotubular TiO₂ on a titanium substrate subsequently coated with a layer of IrO_x [456]. The bipolar plate thus made was only 0.137 mm thick. Stability reached beyond 100 cycles. When compared with a graphitic bipolar plate an increase of efficiency of 3% to 4% was recorded.

Stabilized titanium nitride TiN nanowires were decorated on graphite felt by Wei et al. [457]. Improved electrolyte solution utilization and an energy efficiency of 77.4% at current densities up to 300 $\text{mA} \cdot \text{cm}^{-2}$ were ascribed to faster electrochemical kinetics and more active sites at the negative electrode. Performance was stable during 50 cycles. TiN nanowire directly prepared on titanium foil by a hydrothermal process have been examined as the negative electrode by Zhao et al. [458,459]. Significant improvements in comparison to TiO₂ and plain graphite were noted; a rate constant for

the V^{3+}/V^{2+} reaction of $k = 5.21 \times 10^{-4} \text{ cm}\cdot\text{s}^{-1}$ was found. Titanium carbide TiC nanoparticles were decorated on carbon paper by Wei et al. [460]. Compared to carbon paper decorated with carbon nanoparticles only or to pristine carbon paper significant reductions of overpotentials and peak current increases for the negative electrode reaction were achieved. In a VRFB this resulted in 80.7% energy efficiency at $100 \text{ mA}\cdot\text{cm}^{-2}$, 12.3% better than with pristine carbon paper at the negative electrode. TiN nanoparticles deposited on carbon paper have been examined as catalysts for the negative electrode in a VRFB [461]. A significant improvement in comparison to a negative electrode of plain carbon paper stable for more than 50 cycles was registered. Graphitic C_3N_4 deposited on carbon felt by a hydrothermal procedure using melamine as a nitrogen source has been suggested as a material for the positive VRFB electrode [462]. CVs showed significant improvements in terms of diminished peak separation and increased peak currents resulting in improved cell performance data. Urea pyrolysis in the presence of graphite felt yielded a highly active material for use as the positive electrode [192]. According to DFT-results pyridinic nitrogen atoms were identified as the catalytically particularly active sites. Energy efficiency close to 80% at $j = 150 \text{ mA}\cdot\text{cm}^{-2}$ was almost constant over 800 cycles. Phosphorous-doped C_3N_4 was formed on graphite felt and tested for both VRFB electrodes [463]. Enhanced wettability and improved electrocatalysis evident from decreased peak separation were observed, larger peak currents may be due to both influences. At the negative electrode this increased activity resulted in smaller losses due to parasitic hydrogen evolution. 50% capacity loss were found after 356 cycles, without the applied coating this loss was already registered after 186 cycles. Energy efficiency of 74.1% was observed at $j = 150 \text{ mA}\cdot\text{cm}^{-2}$.

Carbon-coated titanium has been examined for possible use as an electrode in a VRFB [464]. The positive electrode reaction was found to be irreversible because the carbon coating was oxidized. CVs obtained with the negative reaction show a couple of redox peaks with considerable peak separation. Titanium coated with a mixture of iridium(V) oxide and tantalum pentoxide has been examined as positive VRFB electrode [465]. A slightly higher electrocatalytic activity and decreased energy efficiency in comparison to a plain graphite electrode were found.

Mesoporous tungsten oxynitride has been suggested as catalyst for the positive electrode [466]. Details of the actual electrode were missing in the report. Energy efficiency around 80% was found.

Silicon has been studied as a photocathode material in a solar rechargeable VRFB [467]. Bismuth was found to effect a significant electrochemical improvement of the negative electrode reaction. Both acceleration of V^{3+} -reduction and suppression of hydrogen evolution were noticed.

Addition of In^{3+} at a concentration of 10 **mM** to the positive electrolyte solution resulted in slight improvement of kinetic parameters [468]. Changes of the solvation shell of the reactant ions by the indium ions were invoked as possible explanation. Cr^{3+} has been also added to the anolyte [469]. At optimum concentration ($0.3 \text{ g}\cdot\text{L}^{-1}$) improvement of various parameters related to electrode kinetics was noticed. Similar effects in particular regarding apparent diffusion coefficients of vanadium species in the positive electrolyte solution were observed upon addition of Mn^{2+} -ions [470]. Addition of millimolar (0 ... 5 **mM**) concentrations of WCl_6 resulted in smaller peak separations in CVs for both VRFB electrodes and [471]. With tungsten at the positive electrode the anodic peak current was halved, CVs show a major irreversibility. Nevertheless an energy efficiency of 83% was reported for 3 **mM** concentration of WCl_6 during 100 cycles.

Addition of various organic compounds (fructose, mannitol, glucose, D-sorbitol) to electrolyte solutions containing the V^{4+}/V^{5+} redox couple at the positive electrode has been proposed [472]. The most effective additive D-sorbitol apparently caused an increase in surface density of OH-groups being involved in the redox reaction, in addition D-sorbitol increases solubility of the V^{5+} -compound. This finding in general corroborates earlier reports by Sun and Skyllas-Kazacos regarding the effect of surface oxygen functional groups, in particular C-O-H moieties [174,333,393] as well as the early work by Kazacos and Skyllas-Kazacos on the use of organic and inorganic additives as stabilizing agents to inhibit precipitation in supersaturated vanadium electrolytes [473–475]. Beneficial effects of the addition of taurine to the positive electrolyte have been reported [476,477]. Glycerin has been

found to improve electrochemical performance of the positive electrode [478]. Effects of added inositol and phytic acid in the positive electrolyte solution have been examined [479]. Enhanced diffusion of vanadium species and increase exchange current density of the electrode reaction were noted. Addition of dipicolinic and quinolinic acid to the positive electrolyte solution improved electrode kinetics and helped in preventing precipitation of V_2O_5 [480]. The suitability of ionic organic additives in the positive electrolyte solution has been examined [481]. Wu et al. have added hexadecyl trimethyl ammonium bromide CTAB to the electrolyte solution of a VRFB [482]. Evidence gathered with various methods indicates that CTAB interacts with V(V)-ions keeping them from further polymerization helping this way to suppress crystallization. At the electrode they participate in micellar catalysis. Doubling of C_{DL} and reduction of R_{CT} were found. Beneficial effects of both organic amines and inorganic ammonium salts for stability of the positive electrolyte and associated electrode kinetics have been observed [473,474,483]. Various organic compounds have been examined as additives in the positive electrolyte solution [484]. Amino acids have been added to the negative electrolyte solution of a VRFB [485]. Delayed precipitation and improved energy efficiency were found. L-glutamic acid has been examined as an additive to the positive electrolyte solution [486]. Reduced electrolyte salt precipitation was found as well as improved electrode performance. XPS date indicate changes of carbon felt surface composition induced by chemical reaction with the additive. Methanesulfonic acid and aminomethanesulfonic acid have been proposed as additive to the positive electrolyte solution [487]. Beneficial effects have been tentatively attributed to increased hydrophilicity of the electrode surface; the additives may have acted as surfactants. Coulter dispersants (mixtures of water and various surfactants) added to the positive electrolyte solution have been examined [473,474,488]. Dispersant IIIA delayed precipitation of vanadium salts significantly without causing undesirable side effects. The beneficial effects of some additives have been questioned [473,489]. Oxidation of the additive associated with reduction of V(V) ions was suggested as the cause. Frequently enhanced diffusion reported as increased diffusion coefficient has been noted. A careful examination of viscosity changes possible affecting diffusions seems to be warranted, this conceivable explanation has been barely addressed.

The limited solubility of various vanadium salts in the employed electrolyte solutions currently restricts the energy density of VRFBs. This situation is further aggravated by temperature-depending precipitation of constituents. Attempts to enhance solubility by using mixed chloride-containing electrolyte solutions have been reported [490], further options have been discussed above. Additives to stabilize highly concentrated electrolyte solutions and suppress thermally stimulated precipitation have been studied [491–502].

The contact resistance between porous electrodes like graphite felt and the bipolar plate acting as a current collector and mechanical support is mostly overlooked. Lim and Lee have prepared a suitably structured and composed material to be used as bipolar plate addressing this problem [503]. A significant improvement was observed. Another option using an adhesive conducting layer between the graphite felt and the bipolar plate was reported by Qian et al. [504]. Improved cell performance in terms of energy efficiency from 73% for a conventional setup to 81% for this design was observed.

4.4. Catalysis and Surface Enlargement Effects—Concluding Remarks

In most reported studies no attempt has been made to clearly assign observed effects to real catalysis, i.e., an increase of the exchange current density j_0 , or simply to an increase of EASA. Sometimes a change of j_0 by several orders of magnitude when for example going from a flat graphite disc to graphite felt is stated without even mentioning that most likely this is due simply to the enlarged (three-dimensional) surface area of the electrode [505]. Given the large number of methods available for the determination of electrochemically active surface areas [107] this appears to be a minor problem. Beyond the fact that many authors do not even mention this problem and are thus completely unaware of it, the data available from these methods have always been subject of heated debate. At first glance double layer capacity C_{DL} values are the answer. An increase of j_0 or decrease of η_{ct} at a constant value

of C_{DL} would certainly imply true catalysis. In practice this situation is rather unlikely. Any change in surface property—and without such change catalysis is hardly conceivable—may inadvertently result in a change of C_{DL} . Because of lack of data speculation about such cases is inappropriate here. A change of C_{DL} in turn does not necessarily imply a simple surface enlargement effect because C_{DL} yields information on an atomic or at least nanometer scale—well within the thickness of the diffusion layer. Thus changes in EASA do not necessarily exclude catalytic effects. Changes of EASA with typical surface features in the range of the diffusion layer thickness do not have a measurable effect on values of j_0 in kinetic studies with controlled flow (e.g., turbulent pipe or channel flow [506,507]).

In light of these arguments effects caused by sandblasting and ion etching may be discussed. Sandblasting will result certainly in surface roughening and presumably in an enlarged EASA. Further chemical changes, formation of catalytically more active functional groups and of defects is conceivable with ion etching. Not even an attempt is made unfortunately to address this question in this study.

5. Conclusions

The number of materials showing superior catalytic activity for the electrode reactions in a VRFB is overwhelming, the choice of procedures ranging from simple one-pot ones to highly elaborate ones is impressive. For practical use stability and economic aspects are presumably as important as the previous aspects. Thus the absence of stability data in most reports is deplorable; the growing number of studies at least also addressing stability and deterioration aspects is a welcome sign. The term stability applies to all performance-relevant parameters. Providing only stability data on energy efficiency for a system showing rapid loss of storage capability (e.g., in terms of energy density) is a rather useless information. Experimental conditions, in particular current density preferably with respect to the geometric surface area of the used electrodes, should be specified completely. Setting standard current densities preferably applied, would be a major progress. Certainly sophisticated procedures are interesting, even fascinating. Sometimes simplification with respect to a more economic realization may provide a route to reality. Otherwise these studies may stay in the realm of basic research. Careful examination of stability aspects in particular for catalysts showing promising short-term performance and reasonable economic data will be welcome. They will also be needed to enable wider use of VRFBs as an important contributor in a changing energy landscape.

Author Contributions: All authors contributed equally.

Funding: This work received no external funding

Acknowledgments: Alexander von Humboldt-Stiftung, Deutscher Akademischer Austauschdienst, Fonds der Chemischen Industrie, Deutsche Forschungsgemeinschaft, National Materials Genome Project (2016YFB0700600), National Natural Science Foundation Committee of China (Distinguished Youth Scientists Project of 51425301, U1601214, 51502137, and 51573013) supported this report in various ways. The hospitality of X. Xie and L. Liu at the Institute of Metal Research, Shenyang, provided a conducive environment for preparing this report. It was finished within a research project at St. Petersburg State University supported by grant No 26455158. Help in preparation of the manuscript by J. Roscher is gratefully appreciated.

Conflicts of Interest: The authors declare no conflict of interest.

References and Notes

1. Kangro, W. Verfahren zur Speicherung von Elektrischer Energie. German Patent DE914264C, 28 June 1954.
2. Kangro, W.; Pieper, H. Zur Frage der Speicherung von Elektrischer Energie in Flüssigkeiten. *Electrochim. Acta* **1962**, *7*, 435–448. [[CrossRef](#)]
3. Thaller, L.H. Electrically rechargeable redox flow cells. In Proceedings of the 9th Intersociety Energy Conversion Engineering Conference, San Francisco, CA, USA, 26–30 August 1974; pp. 924–928.
4. Hagedorn, N.H.; Thaller, L.H. Redox storage systems for solar applications. *Power Sources* **1981**, *8*, 227–243.
5. Skyllas-Kazacos, M.; Robins, R. All-Vanadium Redox Battery. U.S. Patent 4,786,567, 11 February 1986.
6. Bartolozzi, M. Development of redox flow batteries. A historical bibliography. *J. Power Sources* **1989**, *27*, 219–234. [[CrossRef](#)]

7. Giner, J.; Jalan, V.; Swette, L. Redox Storage Batteries. In *DECHEMA-Monographie*; Vielstich, W., Ed.; Verlag Chemie: Weinheim, Germany, 1982; Volume 92, pp. 381–393.
8. Skyllas-Kazacos, M.; Chakrabarti, M.H.; Hajimolana, S.A.; Mjalli, F.S.; Saleem, M. Progress in Flow Battery Research and Development. *J. Electrochem. Soc.* **2011**, *158*, R55–R79. [[CrossRef](#)]
9. Tomazic, G.; Skyllas-Kazacos, M. Redox Flow Batteries. In *Electrochemical Energy Storage for Renewable Sources and Grid Balancing*; Moseley, P.T., Garche, J., Eds.; Elsevier: Amsterdam, The Netherlands, 2015; pp. 309–336.
10. Kear, G.; Shah, A.A.; Walsh, F.C. Development of the all-vanadium redox flow battery for energy storage: A review of technological, financial and policy aspects. *Int. J. Energy Res.* **2012**, *36*, 1105–1120. [[CrossRef](#)]
11. Guarneri, M.; Mattavelli, P.; Petrone, G.; Spagnuolo, G. Vanadium Redox Flow Batteries. *IEEE Ind. Electron. Mag.* **2016**, *10*, 20–31. [[CrossRef](#)]
12. Ravikumar, M.K.; Rathod, S.; Jaiswal, N.; Patil, S.; Shukla, A. The renaissance in redox flow batteries. *J. Solid State Electrochem.* **2017**, *21*, 2467–2488. [[CrossRef](#)]
13. Weber, A.Z.; Mench, M.M.; Meyers, J.P.; Ross, P.N.; Gostick, J.T.; Liu, Q. Redox flow batteries: A review. *J. Appl. Electrochem.* **2011**, *41*, 1137–1164. [[CrossRef](#)]
14. Shigematsu, T. Redox flow battery for energy storage. *SEI Tech. Rev.* **2011**, *73*, 5–13.
15. Skyllas-Kazacos, M.; Kazacos, G.; Poon, G.; Verseema, H. Recent advances with UNSW vanadium-based redox flow batteries. *Int. J. Energy Res.* **2010**, *34*, 182–189. [[CrossRef](#)]
16. Fabjan, C.; Garche, J.; Harrer, B.; Jörissen, L.; Kolbeck, C.; Philipp, F.; Tomazic, G.; Wagner, F. The vanadium redox-battery: An efficient storage unit for photovoltaic systems. *Electrochim. Acta* **2007**, *47*, 825–831. [[CrossRef](#)]
17. Alotto, P.; Guarneri, M.; Moro, F. Redox flow batteries for the storage of renewable energy: A review. *Renew. Sustain. Energy Rev.* **2014**, *29*, 325–335. [[CrossRef](#)]
18. Cunha, A.; Martins, J.; Rodrigues, N.; Brito, F.P. Vanadium redox flow batteries: A technology review. *Int. J. Energy Res.* **2015**, *39*, 889–918. [[CrossRef](#)]
19. Liu, J.; Hu, J.; Deng, Q.; Mo, J.; Xie, H.; Liu, Z.; Xiong, Y.; Wu, X.; Wu, Y. Aqueous Rechargeable Batteries for Large-scale Energy Storage. *Israel J. Chem.* **2015**, *55*, 521–536. [[CrossRef](#)]
20. Walsh, F.C.; Ponce de Leon, C.; Berlouis, L.; Nikiforidis, G.; Arenas-Martinez, L.F.; Hodgson, D.; Hall, D. The Development of Zn-Ce Hybrid Redox Flow Batteries for Energy Storage and Their Continuing Challenges. *ChemPlusChem* **2015**, *80*, 288–311. [[CrossRef](#)]
21. Wu, X.; Liu, J.; Xiang, X.; Zhang, J.; Hu, J.; Wu, Y. Electrolytes for vanadium redox flow batteries. *Pure Appl. Chem.* **2014**, *86*, 661–669. [[CrossRef](#)]
22. Soloveichik, G.L. Flow Batteries: Current Status and Trends. *Chem. Rev.* **2015**, *115*, 11533–11558. [[CrossRef](#)] [[PubMed](#)]
23. Leung, P.; Li, X.; Ponce De León, C.; Berlouis, L.; Low, C.T.J.; Walsh, F.C. Progress in redox flow batteries, remaining challenges and their applications in energy storage. *RSC Adv.* **2012**, *2*, 10125–10156. [[CrossRef](#)]
24. Skyllas-Kazacos, M.; Cao, L.; Kazacos, M.; Kausar, N.; Mousa, A. Vanadium Electrolyte Studies for the Vanadium Redox Battery A Review. *ChemSusChem* **2016**, *9*, 1521–1543. [[CrossRef](#)] [[PubMed](#)]
25. Ding, C.; Zhang, H.; Li, X.; Liu, T.; Xing, F. Vanadium Flow Battery for Energy Storage: Prospects and Challenges. *J. Phys. Chem. Lett.* **2013**, *4*, 1281–1294. [[CrossRef](#)] [[PubMed](#)]
26. Liu, J.; Zhang, J.-G.; Yang, Z.; Lemmon, J.P.; Imhoff, C.; Graff, G.L.; Li, L.; Hu, J.; Wang, C.; Xiao, J.; et al. Materials Science and Materials Chemistry for Large Scale Electrochemical Energy Storage: From Transportation to Electrical Grid. *Adv. Funct. Mater.* **2013**, *23*, 929–946. [[CrossRef](#)]
27. Parasuraman, A.; Mariana Lim, T.; Menictas, C.; Skyllas-Kazacos, M. Review of material research and development for vanadium redox flow battery applications. *Electrochim. Acta* **2013**, *101*, 27–40. [[CrossRef](#)]
28. Chakrabarti, M.H.; Hajimolana, S.A.; Mjalli, F.S.; Saleem, M.; Mustafa, I. Redox Flow Battery for Energy Storage. *Arab. J. Sci. Eng.* **2013**, *38*, 723–739. [[CrossRef](#)]
29. Kim, K.J.; Park, M.-S.; Kim, Y.-J.; Kim, J.H.; Dou, S.X.; Skyllas-Kazacos, M. A technology review of electrodes and reaction mechanisms in vanadium redox flow batteries. *J. Mater. Chem.* **2015**, *A3*, 16913–16933. [[CrossRef](#)]
30. Ulaganathan, M.; Aravindan, V.; Yan, Q.; Madhavi, S.; Skyllas-Kazacos, M.; Mariana Lim, T. Recent Advancements in All-Vanadium Redox Flow Batteries. *Adv. Mater. Interfaces* **2016**, *3*, 1500309. [[CrossRef](#)]
31. Wei, G.-J.; Fan, X.-Z.; Liu, J.-G.; Yan, C.-W. A review of the electrochemical activity of carbon materials in vanadium redox flow batteries. *Xinxing Tan Cailao/New Carbon Mater.* **2014**, *29*, 272–279; reprinted in *Carbon* **2015**, *81*, 850. [[CrossRef](#)]

32. Zhang, H. Liquid Redox Rechargeable Batteries. In *Electrochemical Technologies for Energy Storage and Conversion*; Liu, R.S., Zhang, L., Sun, X., Liu, H., Zhang, J., Eds.; WILEY-VCH: Weinheim, Germany, 2012; pp. 279–316.
33. Park, M.; Ryu, J.; Wang, W.; Cho, J. Material design and engineering of next-generation flow-battery technologies. *Nat. Rev. Mater.* **2017**, *2*, 16080. [[CrossRef](#)]
34. Zeng, Y.K.; Zhao, T.S.; An, L.; Zhou, X.L.; Wei, L. A comparative study of all-vanadium and iron-chromium redox flow batteries for large-scale energy storage. *J. Power Sources* **2015**, *300*, 438–443. [[CrossRef](#)]
35. Wu, X.; Hu, J.; Liu, J.; Zhou, Q.; Zhou, W.; Li, H.; Wu, Y. Ion exchange membranes for vanadium redox flow batteries. *Pure Appl. Chem.* **2014**, *86*, 633–649. [[CrossRef](#)]
36. Maurya, S.; Shin, S.-H.; Kim, Y.; Moon, S.-H. A review on recent developments of anion exchange membranes for fuel cells and redox flow batteries. *RSC Adv.* **2015**, *5*, 37206–37230. [[CrossRef](#)]
37. Li, X.F.; Zhang, H.M.; Mai, Z.S.; Zhang, H.Z.; Vankelecom, I. Ion exchange membranes for vanadium redox flow battery (VRB) applications. *Energy Environ. Sci.* **2011**, *4*, 1147–1160. [[CrossRef](#)]
38. Wei, X.; Li, B.; Wang, W. Porous Polymeric Composite Separators for Redox Flow Batteries. *Polym. Rev.* **2015**, *55*, 247–272. [[CrossRef](#)]
39. Prifti, H.; Parasuraman, A.; Winardi, S.; Lim, T.M.; Skyllas-Kazacos, M. Membranes for redox flow battery applications. *Membranes* **2012**, *2*, 275–306. [[CrossRef](#)] [[PubMed](#)]
40. Schwenzer, B.; Zhang, J.; Kim, S.; Li, L.; Liu, J.; Yang, Z. Membrane development for vanadium redox flow batteries. *ChemSusChem* **2011**, *4*, 1388–1406. [[CrossRef](#)] [[PubMed](#)]
41. Wei, X.; Pan, W.; Duan, W.; Hollas, A.; Yang, Z.; Li, B.; Nie, Z.; Liu, J.; Reed, D.; Wang, W.; et al. Materials and Systems for Organic Redox Flow Batteries: Status and Challenges. *ACS Energy Lett.* **2017**, *2*, 2187–2204. [[CrossRef](#)]
42. Rosenberg, D.; Pansegrouw, S.; Wachholz, M.; Rehling, A.; Busker, M.; Jansen, W. Redox Flow Batteries—Organic Batteries with Future Prospects. *CHEMKON* **2017**, *24*, 325–340. [[CrossRef](#)]
43. Leung, P.; Shah, A.A.; Sanz, L.; Flox, C.; Morante, J.R.; Xu, Q.; Mohamed, M.R.; Ponce de Leon, C.; Walsh, F.C. Recent developments in organic redox flow batteries: A critical review. *J. Power Sources* **2017**, *360*, 243–283. [[CrossRef](#)]
44. Chakrabarti, M.H.; Dryfe, R.A.W.; Roberts, E.P.L. Evaluation of electrolytes for redox flow battery applications. *Electrochim. Acta* **2007**, *52*, 2189–2195. [[CrossRef](#)]
45. Chu, S.; Cui, Y.; Liu, N. The path towards sustainable energy. *Nat. Mater.* **2017**, *16*, 16–22. [[CrossRef](#)] [[PubMed](#)]
46. Ould Amrouche, S.; Rekioua, D.; Rekioua, T.; Bacha, S. Overview of energy storage in renewable energy systems. *Int. J. Hydrogen Energy* **2016**, *41*, 20914–20927. [[CrossRef](#)]
47. Minke, C.; Turek, T. Materials, system designs and modelling approaches in techno-economic assessment of all-vanadium redox flow batteries—A review. *J. Power Sources* **2018**, *376*, 66–81. [[CrossRef](#)]
48. Arbabzadeh, M.; Johnson, J.X.; Kleine, R.De; Keoleian, G.A. Vanadium redox flow batteries to reach greenhouse gas emissions targets in an off-grid configuration. *Appl. Energy* **2015**, *146*, 397–408. [[CrossRef](#)]
49. Zhao, P.; Zhang, H.; Zhou, H.; Chen, J.; Gao, S.; Yi, B. Characteristics and performance of 10 kW class all-vanadium redox-flow battery stack. *J. Power Sources* **2006**, *162*, 1416–1420. [[CrossRef](#)]
50. Chen, J.; Xu, Z.; Li, B. Research on the characteristics of the vanadium redox-flow battery in power systems applications. *J. Power Sources* **2013**, *241*, 396–399.
51. Arbabzadeh, M.; Johnson, J.X.; Keoleian, G.A.; Rasmussen, P.G.; Thompson, L.T. Twelve Principles for Green Energy Storage in Grid Applications. *Environ. Sci. Technol.* **2016**, *50*, 1046–1055. [[CrossRef](#)] [[PubMed](#)]
52. Lopez-Vizcaino, R.; Mena, E.; Millan, M.; Rodrigo, M.A.; Lobato, J. Performance of a vanadium redox flow battery for the storage of electricity produced in photovoltaic solar panels. *Renew. Energy* **2017**, *114*, 1123–1133. [[CrossRef](#)]
53. Zhou, Z.; Benbouzid, M.E.H.; Charpentier, J.F.; Scuiller, F. Hybrid Diesel/MCT/Battery Electricity Power Supply System for Power Management in Small Islanded Sites: Case Study for the Ouessant French Island. In *Smart Energy Grid Design for Island Countries: Challenges and Opportunities*; Rabiul Islam, F.M., Al Mamun, K., Oo Amanullah, M.T., Eds.; Springer: New York, NY, USA, 2017; pp. 415–445.
54. Lawder, M.T.; Suthar, B.; Northrop, P.W.C.; De, S.; Hoff, C.M.; Leitermann, O.; Crow, M.L.; Santhanagopalan, S.; Subramanian, V.R. Battery Energy Storage System (BESS) and Battery Management System (BMS) for Grid-Scale Applications. *Proc. IEEE* **2014**, *102*, 1014–1030. [[CrossRef](#)]

55. Alotto, P.; Guarnieri, M.; Moro, F.; Stella, A. Large scale energy storage with redox flow batteries. *COMPEL* **2013**, *32*, 1459–1470. [[CrossRef](#)]
56. Zhou, Z.; Scuiller, F.; Charpentier, J.F.; Benbouzid, M.; Tang, T. Application of Flow Battery in Marine Current Turbine System for Daily Power Management. In Proceedings of the 2014 International Conference on Green Energy, Sfax, Tunisia, 25–27 March 2014; pp. 8–13.
57. Baumann, M.; Peters, J.F.; Weil, M.; Grunwald, A. CO₂ Footprint and Life-Cycle Costs of Electrochemical Energy Storage for Stationary Grid Applications. *Energy Technol.* **2017**, *5*, 1071–1083. [[CrossRef](#)]
58. Lei, J.; Gong, Q. Operating strategy and optimal allocation of large-scale VRB energy storage system in active distribution networks for solar/wind power applications. *IET Gener. Transm. Distrib.* **2017**, *11*, 2403–2411. [[CrossRef](#)]
59. Ontiveros, L.J.; Suvire, G.O.; Mercado, P.E. Power conditioning system coupled with a flow battery for wind energy applications: Modelling and control design. *IET Renew. Power Gener.* **2017**, *11*, 987–995. [[CrossRef](#)]
60. Shibata, A.; Sato, K. Development of vanadium redox flow battery for electricity storage. *Power Eng. J.* **1999**, *13*, 130–135. [[CrossRef](#)]
61. Vanýsek, P.; Novák, V. Redox flow batteries as the means for energy storage. *J. Energy Storage* **2017**, *13*, 435–441. [[CrossRef](#)]
62. Soloveichik, G.L. Battery Technologies for Large-Scale Stationary Energy Storage. *Annu. Rev. Chem. Biomol. Eng.* **2011**, *2*, 503–527. [[CrossRef](#)] [[PubMed](#)]
63. Li, M.-J.; Zhao, W.; Chen, X.; Tao, W.-Q. Economic analysis of a new class of vanadium redox-flow battery for medium- and large-scale energy storage in commercial applications with renewable energy. *Appl. Therm. Energy* **2017**, *114*, 802–814. [[CrossRef](#)]
64. Holze, R. *Beiträge der Elektrochemie zu einer sich wandelnden Energielandschaft*; Sitzungsberichte der Sächsischen Akademie der Wissenschaften zu Leipzig Mathematisch-Naturwissenschaftliche Klasse; S. Hirzel: Stuttgart/Leipzig, Germany, 2018; Volume 133.
65. Vanysek, P.; Novak, V. Availability of Suitable Raw Materials Determining the Prospect for Energy Storage Systems Based on Redox Flow Batteries. *Acta Montan. Slov.* **2018**, *23*, 90–99.
66. Wu, X.; Yuan, X.; Wang, Z.; Liu, J.; Hu, Y.; Deng, Q.; Yin, X.; Zhou, Q.; Zhou, W.; Wu, Y. Electrochemical performance of 5 kW all-vanadium redox flow battery stack with a flow frame of multi-distribution channels. *J. Solid State Electrochem.* **2017**, *21*, 429–435. [[CrossRef](#)]
67. Mena, E.; Lopez-Vizcaino, R.; Millan, M.; Canizares, P.; Lobato, J.; Rodrigo, M.A. Vanadium redox flow batteries for the storage of electricity produced in wind turbines. *Int. J. Energy Res.* **2018**, *42*, 720–730. [[CrossRef](#)]
68. Aaron, D.S.; Liu, Q.; Tang, Z.; Grim, G.M.; Papandrew, A.B.; Turhan, A.; Zawodzinski, T.A.; Mench, M.M. Dramatic performance gains in vanadium redox flow batteries through modified cell architecture. *J. Power Sources* **2012**, *206*, 450–453. [[CrossRef](#)]
69. Goulet, M.-A.; Habisch, A.; Kjeang, E. In Situ Enhancement of Flow-through Porous Electrodes with Carbon Nanotubes via Flowing Deposition. *Electrochim. Acta* **2016**, *206*, 36–44. [[CrossRef](#)]
70. Zhang, Y.; Zhao, J.; Wang, P.; Skyllas-Kazacos, M.; Xiong, B.; Badrinarayanan, R. A comprehensive equivalent circuit model of all-vanadium redox flow battery for power system analysis. *J. Power Sources* **2015**, *290*, 14–24. [[CrossRef](#)]
71. Houser, J.; Clement, J.; Pezeshki, A.; Mench, M.M. Influence of architecture and material properties on vanadium redox flow battery performance. *J. Power Sources* **2016**, *302*, 369–377. [[CrossRef](#)]
72. Luo, S.-W.; Lee, S.; Fuh, Y.-K. Micro-pillars enhanced all vanadium redox flow batteries and the effect of assembly torque on the electrochemical performance. *Microsyst. Technol.* **2017**, *23*, 2065–2074. [[CrossRef](#)]
73. Gencen, M.; Gursu, H.; Sahin, Y. Effect of alpha- and gamma-alumina on the precipitation of positive electrolyte in vanadium redox battery. *Int. J. Hydrogen Energy* **2017**, *42*, 25598–25607. [[CrossRef](#)]
74. Gencen, M.; Gursu, H.; Sahin, Y. Anti-precipitation effects of TiO₂ and TiOSO₄ on positive electrolyte of vanadium redox battery. *Int. J. Hydrogen Energy* **2017**, *42*, 25608–25618. [[CrossRef](#)]
75. Wang, G.; Ciobotaru, M.; Agelidis, V.G. Power Management for Improved Dispatch of Utility-Scale PV Plants. *IEEE Trans. Power Syst.* **2016**, *31*, 2297–2306. [[CrossRef](#)]
76. Viswanathan, V.; Crawford, A.; Stephenson, D.; Kim, S.; Wang, W.; Li, B.; Coffey, G.; Thomsen, E.; Graff, G.; Balducci, P.; et al. Cost and performance model for redox flow batteries. *J. Power Sources* **2014**, *247*, 1040–1051. [[CrossRef](#)]

77. Zhou, X.L.; Zhao, T.S.; An, L.; Zeng, Y.K.; Wie, L. Critical transport issues for improving the performance of aqueous redox flow batteries. *J. Power Sources* **2017**, *339*, 1–12. [[CrossRef](#)]
78. Monteiro, R.; Lerès, J.; Boaventura, M.; Mendes, A. Insights into all-vanadium redox flow battery: A case study on components and operational conditions. *Electrochim. Acta* **2018**, *267*, 80–93. [[CrossRef](#)]
79. Pan, J.; Huang, M.; Li, X.; Wang, S.; Li, W.; Ma, T.; Xie, X.; Ramani, V. The performance of all vanadium redox flow batteries at below-ambient temperatures. *Energy* **2016**, *107*, 784–790. [[CrossRef](#)]
80. Zheng, Q.; Li, X.; Cheng, Y.; Ning, G.; Xing, F.; Zhang, H. Development and perspective in vanadium flow battery modeling. *Appl. Energy* **2014**, *132*, 254–266. [[CrossRef](#)]
81. Qiu, G.; Joshi, A.S.; Dennison, C.R.; Knehr, K.W.; Kumbur, E.C.; Sun, Y. 3-D pore-scale resolved model for coupled species/charge/fluid transport in a vanadium redox flow battery. *Electrochim. Acta* **2012**, *64*, 46–64. [[CrossRef](#)]
82. Rychcik, M.; Skyllas-Kazacos, M. Characteristics of a new All-Vanadium Redox Flow Battery. *J. Power Sources* **1988**, *22*, 59–67. [[CrossRef](#)]
83. Crawford, A.; Viswanathan, V.; Stephenson, D.; Wang, W.; Thomsen, E.; Reed, D.; Li, B.; Balducci, P.; Kintner-Meyer, M.; Sprenkle, V. Comparative analysis for various redox flow batteries chemistries using a cost performance model. *J. Power Sources* **2015**, *293*, 388–399. [[CrossRef](#)]
84. Fares, R.L.; Webber, M.E. What are the tradeoffs between battery energy storage cycle life and calendar life in the energy arbitrage application? *J. Energy Storage* **2018**, *16*, 37–45. [[CrossRef](#)]
85. Hiksas, M.M.; Aninditio, M.L. Redox Flow Batteries for Small Scale Energy Storage. In Proceedings of the 2016 IEEE Conference on Technologies for Sustainability (SUSTECH), Phoenix, AZ, USA, 9–11 October 2016.
86. Hosseina, M.; Bathaee, S.M.T. Optimal scheduling for distribution network with redox flow battery storage. *Energy Convers. Manag.* **2016**, *121*, 145–151. [[CrossRef](#)]
87. He, G.; Chen, Q.; Kang, C.; Xia, Q. Optimal operating strategy and revenue estimates for the arbitrage of a vanadium redox flow battery considering dynamic efficiencies and capacity loss. *IET Gener. Transm. Distrib.* **2016**, *10*, 1278–1285. [[CrossRef](#)]
88. Yamamura, T.; Wu, X.W.; Ohta, S.; Shirasaki, K.; Sakuraba, H.; Satoh, I.; Shikama, T. Vanadium solid-salt battery: Solid state with two redox couples. *J. Power Sources* **2011**, *196*, 4003–4011. [[CrossRef](#)]
89. Wang, Z.; Hu, J.; Wu, X.; Ye, H.; Zhou, W.; Wu, Y.; Holze, R. Amembrane based on sulfonated polystyrene for a vanadium solid-salt battery. *J. Solid State Electrochem.* **2016**, *20*, 943–948. [[CrossRef](#)]
90. Shinkle, A.A.; Sleightholme, A.E.S.; Thompson, L.T.; Monroe, C.W. Electrode kinetics in non-aqueous vanadium acetylacetone redox flow batteries. *J. Appl. Electrochem.* **2011**, *41*, 1191–1199. [[CrossRef](#)]
91. Lee, K.; Lee, J.; Kwon, K.W.; Park, M.-S.; Hwang, J.-H.; Kim, K.J. 3D Graphene-Ni Foam as an Advanced Electrode for High-Performance Nonaqueous Redox Flow Batteries. *ACS Appl. Mater. Interfaces* **2017**, *9*, 22502–22508. [[CrossRef](#)] [[PubMed](#)]
92. Mustafa, I.; Bamgbopa, M.O.; Alraeesi, E.; Shao-Horn, Y.; Sun, H.; Almheiri, S. Insights on the Electrochemical Activity of Porous Carbonaceous Electrodes in Non-Aqueous Vanadium Redox Flow Batteries. *J. Electrochem. Soc.* **2017**, *164*, A3673–A3683. [[CrossRef](#)]
93. Lee, J.; Park, M.-S.; Kim, K.J. Highly enhanced electrochemical activity of Ni foam electrodes decorated with nitrogen-doped carbon nanotubes for non-aqueous redox flow batteries. *J. Power Sources* **2017**, *341*, 212–218. [[CrossRef](#)]
94. Sun, C.-N.; Delnick, F.M.; Aaron, D.S.; Papandrew, A.B.; Mench, M.M.; Zawodzinski, T.A. Probing Electrode Losses in All-Vanadium Redox Flow Batteries with Impedance Spectroscopy. *ECS Electrochem. Lett.* **2013**, *2*, A43–A45. [[CrossRef](#)]
95. Sun, C.-N.; Delnick, F.M.; Aaron, D.S.; Papandrew, A.B.; Mench, M.M.; Zawodzinski, T.A., Jr. Resolving Losses at the Negative Electrode in All-Vanadium Redox Flow Batteries Using Electrochemical Impedance Spectroscopy. *J. Electrochem. Soc.* **2014**, *161*, A981–A988. [[CrossRef](#)]
96. Holze, R. *Landolt-Börnstein: Numerical Data and Functional Relationships in Science and Technology, New Series, Group IV: Physical Chemistry, Volume 9: Electrochemistry, Subvolume A: Electrochemical Thermodynamics and Kinetics*; Martienssen, W., Lechner, M.D., Eds.; Springer: Berlin, Germany, 2007.
97. The acronym ASA for active surface area seems to apply only on surface area determined by dioxygen chemisorption [117], it should not be confused with EASA.
98. Trasatti, S.; Petrii, O.A. Real Surface-Area Measurements in Electrochemistry. *J. Electroanal. Chem.* **1992**, *327*, 353–376. [[CrossRef](#)]

99. Trasatti, S.; Petrii, O.E. Real surface area measurements in electrochemistry. *Pure Appl. Chem.* **1991**, *63*, 711–734. [[CrossRef](#)]
100. Watt-Smith, M.J.; Friedrich, J.M.; Rigby, S.P.; Ralph, T.R.; Walsh, F.C. Determination of the electrochemically active surface area of Pt/C PEM fuel cell electrodes using different adsorbates. *J. Phys. D Appl. Phys.* **2008**, *41*, 74004. [[CrossRef](#)]
101. Binninger, T.; Fabbri, E.; Koetz, R.; Schmidt, T.J. Determination of the Electrochemically Active Surface Area of Metal-Oxide Supported Platinum Catalyst. *J. Electrochem. Soc.* **2014**, *161*, H121–H128. [[CrossRef](#)]
102. Ganassin, A.; Maljusch, A.; Colic, V.; Spanier, L.; Brandl, K.; Schuhmann, W.; Bandarenka, A. Benchmarking the Performance of Thin-Film Oxide Electrocatalysts for Gas Evolution Reactions at High Current Densities. *ACS Catal.* **2016**, *6*, 3017–3024. [[CrossRef](#)]
103. Maksimov, Y.M.; Podlovchenko, B.I. Use of silver adatoms for the determination of the electrochemically active surface area of polycrystalline gold. *Mendeleev Commun.* **2017**, *27*, 64–66. [[CrossRef](#)]
104. Watzele, S.; Bandarenka, A.S. Quick Determination of Electroactive Surface Area of Some Oxide Electrode Materials. *Electroanalysis* **2016**, *28*, 2394–2399. [[CrossRef](#)]
105. Wiberg, G.K.H.; Mayrhofer, K.J.J.; Arenz, M. Investigation of the Oxygen Reduction Activity on Silver—A Rotating Disc Electrode Study. *Fuel Cells* **2010**, *10*, 575–581. [[CrossRef](#)]
106. Xie, X.; Holze, R. Electrode kinetic data: Geometric vs. real surface area. 2018; in progress.
107. Ahn, J.; Holze, R. Bifunctional Electrodes for an Integrated Water-Electrolysis and Hydrogen-Oxygen Fuel Cell with a Solid Polymer Electrolyte. *J. Appl. Electrochem.* **1992**, *22*, 1167–1174. [[CrossRef](#)]
108. Friedl, J.; Stimming, U. Determining Electron Transfer Kinetics at Porous Electrodes. *Electrochim. Acta* **2017**, *227*, 235–245. [[CrossRef](#)]
109. Friedl, J.; Bauer, C.M.; Rinaldi, A.; Stimming, U. Electron transfer kinetics of the $\text{VO}^{2+}/\text{VO}_2^+$ Reaction on multi-walled carbon nanotubes. *Carbon* **2013**, *63*, 228–239. [[CrossRef](#)]
110. Thommes, M.; Kaneko, K.; Neimark, A.V.; Olivier, J.P.; Rodriguez-Reinoso, F.; Rouquerol, J.; Sing, K.S.W. Physisorption of gases, with special reference to the evaluation of surface area and pore size distribution. *Pure Appl. Chem.* **2015**, *87*, 1051–1069. [[CrossRef](#)]
111. Jagiello, J.; Ania, C.; Parra, J.B.; Cook, C. Dual gas analysis of microporous carbons using 2D-NL heterogeneous surface model and combined adsorption data of N_2 and CO_2 . *Carbon* **2015**, *91*, 330–337. [[CrossRef](#)]
112. Jagiello, J.; Ania, C.O.; Parra, J.B.; Jagiello, L.; Pis, J.J. Using DFT analysis of adsorption data of multiple gases including H_2 for the comprehensive characterization of microporous carbons. *Carbon* **2007**, *45*, 1066–1071. [[CrossRef](#)]
113. Holze, R.; Vielstich, W. Double-Layer Capacity Measurements as a Method to Characterize Porous Fuel Cell Electrodes. *Electrochim. Acta* **1984**, *29*, 607–610. [[CrossRef](#)]
114. Kneten Cline, K.; McDermott, M.T.; McCreery, R.L. Anomalously Slow-Electron Transfer at Ordered Graphite-Electrodes—Influence of Electronic Factors and Reactive Sites. *J. Phys. Chem.* **1994**, *98*, 5314–5319. [[CrossRef](#)]
115. McCreery, R.L.; Kneten Cline, K.; McDermott, C.A.; McDermott, M.T. Control of reactivity at carbon electrode surfaces. *Colloid. Surf.* **1994**, *A93*, 211–219. [[CrossRef](#)]
116. Wei, G.; Su, W.; Wei, Z.; Fan, X.; Liu, J.; Yan, C. Electrocatalytic effect of the edge planes sites at graphite electrode on the vanadium redox couples. *Electrochim. Acta* **2016**, *204*, 263–269. [[CrossRef](#)]
117. Rabbow, T.J.; Whitehead, A.H. Deconvolution of electrochemical double layer capacitance between fractions of active and total surface area of graphite felts. *Carbon* **2017**, *111*, 782–788. [[CrossRef](#)]
118. Pour, N.; Kwabi, D.G.; Carney, T.; Darling, R.M.; Perry, M.L.; Shao-Horn, Y. Influence of Edge- and Basal-Plane Sites on the Vanadium Redox Kinetics for Flow Batteries. *J. Phys. Chem.* **2015**, *C119*, 5311–5318. [[CrossRef](#)]
119. Jow, J.-J.; Hsieh, L.-Y.; Cho, H.-P.; Chen, H.-R.; Kuo, C.-W. Determination of surface area of carbon-black by simple cyclic-voltammetry measurements in aqueous H_2SO_4 . *J. Ind. Eng. Chem.* **2013**, *19*, 1730–1734. [[CrossRef](#)]
120. Lasia, A. *Electrochemical Impedance Spectroscopy and Its Applications*; Springer: New York, NY, USA, 2014.
121. Holze, R. Electrode impedance measurements: A versatile tool for electrochemists. *Bull. Electrochem.* **1994**, *10*, 56–67.
122. Barsoukov, E.; Macdonald, J.R. *Impedance Spectroscopy*; WILEY-Interscience: Hoboken, NJ, USA, 2005.

123. Fink, H.; Friedl, J.; Stimming, U. Composition of the Electrode Determines Which Half-Cell's Rate Constant is Higher in a Vanadium Flow Battery. *J. Phys. Chem.* **2016**, *C120*, 15893–15901. [[CrossRef](#)]
124. Pezeshki, A.M.; Sacci, R.L.; Delnick, F.M.; Aaron, D.S.; Mench, M.M. Elucidating effects of cell architecture, electrode material, and solution composition on overpotentials in redox flow batteries. *Electrochim. Acta* **2017**, *229*, 261–270. [[CrossRef](#)]
125. Darling, R.M.; Perry, M.L. Half-Cell Steady-State Flow-Battery Experiments. *ECS Trans.* **2013**, *53*, 31–38. [[CrossRef](#)]
126. Aaron, D.S.; Tang, Z.; Lawton, J.S.; Papandrew, A.B.; Zawodzinski, T.A., Jr. In-situ single electrode studies of an all-vanadium redox flow battery. *ECS Trans.* **2012**, *41*, 43–51.
127. Schweiss, R.; Meiser, C.; Goh, F.W.T. Steady-State Measurements of Vanadium Redox-Flow Batteries to Study Particular Influences of Carbon Felt Properties. *ChemElectroChem* **2017**, *4*, 1969–1974. [[CrossRef](#)]
128. Fu, L.; Qu, Q.; Holze, R.; Wu, Y. On the difference between cell and electrode impedances. *Electrochem. Energy Technol.* **2018**, submitted.
129. Park, J.H.; Park, J.J.; Park, O.O.; Jin, C.-S.; Yang, J.H. Highly accurate apparatus for electrochemical characterization of the felt electrodes used in redox flow batteries. *J. Power Sources* **2016**, *310*, 137–144. [[CrossRef](#)]
130. Diener, F.; Roscher, J.; Holze, R. A miniature flow cell for electrochemical studies of graphite electrodes. 2018; in progress.
131. Wang, Q.; Qu, Z.G.; Jiang, Z.Y.; Yang, W.W. Experimental study on the performance of a vanadium redox flow battery with non-uniformly compressed carbon felt electrode. *Appl. Energy* **2018**, *213*, 293–305. [[CrossRef](#)]
132. Park, S.-K.; Shim, J.; Yang, J.H.; Jin, C.-S.; Lee, B.S.; Lee, Y.-S.; Shin, K.-H.; Jeon, J.-D. The influence of compressed carbon felt electrodes on the performance of a vanadium redox flow battery. *Electrochim. Acta* **2014**, *116*, 447–452. [[CrossRef](#)]
133. Becker, M.; Bredemeyer, N.; Tenhumberg, N.; Turek, T. Polarization curve measurements combined with potential probe sensing for determining current density distribution in vanadium redox-flow batteries. *J. Power Sources* **2016**, *307*, 826–833. [[CrossRef](#)]
134. Goulet, M.-A.; Eikerling, M.; Kjeang, E. Direct measurement of electrochemical reaction kinetics in flow-through porous electrodes. *Electrochim. Commun.* **2015**, *57*, 14–17. [[CrossRef](#)]
135. Li, L.; Nikiforidis, G.; Leung, M.K.H.; Daoud, W.A. Vanadium microfluidic fuel cell with novel multi-layer flow-through porous electrodes: Model, simulations and experiments. *Appl. Energy* **2016**, *177*, 729–739. [[CrossRef](#)]
136. Lee, J.W.; Hong, J.K.; Kjeang, E. Electrochemical characteristics of vanadium redox reactions on porous carbon electrodes for microfluidic fuel cell applications. *Electrochim. Acta* **2012**, *83*, 430–438. [[CrossRef](#)]
137. Sato, Y.; Narita, A.; Kaneko, Y.; Negishi, A.; Nozaki, K.; Kato, T. Characterization of Carbon Materials for Redox Flow Battery Electrodes by Voltage-Step Coulometry. *ECS Trans.* **2017**, *75*, 37–47. [[CrossRef](#)]
138. Jing, M.; Qin, Y.; Shi, Q.; Liu, J.; Yan, C. A new insight into electrode processes of vanadium redox flow battery by thermo-electro-chemistry method. *J. Energy Storage* **2017**, *14*, 163–167. [[CrossRef](#)]
139. Ashraf Gandomi, Y.; Aaron, D.S.; Houser, J.R.; Daugherty, M.C.; Clement, J.T.; Pezeshki, A.M.; Ertugrul, T.Y.; Moseley, D.P.; Mench, M.M. Critical Review—Experimental Diagnostics and Material Characterization Techniques Used on Redox Flow Batteries. *J. Electrochem. Soc.* **2018**, *165*, A970–A1010. [[CrossRef](#)]
140. Tang, Z. Characterization Techniques and Electrolyte Separator Performance Investigation for All Vanadium Redox Flow Battery. Ph.D. Thesis, University of Tennessee, Knoxville, TN, USA, 2013.
141. Wu, L.; Wang, J.; Shen, Y.; Liu, L.; Xi, J. Electrochemical evaluation methods of vanadium flow battery electrodes. *Phys. Chem. Chem. Phys.* **2017**, *19*, 14708–14717. [[CrossRef](#)] [[PubMed](#)]
142. Becker, M.; Bredemeyer, N.; Tenhumberg, N.; Turek, T. Kinetic studies at carbon felt electrodes for vanadium redox-flow batteries under controlled transfer current density conditions. *Electrochim. Acta* **2017**, *252*, 12–24. [[CrossRef](#)]
143. Cheng, F.Y.; Liang, J.; Tao, Z.L.; Chen, J. Functional Materials for Rechargeable Batteries. *Adv. Mater.* **2011**, *23*, 1695–1715. [[CrossRef](#)] [[PubMed](#)]
144. Chakrabarti, M.H.; Brandon, N.P.; Hajimolana, S.A.; Tariq, E.; Yufit, V.; Hashim, M.A.; Hussain, M.A.; Low, C.T.J.; Aravind, P.V. Application of carbon materials in redox flow batteries. *J. Power Sources* **2014**, *253*, 150–166. [[CrossRef](#)]

145. Satola, B.; Komsyksa, L.; Wittstock, G. Corrosion of Graphite-Polypropylene Current Collectors during Overcharging in Negative and Positive Vanadium Redox Flow Battery Half-Cell Electrolytes. *J. Electrochem. Soc.* **2018**, *165*, A963–A969. [[CrossRef](#)]
146. Satola, B.; Komsyksa, L.; Wittstock, G. Bulk Aging of Graphite-Polypropylene Current Collectors Induced by Electrochemical Cycling in the Positive Electrolyte of Vanadium Redox Flow Batteries. *J. Electrochem. Soc.* **2017**, *164*, A2566–A2572. [[CrossRef](#)]
147. Satola, B.; Nunes Kirchner, C.; Komsyksa, L.; Wittstock, G. Chemical Stability of Graphite-Polypropylene Bipolar Plates for the Vanadium Redox Flow Battery at Resting State. *J. Electrochem. Soc.* **2016**, *163*, A2318–A2325. [[CrossRef](#)]
148. Mohammadi, F.; Timbrell, P.; Zhong, S.; Padeste, C.; Skyllas-Kazacos, M. Overcharge in the Vanadium Redox Battery and Changes in Electrical Resistivity and Surface Functionality of Graphite Felt Electrodes. *J. Power Sources* **1994**, *52*, 61–68. [[CrossRef](#)]
149. Haddadi-Asl, V.; Rabbani, M.S. Effect of electrochemical cell overcharge on electrical and electrochemical properties of polymer composite electrodes (II): Mechanism of electrode deterioration. *Iran. Polym. J.* **1998**, *7*, 185–194.
150. Lee, N.J.; Lee, S.-W.; Kim, K.J.; Kim, J.-H.; Park, M.-S.; Jeong, G.; Kim, Y.-J.; Byun, D. Development of Carbon Composite Bipolar Plates for Vanadium Redox Flow Batteries. *Bull. Korean Chem. Soc.* **2012**, *33*, 3589–3592. [[CrossRef](#)]
151. Kim, K.H.; Kim, B.G.; Lee, D.G. Development of carbon composite bipolar plate (BP) for vanadium redox flow battery (VRFB). *Compos. Struct.* **2014**, *109*, 253–259. [[CrossRef](#)]
152. Nam, S.; Lee, D.; Lee, D.G.; Kim, J. Nano carbon/fluoroelastomer composite bipolar plate for a vanadium redox flow battery (VRFB). *Compos. Struct.* **2017**, *159*, 220–227. [[CrossRef](#)]
153. Li, W.; Jing, S.; Wang, S.; Wang, C.; Xie, X. Experimental investigation of expanded graphite/phenolic resin composite bipolar plate. *Int. J. Hydrogen Energy* **2016**, *41*, 16240–16246. [[CrossRef](#)]
154. Choe, J.; Kim, K.H.; Lee, D.G. Corrugated carbon/epoxy composite bipolar plate for vanadium redox flow batteries. *Compos. Struct.* **2015**, *119*, 534–542. [[CrossRef](#)]
155. Park, M.; Jung, Y.-J.; Ryu, J.; Cho, J. Material selection and optimization for highly stable composite bipolar plates in vanadium redox flow batteries. *J. Mater. Chem.* **2014**, *2*, 15808–15815. [[CrossRef](#)]
156. Liu, H.; Xu, Q.; Yan, C. On-line mass spectrometry study of electrochemical corrosion of the graphite electrode for vanadium redox flow battery. *Electrochim. Commun.* **2013**, *28*, 58–62. [[CrossRef](#)]
157. Hagg, C.M.; Skyllas-Kazacos, M. Novel bipolar electrodes for battery applications. *J. Appl. Electrochem.* **2002**, *32*, 1063–1069. [[CrossRef](#)]
158. Caglar, B.; Fischer, P.; Kauranen, P.; Karttunen, M.; Eisner, P. Development of carbon nanotube and graphite filled polyphenylene sulfide based bipolar plates for all-vanadium redox flow batteries. *J. Power Sources* **2014**, *256*, 88–95. [[CrossRef](#)]
159. Derr, I.; Przyrembel, D.; Schweer, J.; Fetyan, A.; Langner, J.; Melke, J.; Weinelt, M.; Roth, C. Electroless chemical aging of carbon felt electrodes for the all-vanadium redox flow battery (VRFB) investigated by Electrochemical Impedance and X-ray Photoelectron Spectroscopy. *Electrochim. Acta* **2017**, *246*, 783–793. [[CrossRef](#)]
160. Derr, I.; Bruns, M.; Langner, J.; Fetyan, A.; Melke, J.; Roth, C. Degradation of all-vanadium redox flow batteries (VRFB) investigated by electrochemical impedance and X-ray photoelectron spectroscopy: Part 2 electrochemical degradation. *J. Power Sources* **2016**, *325*, 351–359. [[CrossRef](#)]
161. Derr, I.; Fetyan, A.; Schutjajew, K.; Roth, C. Electrochemical analysis of the performance loss in all vanadium flow batteries using different cut-off voltages. *Electrochim. Acta* **2017**, *224*, 9–16. [[CrossRef](#)]
162. Nibel, O.; Taylor, S.M.; Patru, A.; Fabbri, E.; Gubler, L.; Schmidt, T.J. Performance of Different Carbon Electrode Materials: Insights into Stability and Degradation under Real Vanadium Redox Flow Battery Operating Conditions. *J. Electrochem. Soc.* **2017**, *164*, A1608–A1615. [[CrossRef](#)]
163. Mayer, P.; Holze, R. Electrocatalysis of redox reactions by metal nanoparticles on graphite electrodes. *J. Solid State Electrochem.* **2001**, *5*, 402–411. [[CrossRef](#)]
164. Climent, M.A.; Garces, P.; Aldaz, A. Cyclic voltammetric study of $\text{Fe}^{3+}/\text{Fe}^{2+}$ electroodic reaction for use in a Fe/Cr battery. *Bull. Electrochem.* **1988**, *4*, 845–848.
165. Kaneko, H.; Nozaki, K.; Wada, Y.; Aoki, T.; Negishi, A.; Kamimoto, M. Vanadium Redox Reactions and Carbon Electrodes for Vanadium Redox Flow Battery. *Electrochim. Acta* **1991**, *36*, 1191–1196. [[CrossRef](#)]

166. Kim, H.S. Electrochemical Properties of Graphite-based Electrodes for Redox Flow Batteries. *Bull. Korean Chem. Soc.* **2011**, *32*, 571–575. [[CrossRef](#)]
167. Cnobloch, H.; Nischik, H.; Pantel, K.; Ledjeff, K.; Heinzel, A. Application of carbon as a construction material in redox-flow-storage-batteries. In Proceedings of the 4th International Carbon Conference (Carbon'86), Baden-Baden, Germany, 30 June–4 July 1986; pp. 367–369.
168. Holze, R. Underpotential deposit electrocatalysis of fast redox reactions for electrochemical energy storage systems. *J. Solid State Electrochem.* **1998**, *2*, 73–77. [[CrossRef](#)]
169. Yang, C.Y. Catalytic electrodes for the Redox Flow Cell energy storage device. *J. Appl. Electrochem.* **1982**, *12*, 425–434. [[CrossRef](#)]
170. Zhou, X.L.; Zhao, T.S.; Zeng, Y.K.; An, L.; Wie, L. A highly permeable and enhanced surface area carbon-cloth electrode for vanadium redox flow batteries. *J. Power Sources* **2016**, *329*, 247–254. [[CrossRef](#)]
171. Aaron, D.; Sun, C.-N.; Bright, M.; Papandrew, A.B.; Mench, M.M.; Zawodzinski, T.A. In Situ Kinetics Studies in All-Vanadium Redox Flow Batteries. *ECS Electrochem. Lett.* **2013**, *2*, A29–A31. [[CrossRef](#)]
172. Maruyama, J.; Shinagawa, T.; Hayashida, A.; Matsuo, Y.; Nishihara, H.; Kyotani, T. Vanadium-Ion Redox Reactions in a Three-Dimensional Network of Reduced Graphite Oxide. *ChemElectroChem* **2016**, *3*, 650–657. [[CrossRef](#)]
173. Park, S.; Kim, H. Fabrication of nitrogen-doped graphite felts as positive electrodes using polypyrrole as a coating agent in vanadium redox flow batteries. *J. Mater. Chem.* **2015**, *3*, 12276–12283. [[CrossRef](#)]
174. Kim, K.J.; Park, M.-S.; Kim, J.-H.; Hwang, U.; Lee, N.J.; Jeong, G.; Kim, Y.-J. Novel catalytic effects of Mn_3O_4 for all vanadium redox flow batteries. *Chem. Commun.* **2012**, *48*, 5455–5457. [[CrossRef](#)] [[PubMed](#)]
175. Moghim, M.H.; Eqra, R.; Babaiee, M.; Zarei-Jelyani, M.; Mohsen Loghavi, M. Role of reduced graphene oxide as nano-electrocatalyst in carbon felt electrode of vanadium redox flow battery. *J. Electroanal. Chem.* **2017**, *789*, 67–75. [[CrossRef](#)]
176. Sun, B.; Sykllas-Kazacos, M. Modification of Graphite Electrode Materials for Vanadium Redox Flow Battery Application—1. Thermal-Treatment. *Electrochim. Acta* **1992**, *37*, 1253–1260. [[CrossRef](#)]
177. Flox, C.; Rubio-Garcia, J.; Skoumal, M.; Andreu, T.; Ramon Morante, J. Thermo-chemical treatments based on NH_3/O_2 for improved graphite-based fiber electrodes in vanadium redox flow batteries. *Carbon* **2013**, *60*, 280–288. [[CrossRef](#)]
178. Zhang, W.; Xi, J.; Li, Z.; Zhou, H.; Liu, L.; Wu, Z.; Qiu, X. Electrochemical activation of graphite felt electrode for VO^{2+}/VO_2^+ redox couple application. *Electrochim. Acta* **2013**, *89*, 429–435. [[CrossRef](#)]
179. Gonzalez, Z.; Flox, C.; Blanco, C.; Granda, M.; Morante, J.R.; Menendez, R.; Santamaria, R. Outstanding electrochemical performance of a graphene-modified graphite felt for vanadium redox flow battery application. *J. Power Sources* **2017**, *338*, 155–162. [[CrossRef](#)]
180. Gonzalez, Z.; Sanchez, A.; Blanco, C.; Granda, M.; Menendez, R.; Santamaria, R. Enhanced performance of a Bi-modified graphite felt as the positive electrode of a vanadium redox flow battery. *Electrochim. Commun.* **2011**, *13*, 1379–1382. [[CrossRef](#)]
181. Zhong, S.; Padeste, C.; Kazacos, M.; Skyllas-Kazacos, M. Comparison of the Physical, Chemical and Electrochemical Properties of Rayon-Based and Polyacrylonitrile-Based Graphite Felt Electrodes. *J. Power Sources* **1993**, *45*, 29–41. [[CrossRef](#)]
182. Oriji, G.; Katayama, Y.; Miura, T. Investigation on V(IV)/V(V) species in a vanadium redox flow battery. *Electrochim. Acta* **2004**, *49*, 3091–3095. [[CrossRef](#)]
183. Wen, Y.H.; Zhang, H.M.; Qian, P.; Zhao, P.; Zhou, H.T.; Yi, B.L. Investigations on the electrode process of concentrated V(IV)/V(V) species in a vanadium redox flow battery. *Act. Phys.-Chim. Sin.* **2006**, *22*, 403–408. [[CrossRef](#)]
184. Wang, Q.; Daoud, W.A. Temperature influence on the reaction kinetics of V(IV)/V(V) in methanesulfonic acid for all-vanadium redox flow battery. *Electrochim. Acta* **2016**, *214*, 11–18. [[CrossRef](#)]
185. Le, T.X.H.; Bechelany, M.; Cretin, M. Carbon felt based-electrodes for energy and environmental applications: A review. *Carbon* **2017**, *122*, 564–591.
186. Noack, J.; Tübke, J. A Comparison of Materials and Treatment of Materials for Vanadium Redox Flow Battery. *ECS Trans.* **2010**, *25*, 235–245.
187. Gang, W.; Jinwei, C.; Shifu, Z.; Jie, Z.; Xiaojiang, L.; Ruilin, W. Activation of Carbon Electrodes for All-Vanadium Redox Flow Battery. *Prog. Chem.* **2015**, *27*, 1343–1355.

188. Goulet, M.-A.; Skyllas-Kazacos, M.; Kjeang, E. The importance of wetting in carbon paper electrodes for vanadium redox reactions. *Carbon* **2016**, *101*, 390–398. [[CrossRef](#)]
189. Certainly any combination of two materials can be called a composite; a generally accepted definition of this term is absent. According to common usage a composite can be a combination of two distinctly different materials yielding a new one—A composite—with properties distinctly different from those of the constituents. Accordingly the combination of CNF and MnO₂ may be called a composite whereas graphene platelets deposited on carbon fiber hardly qualify. The latter can be called modified carbon fiber—And this classification is observed in the present text.
190. Rychcik, M.; Skyllas-Kazacos, M. Evaluation of electrode materials for vanadium redox cell. *J. Power Sources* **1987**, *19*, 45–54. [[CrossRef](#)]
191. Jiang, Z.; Klyukin, K.; Alexandrov, V. First-principles study of adsorption-desorption kinetics of aqueous V²⁺/V³⁺ redox species on graphite in a vanadium redox flow battery. *Phys. Chem. Chem. Phys.* **2017**, *19*, 14897–14901. [[CrossRef](#)] [[PubMed](#)]
192. Ma, Q.; Zeng, X.-X.; Zhou, C.; Deng, Q.; Wang, P.-F.; Zuo, T.-T.; Zhang, X.-D.; Yin, Y.-X.; Wu, X.; Chai, L.-Y.; et al. Designing High-Performance Composite Electrodes for Vanadium Redox Flow Batteries: Experimental and Computational Investigation. *ACS Appl. Mater. Interface* **2018**, *10*, 22381–22388. [[CrossRef](#)] [[PubMed](#)]
193. Jiang, H.R.; Shyy, W.; Zeng, L.; Zhang, R.H.; Zhao, T.S. Highly efficient and ultra-stable boron-doped graphite felt electrodes for vanadium redox flow batteries. *J. Mater. Chem. A* **2018**, *6*, 13244–13253. [[CrossRef](#)]
194. Holze, R. Kinetics of Fast Redox Systems for Energy Storage. In *Springer Handbook of Electrochemical Energy*; Breitkopf, C., Swider-Lyons, K., Eds.; Springer: Dordrecht, The Netherlands, 2016; pp. 591–610.
195. Schweiss, R.; Pritzl, A.; Meiser, C. Parasitic Hydrogen Evolution at Different Carbon Fiber Electrodes in Vanadium Redox Flow Batteries. *J. Electrochem. Soc.* **2016**, *163*, A2089–A2094. [[CrossRef](#)]
196. Chen, F.; Liu, J.; Chen, H.; Yan, C. Study on hydrogen evolution reaction at a graphite electrode in the all-vanadium redox flow battery. *Int. J. Electrochem. Sci.* **2012**, *7*, 3750–3764.
197. Gahn, R.F.; Hagedorn, N.H.; Johnson, J.A. Cycling performance of the iron-chromium redox energy storage system. In Proceedings of the 20th Intersociety Energy Conversion Engineering Conference 1985, Miami Beach, FL, USA, 18–23 August 1985; Volume 2, pp. 91–97.
198. Skyllas-Kazacos, M. All-Vanadium Redox Battery and Additives. WO Patent Affiliation 89/05526, 15 June 1989.
199. Cnobloch, H.; Nischik, H.; Pantel, K.; Ledjeff, K.; Heinzel, A.; Reiner, A. Eisen-Chrom-Redoxionen-Speicher. In *DECHEMA-Monographie*; VCH Verlagsgesellschaft: Weinheim, Germany, 1987; Volume 109, pp. 427–445.
200. Liu, C.C.; Galasco, R.T.; Savinell, F. Operating Performance of an Fe-Ti Stationary Redox Battery in the Presence of Lead. *J. Electrochem. Soc.* **1982**, *129*, 2502–2505. [[CrossRef](#)]
201. Liu, M.-Y.; Xiang, Z.-P.; Deng, H.-Q.; Wan, K.; Liu, Q.-B.; Piao, J.-H.; Zheng, Y.-Y.; Liang, Z.-X. Electrochemical Behavior of Vanadium Redox Couples on Carbon Electrode. *J. Electrochem. Soc.* **2016**, *163*, H937–H942. [[CrossRef](#)]
202. Nicholson, R.S. Theory and Application of Cyclic Voltammetry for Measurement of Electrode Reaction Kinetics. *Anal. Chem.* **1965**, *37*, 1351–1355. [[CrossRef](#)]
203. Oriji, G.; Katayama, Y.; Miura, T. Investigations on V(IV)/V(V) and V(II)/V(III) redox reactions by various electrochemical methods. *J. Power Sources* **2005**, *139*, 321–324. [[CrossRef](#)]
204. Liu, W.; Luo, D.; Zeng, F.; Meng, X.; Li, D. Investigations on the V(III) Reduction Process of All-Vanadium Redox Flow Battery. *Int. J. Electrochem. Sci.* **2016**, *11*, 3492–3501. [[CrossRef](#)]
205. Roznyatovskaya, N.; Noack, J.; Fühl, M.; Pinkwart, K.; Tübke, J. Towards an all-vanadium redox-flow battery electrolyte: Electropoxidation of V(III) in V(IV)/V(III) redox couple. *Electrochim. Acta* **2016**, *211*, 926–932. [[CrossRef](#)]
206. Gattrell, M.; Qian, J.; Stewar, C.; Graham, P.; MacDougall, B. The electrochemical reduction of VO₂. *Electrochim. Acta* **2005**, *51*, 395–407. [[CrossRef](#)]
207. Taylor, S.M.; Patru, A.; Streich, D.; El Kazzi, M.; Fabbri, E.; Schmidt, T.J. Vanadium (V) reduction reaction on modified glassy carbon electrodes—Role of oxygen functionalities and microstructure. *Carbon* **2016**, *109*, 472–478. [[CrossRef](#)]
208. Melke, J.; Jakes, P.; Langner, J.; Riekehr, L.; Kunz, U.; Zhao-Karger, Z.; Nefedov, A.; Sezen, H.; Woell, C.; Ehrenberg, H.; et al. Carbon materials for the positive electrode in all-vanadium redox flow batteries. *Carbon* **2014**, *78*, 220–230. [[CrossRef](#)]

209. Zhang, H.; Tan, Y.; Li, J.; Xue, B. Studies on properties of rayon- and polyacrylonitrile-based graphite felt electrodes affecting Fe/Cr redox flow battery performance. *Electrochim. Acta* **2017**, *248*, 603–613. [CrossRef]
210. Langner, J.; Bruns, M.; Dixon, D.; Nefedov, A.; Woell, Ch.; Scheiba, F.; Ehrenberg, H.; Roth, C.; Melke, J. Surface properties and graphitization of polyacrylonitrile based fiber electrodes affecting the negative half-cell reaction in vanadium redox flow batteries. *J. Power Sources* **2016**, *321*, 210–218. [CrossRef]
211. Ling, W.; Wang, Z.; Deng, Q.; Wang, H.; Zeng, X.; Hu, Y.; He, S.; Wu, X.; Chen, G.; Wu, Y.; et al. A three-dimensional conducting network from rGO-in-graphite-felt as electrode for vanadium redox flow batteries. *Electrochim. Energy Technol.* **2018**, submitted.
212. Sabou, D.-M.; Dorneanu, S.-A.; Ilea, P. Spectral graphite as electrode material for the all-vanadium redox flow battery. *Stud. Univ. Babes-Bolyai Chem.* **2015**, *60*, 193–203.
213. Yang, H.-Y.; Hsueh, K.-L.; Hsieh, C.-L.; Hung, J.-S. Study of the Kinetics of Vanadium (II)/(III) Redox Reaction. *ECS Trans.* **2013**, *50*, 87–92. [CrossRef]
214. Wang, W.; Fan, X.; Liu, J.; Yan, C.; Zeng, C. Unusual phenomena in the reduction process of vanadium(V) on a graphite electrode at high overpotentials. *Phys. Chem. Chem. Phys.* **2014**, *16*, 19848–19851. [CrossRef] [PubMed]
215. Gattrell, M.; Park, J.; MacDougall, B.; Apte, J.; McCarthy, S.; Wu, C.W. Study of the mechanism of the vanadium 4+/5+ redox reaction in acidic solutions. *J. Electrochem. Soc.* **2004**, *151*, A123–A130. [CrossRef]
216. Wang, W.; Fan, X.; Liu, J.; Yan, C.; Zeng, C. A novel mechanism for the oxidation reaction of VO^{2+} on a graphite electrode in acidic solutions. *J. Power Sources* **2014**, *261*, 212–220. [CrossRef]
217. Yamamura, T.; Watanabe, N.; Yano, T.; Shiokawa, Y. Electron-transfer kinetics of $\text{Np}^{3+}/\text{Np}^{4+}$, $\text{NpO}_2^+/\text{NpO}_2^{2+}$, $\text{V}^{2+}/\text{V}^{3+}$, and $\text{VO}^{2+}/\text{VO}_2^+$ at carbon electrodes. *J. Electrochem. Soc.* **2005**, *152*, A830–A836. [CrossRef]
218. Narita, A.; Kaneko, Y.; Sato, Y.; Negishi, A.; Nozaki, K.; Kato, T. Characterization of Carbon Fiber Electrode for Vanadium-Based Redox Flow Batteries. *ECS Trans.* **2015**, *68*, 89–95. [CrossRef]
219. Maruyama, J.; Hasegawa, T.; Iwasaki, S.; Fukuhara, T.; Nogami, M. Mechanism of Dioxovanadium Ion Reduction on Oxygen-Enriched Carbon Surface. *J. Electrochem. Soc.* **2013**, *160*, A1293–A1298. [CrossRef]
220. Wu, X.W.; Yamamura, T.; Ohta, S.; Zhang, Q.X.; Lv, F.C.; Liu, C.M.; Shirasaki, K.; Satoh, I.; Shikama, T.; Lu, D.; et al. Acceleration of the redox kinetics of $\text{VO}^{2+}/\text{VO}_2^+$ and $\text{V}^{3+}/\text{V}^{2+}$ couples on carbon paper. *J. Appl. Electrochem.* **2011**, *41*, 1183–1190. [CrossRef]
221. Zhou, X.L.; Zeng, Y.K.; Zhu, X.B.; Wei, L.; Zhao, T.S. A high-performance dual-scale porous electrode for vanadium redox flow batteries. *J. Power Sources* **2016**, *325*, 329–336. [CrossRef]
222. Zhang, Z.; Xi, J.; Zhou, H.; Qiu, X. KOH etched graphite felt with improved wettability and activity for vanadium flow batteries. *Electrochim. Acta* **2016**, *218*, 15–23. [CrossRef]
223. Xie, Y.; Cheng, Z.; Guo, B.; Qiu, Y.; Fan, H.; Sun, S.; Wu, T.; Jin, L.; Fan, L. Preparation of activated carbon paper by modified Hummer's method and application as vanadium redox battery. *Ionics* **2015**, *21*, 283–287. [CrossRef]
224. Wu, X.; Xu, H.; Shen, Y.; Xu, P.; Lu, L.; Fu, J.; Zhao, H. Treatment of graphite felt by modified Hummers method for the positive electrode of vanadium redox flow battery. *Electrochim. Acta* **2014**, *138*, 264–269. [CrossRef]
225. Gencten, M.; Gursu, H.; Sahin, Y. Electrochemical investigation of the effects of V(V) and sulfuric acid concentrations on positive electrolyte for vanadium redox flow battery. *Int. J. Hydrogen Energy* **2016**, *41*, 9868–9875. [CrossRef]
226. Yang, H.; Fan, C.; Zhu, Q. Activated Charcoal Modified Graphite Felts Using for Positive Electrodes of Vanadium Redox Flow Battery. *J. Electrochem. Energy Convers. Storage* **2017**, *14*, 041004. [CrossRef]
227. Lee, M.E.; Lee, S.; Jin, H.-J.; Yun, Y.S. Standalone macroporous graphitic nanowebs for vanadium redox flow batteries. *J. Ind. Eng. Chem.* **2018**, *60*, 85–90. [CrossRef]
228. Schmidt, C.N.; Cao, G. Properties of mesoporous carbon modified carbon felt for anode of all-vanadium redox flow battery. *Sci. China Mater.* **2016**, *59*, 1037–1050. [CrossRef]
229. Jeong, S.; An, S.; Jeong, J.; Lee, J.; Kwon, Y. Effect of mesocellular carbon foam electrode material on performance of vanadium redox flow battery. *J. Power Sources* **2015**, *278*, 245–254. [CrossRef]
230. Jeong, S.; Kim, S.; Kwon, Y. Performance enhancement in vanadium redox flow battery using platinum-based electrocatalyst synthesized by polyol process. *Electrochim. Acta* **2013**, *114*, 439–447. [CrossRef]
231. Peng, L.; Fang, Z.; Zhu, Y.; Yan, C.; Yu, G. Holey 2D Nanomaterials for Electrochemical Energy Storage. *Adv. Energy Mater.* **2018**, *8*, 1702179. [CrossRef]

232. Liu, Y.; Shen, Y.; Yu, L.; Liu, L.; Liang, F.; Qiu, X.; Xi, J. Holey-engineered electrodes for advanced vanadium flow batteries. *Nano Energy* **2018**, *43*, 55–62. [[CrossRef](#)]
233. Raccichini, R.; Varzi, A.; Passerini, S.; Scrosati, B. The role of graphene for electrochemical energy storage. *Nat. Mater.* **2015**, *14*, 271–279. [[CrossRef](#)] [[PubMed](#)]
234. Ji, L.; Meduri, P.; Agubra, V.; Xiao, X.; Alcoutlabi, M. Graphene-Based Nanocomposites for Energy Storage. *Adv. Energy Mater.* **2016**, *6*, 1502159. [[CrossRef](#)]
235. Shao, Y.; Cheng, Y.; Duan, W.; Wang, W.; Lin, Y.; Wang, Y.; Li, J. Nanostructured Electrocatalysts for PEM Fuel Cells and Redox Flow Batteries: A Selected Review. *ACS Catal.* **2015**, *5*, 7288–7298. [[CrossRef](#)]
236. Park, M.; Ryu, J.; Cho, J. Nanostructured Electrocatalysts for All-Vanadium Redox Flow Batteries. *Chem. Asian J.* **2015**, *10*, 2096–2110. [[CrossRef](#)] [[PubMed](#)]
237. Wang, F.; Wu, X.; Li, C.; Zhu, Y.; Fu, L.; Wu, Y.; Liu, X. Nanostructured positive electrode materials for post-lithium ion batteries. *Energy Environ. Sci.* **2016**, *9*, 3570–3611. [[CrossRef](#)]
238. Zhou, Y.; Liu, L.; Shen, Y.; Wu, L.; Yu, L.; Liang, F.; Xi, J. Carbon dots promoted vanadium flow batteries for all-climate energy storage. *Chem. Commun.* **2017**, *53*, 7565–7568. [[CrossRef](#)] [[PubMed](#)]
239. Robarts, L.; Santhanam, K.S.V. Interfacial Electron Transfer Involving Vanadium and Graphene Quantum Dots for Redox Flow Battery. *MRS Adv.* **2018**, *3*, 1221–1228. [[CrossRef](#)]
240. Sankar, A.; Michos, I.; Dutta, I.; Dong, J.; Angelopoulos, A.P. Enhanced vanadium redox flow battery performance using graphene nanoplatelets to decorate carbon electrodes. *J. Power Sources* **2018**, *387*, 91–100. [[CrossRef](#)]
241. Park, M.; Jeon, I.-Y.; Ryu, J.; Jang, H.; Back, J.-B.; Cho, J. Edge-halogenated graphene nanoplatelets with F, Cl, or Br as electrocatalysts for all-vanadium redox flow batteries. *Nano Energy* **2016**, *26*, 233–240. [[CrossRef](#)]
242. Zhang, Z.; Lee, C.-S.; Zhang, W. Vertically Aligned Graphene Nanosheet Arrays: Synthesis, Properties and Applications in Electrochemical Energy Conversion and Storage. *Adv. Energy Mater.* **2017**, *7*, 1700678. [[CrossRef](#)]
243. Gonzalez, Z.; Botas, C.; Alvarez, P.; Roldan, S.; Blanco, C.; Santamaria, R.; Granda, M.; Menendez, R. Thermally reduced graphite oxide as positive electrode in Vanadium Redox Flow Batteries. *Carbon* **2012**, *50*, 828–834. [[CrossRef](#)]
244. Shi, L.; Liu, S.; He, Z.J. Shen Nitrogen-Doped Graphene: Effects of nitrogen species on the properties of the vanadium redox flow battery. *Electrochim. Acta* **2014**, *138*, 93–100. [[CrossRef](#)]
245. Han, P.; Wang, H.; Liu, Z.; Chen, X.; Ma, W.; Yao, J.; Zhu, Y.; Cui, G. Graphene oxide nanoplatelets as excellent electrochemical active materials for $\text{VO}^{2+}/\text{VO}_2^+$ and $\text{V}^{2+}/\text{V}^{3+}$ redox couples for a vanadium redox flow battery. *Carbon* **2011**, *49*, 693–700. [[CrossRef](#)]
246. Sun, B.T.; Skyllas-Kazacos, M. Chemical modification of graphite electrode materials for vanadium redox flow battery application—Part II. Acid treatments. *Electrochim. Acta* **1992**, *37*, 2459–2465. [[CrossRef](#)]
247. Chakrabarti, B.; Nir, D.; Yufit, V.; Tariq, F.; Rubio-Garcia, J.; Maher, R.; Kucernak, A.; Aravind, P.V.; Brandon, N. Performance Enhancement of Reduced Graphene Oxide-Modified Carbon Electrodes for Vanadium Redox-Flow Systems. *ChemElectroChem* **2017**, *4*, 194–200. [[CrossRef](#)]
248. Li, W.; Liu, J.; Yan, C. Reduced graphene oxide with tunable C/O ratio and its activity towards vanadium redox pairs for an all vanadium redox flow battery. *Carbon* **2013**, *55*, 313–320. [[CrossRef](#)]
249. Deng, Q.; Huang, P.; Zhou, W.-X.; Ma, Q.; Zhou, N.; Xie, H.; Ling, W.; Zhou, C.-J.; Yin, Y.-X.; Wu, X.-W.; et al. A High-Performance Composite Electrode for Vanadium Redox Flow Batteries. *Adv. Energy Mater.* **2017**, *7*, 1700461. [[CrossRef](#)]
250. Reversibility is used as a term with several meanings frequently confusing. Reversibility in its thermodynamic sense meaning under reversible conditions certainly does not apply here, in its mechanistic sense meaning a reaction going forward and backward in the same direction with opposite orientations may be correct here, but is presumably not intended (The authors statement regarding reaction mechanism are not supported in the article), and the electrochemical meaning of a fast reaction—which obviously applies here.
251. Di Blasi, O.; Briguglio, N.; Busacca, C.; Ferraro, M.; Antonucci, V.; Di Blasi, A. Electrochemical investigation of thermically treated graphene oxides as electrode materials for vanadium redox flow battery. *Appl. Energy* **2015**, *147*, 74–81. [[CrossRef](#)]

252. Etesami, M.; Abouzari-Lotf, E.; Ripin, A.; Nasef, M.M.; Ting, T.M.; Saharkhiz, A.; Ahmad, A. Phosphonated graphene oxide with high electrocatalytic performance for vanadium redox flow battery. *Int. J. Hydrogen Energy* **2018**, *43*, 189–197. [[CrossRef](#)]
253. Gonzalez, Z.; Botas, C.; Blanco, C.; Santamaria, R.; Granda, M.; Alvarez, P.; Menendez, R. Thermally reduced graphite and graphene oxides in VRFBs. *Nano Energy* **2013**, *2*, 1322–1328. [[CrossRef](#)]
254. Gonzalez, Z.; Botas, C.; Blanco, C.; Santamaria, R.; Granda, M.; Alvarez, P.; Menendez, R. Graphite oxide-based graphene materials as positive electrodes in vanadium redox flow batteries. *J. Power Sources* **2013**, *241*, 349–354. [[CrossRef](#)]
255. Ko, Y.-J.; Choi, K.; Kim, J.-Y.; Kim, I.; Jeong, D.S.; Choi, H.-J.; Mizuseki, H.; Lee, W.-S. Onion-like carbon as dopant/modification-free electrocatalyst for $\text{VO}^{2+}/\text{VO}_2^+$ redox reaction: Performance-control mechanism. *Carbon* **2018**, *127*, 31–40. [[CrossRef](#)]
256. Dai, L.; Jiang, Y.; Meng, W.; Zhou, H.; Wang, L.; He, Z. Improving the electrocatalytic performance of carbon nanotubes for $\text{VO}^{2+}/\text{VO}_2^+$ redox reaction by KOH activation. *Appl. Surf. Sci.* **2017**, *401*, 106–113. [[CrossRef](#)]
257. He, Z.; Liu, L.; Gao, C.; Zhou, Z.; Liang, X.; Lei, Y.; He, Z.; Liu, S. Carbon nanofibers grown on the surface of graphite felt by chemical vapour deposition for vanadium redox flow batteries. *RSC Adv.* **2013**, *3*, 19774–19777. [[CrossRef](#)]
258. Lv, Z.; Zhang, J.; Lv, Y.; Cheng, Y.; Jiang, S.P.; Xiang, Y.; Lu, S. The electrocatalytic characterization and mechanism of carbon nanotubes with different numbers of walls for the $\text{VO}^{2+}/\text{VO}_2^+$ redox couple. *Phys. Chem. Chem. Phys.* **2018**, *20*, 7791–7797. [[CrossRef](#)] [[PubMed](#)]
259. Wang, S.; Zhao, X.; Cochell, T.; Manthiram, A. Nitrogen-Doped Carbon Nanotube/Graphite Felts as Advanced Electrode Materials for Vanadium Redox Flow Batteries. *J. Phys. Chem. Lett.* **2012**, *3*, 2164–2167. [[CrossRef](#)] [[PubMed](#)]
260. Yang, D.-S.; Lee, J.Y.; Jo, S.-W.; Yoon, S.J.; Kim, T.-H.; Hong, Y.T. Electrocatalytic activity of nitrogen-doped CNT graphite felt hybrid for all-vanadium redox flow batteries. *Int. J. Hydrogen Energy* **2018**, *43*, 1516–1522. [[CrossRef](#)]
261. Steimecke, M.; Ruemmler, S.; Schuhmacher, N.-F.; Lindenberg, T.; Hartmann, M.; Bron, M. A Comparative Study of Functionalized High-Purity Carbon Nanotubes towards the V(IV)/V(V) Redox Reaction Using Cyclic Voltammetry and Scanning Electrochemical Microscopy. *Electroanalysis* **2017**, *29*, 1056–1061. [[CrossRef](#)]
262. Steimecke, M.; Ruemmler, S.; Kuehhirt, M.; Bron, M. A Linear Sweep Voltammetric Procedure Applied to Scanning Electrochemical Microscopy for the Characterization of Carbon Materials towards the Vanadium(IV)/(V) Redox System. *ChemElectroChem* **2016**, *3*, 318–322. [[CrossRef](#)]
263. Lin, J.; Shang, Y.; Lin, X.; Yang, L.; Yu, A. Study on Nitrogen-Doped Carbon Nanotubes for Vanadium Redox Flow Battery Application. *Int. J. Electrochem. Sci.* **2016**, *11*, 665–674.
264. Chang, Y.-C.; Shih, Y.-C.; Chen, J.-Y.; Lin, G.-Y.; Hsu, N.-Y.; Chou, Y.-S.; Wang, C.-H. High efficiency of bamboo-like carbon nanotubes on functionalized graphite felt as electrode in vanadium redox flow battery. *RSC Adv.* **2016**, *6*, 102068–102075. [[CrossRef](#)]
265. Chang, Y.-C.; Shih, Y.-C.; Chen, J.-Y.; Lin, G.-Y.; Hsu, N.-Y.; Chou, Y.-S.; Wang, C.-H. High efficiency of bamboo-like carbon nanotubes on functionalized graphite felt as electrode in vanadium redox flow battery. *RSC Adv.* **2016**, *6*, 107294. [[CrossRef](#)]
266. Masurenko, I.; Etienne, M.; Francius, G.; Vakulko, I.; Walcarus, A. Macroporous carbon nanotube-carbon composite electrodes. *Carbon* **2016**, *109*, 106–116. [[CrossRef](#)]
267. Fu, S.; Zhu, C.; Song, J.; Engelhard, M.H.; Du, D.; Lin, Y. Three-dimensional Nitrogen-Doped Reduced Graphene Oxide/Carbon Nanotube Composite Catalysts for Vanadium Flow Batteries. *Electroanalysis* **2017**, *29*, 1469–1473. [[CrossRef](#)]
268. Yang, H.; Fan, C.; Zhu, Q. Sucrose pyrolysis assembling carbon nanotubes on graphite felt using for vanadium redox flow battery positive electrode. *J. Energy Chem.* **2018**, *27*, 451–454. [[CrossRef](#)]
269. Li, W.; Liu, J.; Yan, C. Multi-walled carbon nanotubes used as an electrode reaction catalyst for catalyst for $\text{VO}^{2+}/\text{VO}_2^+$ for a vanadium redox flow battery. *Carbon* **2011**, *49*, 3463–3470. [[CrossRef](#)]
270. Li, W.; Liu, J.; Yan, C. The electrochemical catalytic activity of single-walled carbon nanotubes towards $\text{VO}^{2+}/\text{VO}_2^+$ and $\text{V}^{3+}/\text{V}^{2+}$ redox pairs for an all vanadium redox flow battery. *Electrochim. Acta* **2012**, *79*, 102–108. [[CrossRef](#)]
271. Wei, G.; Jia, C.; Liu, J.; Yan, C. Carbon felt supported carbon nanotubes catalysts composite electrode for vanadium redox flow battery application. *J. Power Sources* **2012**, *220*, 185–192. [[CrossRef](#)]

272. Huang, K.-L.; Chen, R.-Y.; Liu, S.-Q.; Shi, X.-H.; Zhang, Q.-H. Characteristics of Carbon Nanotube-graphite Composite Electrodes for Vanadium Redox Flow Battery. *J. Inorg. Mater.* **2010**, *25*, 659–663. [CrossRef]
273. Chu, Y.Q.; Li, D.D.; Li, W.W.; Ma, C.A. Electrocatalytic Activity of Multi-walled Carbon Nanotubes for V^{2+}/VO_2^+ of a Vanadium Redox Flow Battery. In Proceedings of the 2013 International Conference on Materials for Renewable Energy and Environment (ICMREE), Chengdu, China, 19–21 August 2014; Volume 1–3, pp. 537–540.
274. Mustafa, I.; Lopez, I.; Younes, H.; Susantyoko, R.A.; Abu Al-Rub, R.; Almheiri, S. Fabrication of Freestanding Sheets of Multiwalled Carbon Nanotubes (Buckypapers) for Vanadium Redox Flow Batteries and Effects of Fabrication Variables on Electrochemical Performance. *Electrochim. Acta* **2017**, *230*, 222–235. [CrossRef]
275. Mustafa, I.; Al Shehhi, A.; Al Hammadi, A.; Susantyoko, R.; Palmisano, G.; Almheiri, S. Effects of carbonaceous impurities on the electrochemical activity of multiwalled carbon nanotube electrodes for vanadium redox flow batteries. *Carbon* **2018**, *131*, 47–59. [CrossRef]
276. Tenny, K.M.; Lakhanpal, V.S.; Dowd, R.P., Jr.; Yarlagadda, V.; Van Nguyen, T. Impact of Multi-Walled Carbon Nanotube Fabrication on Carbon Cloth Electrodes for Hydrogen-Vanadium Reversible Fuel Cells. *J. Electrochem. Soc.* **2017**, *164*, A2534–A2538. [CrossRef]
277. Zarei Jelyani, M.; Rashid-Nadimi, S.; Asghari, S. Treated carbon felt as electrode material in vanadium redox flow batteries: A study of the use of carbon nanotubes as electrocatalyst. *J. Solid State Electrochem.* **2017**, *21*, 69–79. [CrossRef]
278. González, Z.; Álvarez, P.; Blanco, C.; Vega-Díaz, S.; Tristaán-Lopez, F.; Pulickal Rajukumar, L.; Cruz-Silva, R.; Laura Elias, A.; Terrones, M.; Menéndez, R. The influence of carbon nanotubes characteristics in their performance as positive electrodes in vanadium redox flow batteries. *Sustain. Energy Technol. Assess.* **2015**, *9*, 105–110. [CrossRef]
279. Han, P.; Yue, Y.; Liu, Z.; Xu, W.; Zhang, L.; Xu, H.; Dong, S.; Cui, G. Graphene oxide nanosheets/multi-walled carbon nanotubes hybrid as an excellent electrocatalytic material towards VO^{2+}/VO_2^+ redox couples for vanadium redox flow batteries. *Energy Environ. Sci.* **2011**, *4*, 4710–4717. [CrossRef]
280. Rui, X.; Ohnmar Oo, M.; Sim, D.H.; Raghu, S.C.; Yan, Q.; Lim, T.M.; Skyllas-Kazacos, M. Graphene oxide nanosheets/polymer binders as superior electrocatalytic materials for vanadium bromide redox flow batteries. *Electrochim. Acta* **2012**, *85*, 175–181. [CrossRef]
281. Park, M.; Jung, Y.-J.; Kim, J.; Lee, H.I.; Cho, J. Synergistic Effect of Carbon Nanofiber/Nanotube Composite Catalyst on Carbon Felt Electrode for High-Performance All-Vanadium Redox Flow Battery. *NANO Lett.* **2013**, *13*, 4833–4839. [CrossRef] [PubMed]
282. Zhu, H.Q.; Zhang, Y.M.; Yue, L.; Li, W.S.; Li, G.L.; Shu, D.; Chen, H.Y. Graphite-carbon nanotube composite electrodes for all vanadium redox flow battery. *J. Power Sources* **2008**, *184*, 637–640. [CrossRef]
283. Li, W.; Liu, J.; Yan, C. Modified multiwalled carbon nanotubes as an electrode reaction catalyst for an all vanadium redox flow battery. *J. Solid State Electrochem.* **2013**, *17*, 1369–1376. [CrossRef]
284. Yang, H.; Hung, C.-H.; Wang, S.-P.; Chiang, I.-L. Graphite felt with vapor grown carbon fibers as electrodes for vanadium redox flow batteries. *Rare Met.* **2011**, *30*, 1–4. [CrossRef]
285. Li, W.; Zhang, Z.; Tang, Y.; Bian, H.; Ng, T.-W.; Zhang, W.; Lee, C.-S. Graphene-Nanowall-Decorated Carbon Felt with Excellent Electrochemical Activity Toward VO^{2+}/VO_2^+ Couple for All Vanadium Redox Flow Battery. *Adv. Sci.* **2016**, *3*, 1500276. [CrossRef] [PubMed]
286. Gonzalez, Z.; Vizireanu, S.; Dinescu, G.; Blanco, C.; Santamaria, R. Carbon nanowalls thin films as nanostructured electrode materials in vanadium redox flow batteries. *Nano Energy* **2012**, *1*, 833–839. [CrossRef]
287. Park, M.; Jeon, I.-Y.; Ryu, J.; Baek, J.-B.; Cho, J. Exploration of the Effective Location of Surface Oxygen Defects in Graphene-Based Electrocatalysts for All-Vanadium Redox-Flow Batteries. *Adv. Energy Mater.* **2015**, *5*, 1401550. [CrossRef]
288. Park, M.; Jeon, I.-Y.; Ryu, J.; Baek, J.-B.; Cho, J. Exploration of the effective location of surface oxygen defects in graphene-based electrocatalysts for all-vanadium redox flow batteries. In Proceedings of the 249th National ACS Meeting, Denver, CO, USA, 22–26 March 2015.
289. He, Z.; Cheng, G.; Jiang, Y.; Wang, L.; Dai, L. Sulfonated Carbon Nanotubes as Superior Catalysts towards V^{3+}/V^{2+} Redox Reaction for Vanadium Redox Flow Battery. *J. Electrochem. Soc.* **2018**, *165*, A932–A938. [CrossRef]

290. Noh, C.; Moon, S.; Chung, Y.; Kwon, Y. Chelating functional group attached to carbon nanotubes prepared for performance enhancement of vanadium redox flow battery. *J. Mater. Chem.* **2017**, *5*, 21334–21342. [CrossRef]
291. Wu, L.; Shen, Y.; Yu, L.; Xi, J.; Qiu, X. Boosting vanadium flow battery performance by Nitrogen-doped carbon nanospheres electrocatalyst. *Nano Energy* **2016**, *28*, 19–28. [CrossRef]
292. He, Z.; Jiang, Y.; Wei, Y.; Zhao, C.; Jiang, F.; Li, L.; Zhou, H.; Meng, W.; Wang, L.; Dai, L. N,P co-doped carbon microsphere as superior electrocatalyst for $\text{VO}^{2+}/\text{VO}_2^+$ redox reaction. *Electrochim. Acta* **2018**, *259*, 122–130. [CrossRef]
293. Han, M.; Kim, H. Development of Boron Doped Carbon Using CO_2 Reduction with NaBH_4 for Vanadium Redox Flow Battery. *J. Korean Electrochem. Soc.* **2018**, *21*, 1–5.
294. Gursu, H.; Gencen, M.; Sahin, Y. Preparation of Sulphur-Doped Graphene-Based Electrodes by Cyclic Voltammetry: A Potential Application for Vanadium Redox Flow Battery. *Int. J. Electrochem. Sci.* **2018**, *13*, 875–885. [CrossRef]
295. Jiang, H.R.; Shyy, W.; Wu, M.C.; Wei, L.; Zhao, T.S. Highly active, bi-functional and metal-free B4C-nanoparticle-modified graphite felt electrodes for vanadium redox flow batteries. *J. Power Sources* **2017**, *365*, 34–42. [CrossRef]
296. Abbas, S.; Lee, H.; Hwang, J.; Mehmood, A.; Shin, H.-J.; Mehboob, S.; Lee, J.-Y.; Ha, H.Y. A novel approach for forming carbon nanorods on the surface of carbon felt electrode by catalytic etching for high-performance vanadium redox flow battery. *Carbon* **2018**, *128*, 31–37. [CrossRef]
297. Li, W.; Liu, J.; Yan, C. Graphite–graphite oxide composite electrode for vanadium redox flow battery. *Electrochim. Acta* **2011**, *56*, 5290–5294. [CrossRef]
298. Liu, J.; Wang, Z.A.; Wu, X.W.; Yuan, X.H.; Hu, J.P.; Zhou, Q.M.; Liu, Z.H.; Wu, Y.P. Porous carbon derived from disposable shaddock peel as an excellent catalyst toward $\text{VO}^{2+}/\text{VO}_2^+$ couple for vanadium redox battery. *J. Power Sources* **2015**, *299*, 301–308. [CrossRef]
299. Maharjan, M.; Bhattacharai, A.; Ulaganathan, M.; Wai, N.; Oo, M.O.; Wang, J.-Y.; Lim, T.M. High surface area bio-waste based carbon as a superior electrode for vanadium redox flow battery. *J. Power Sources* **2017**, *362*, 50–56. [CrossRef]
300. Ryu, J.; Park, M.; Cho, J. Catalytic Effects of B/N-co-Doped Porous Carbon Incorporated with Ketjenblack Nanoparticles for All-Vanadium Redox Flow Batteries. *J. Electrochem. Soc.* **2016**, *163*, A5144–A5149. [CrossRef]
301. Ulaganathan, M.; Jain, A.; Aravindan, V.; Jayaraman, S.; Ling, W.C.; Lim, T.M.; Srinivasan, M.P.; Yan, Q.; Madhavi, S. Bio-mass derived mesoporous carbon as superior electrode in all vanadium redox flow battery with multicouple reactions. *J. Power Sources* **2015**, *274*, 846–850. [CrossRef]
302. Park, M.; Ryu, J.; Kim, Y.; Cho, J. Corn protein-derived nitrogen-doped carbon materials with oxygen-rich functional groups: A highly efficient electrocatalyst for all-vanadium redox flow batteries. *Energy Environ. Sci.* **2014**, *7*, 3727–3735. [CrossRef]
303. Wei, L.; Zhao, T.S.; Zhao, G.; An, L.; Zeng, L. A high-performance carbon nanoparticle-decorated graphite felt electrode for vanadium redox flow batteries. *Appl. Energy* **2016**, *176*, 74–79. [CrossRef]
304. Zhang, Z.H.; Zhao, T.S.; Bai, B.F.; Zeng, L.; Wie, L. A highly active biomass-derived electrode for all vanadium redox flow batteries. *Electrochim. Acta* **2017**, *248*, 197–205. [CrossRef]
305. Lee, H.; Kim, H. Development of nitrogen-doped carbons using the hydrothermal method as electrode materials for vanadium redox flow batteries. *J. Appl. Electrochem.* **2013**, *43*, 553–557. [CrossRef]
306. Schnucklak, M.; Kuecken, S.; Fetyan, A.; Schmidt, J.; Thomas, A.; Roth, C. Salt-templated porous carbon-carbon composite electrodes for application in vanadium redox flow batteries. *J. Mater. Chem.* **2017**, *5*, 25193–25199. [CrossRef]
307. Mazur, P.; Mrlik, J.; Benes, J.; Pocedic, J.; Vrana, J.; Dundalek, J.; Kosek, J. Performance evaluation of thermally treated graphite felt electrodes for vanadium redox flow battery and their four-point single cell characterization. *J. Power Sources* **2018**, *380*, 105–114. [CrossRef]
308. Noh, T.H.; Kim, M.Y.; Kim, D.H.; Yang, S.H.; Lee, J.H.; Park, H.S.; Noh, H.S.; Lee, M.S.; Kim, H.S. Electrochemical Studies of Carbon Felt Electrode Modified Under Airless Conditions for Redox Flow Batteries. *J. Electrochem. Sci. Technol.* **2017**, *8*, 155–161.
309. Liu, S.-Q.; Shi, X.-H.; Huang, K.-L.; Li, X.-G. Characteristics of Carbon Paper as Electrode for Vanadium Redox Flow Battery. *J. Inorg. Mater.* **2009**, *24*, 798–802. [CrossRef]

310. Cho, Y.I.; Park, S.J.; Hwang, H.J.; Lee, J.G.; Jeon, Y.K.; Chu, Y.H.; Shul, Y.-G. Effects of Microwave Treatment on Carbon Electrode for Vanadium Redox Flow Battery. *ChemElectroChem* **2015**, *2*, 872–876. [CrossRef]
311. Wu, X.; Xu, H.; Xu, P.; Shen, Y.; Lu, L.; Shi, J.; Fu, J.; Zhao, H. Microwave-treated graphite felt as the positive electrode for all-vanadium redox flow battery. *J. Power Sources* **2014**, *263*, 104–109. [CrossRef]
312. Boehm, H.-P. Funktionelle Gruppen an Festkörper-Oberflächen. *Angew. Chem.* **1966**, *78*, 617–628. [CrossRef]
313. Di Blasi, A.; Di Blasi, O.; Briguglio, N.; Arico, A.S.; Sebastian, D.; Lazaro, M.J.; Monforte, G.; Antonucci, V. Investigation of several graphite-based electrodes for vanadium redox flow cell. *J. Power Sources* **2013**, *227*, 15–23. [CrossRef]
314. Kim, K.J.; Kim, Y.-J.; Kim, J.-H.; Park, M.-S. The effects of surface modification on carbon felt electrodes for use in vanadium redox flow batteries. *Mater. Chem. Phys.* **2011**, *131*, 547–553. [CrossRef]
315. Zeng, L.; Zhao, T.; Wie, L. Revealing the Performance Enhancement of Oxygenated Carbonaceous Materials for Vanadium Redox Flow Batteries: Functional Groups or Specific Surface Area? *Adv. Sustain. Syst.* **2018**, *2*, 1700148. [CrossRef]
316. Maruyama, J.; Maruyama, S.; Fukuhara, T.; Hanafusa, K. Efficient Edge Plane Exposure on Graphitic Carbon Fiber for Enhanced Flow-Battery Reactions. *J. Phys. Chem.* **2017**, *C121*, 24425–24433. [CrossRef]
317. Mayrhuber, I.; Dennison, C.R.; Kalra, V.; Kumbur, E.C. Laser-perforated carbon paper electrodes for improved mass-transport in high power density vanadium redox flow batteries. *J. Power Sources* **2014**, *260*, 251–258. [CrossRef]
318. He, Z.; Jiang, Y.; Li, Y.; Zhu, J.; Zhou, H.; Meng, W.; Wang, L.; Dai, L. Carbon layer-exfoliated, wettability-enhanced, SO_3H -functionalized carbon paper: A superior positive electrode for vanadium redox flow battery. *Carbon* **2018**, *127*, 297–304. [CrossRef]
319. Kötz, R.; Barbero, C.; Schnyder, B.; Haas, O. Spectroscopic Ellipsometry of Carbon Electrodes during Electrochemical Activation. *Thin Solid Films* **1993**, *233*, 69–73. [CrossRef]
320. Sullivan, M.G.; Schnyder, B.; Bartsch, M.; Alliata, D.; Barbero, C.; Imhof, R.; Kötz, R. Electrochemically modified glassy carbon for capacitor electrodes characterization of thick anodic layers by cyclic voltammetry, differential electrochemical mass spectrometry, spectroscopic ellipsometry, X-ray photoelectron spectroscopy, FTIR, and AFM. *J. Electrochem. Soc.* **2000**, *147*, 2636–2643. [CrossRef]
321. Kabir, H.; Gyan, I.O.; Cheng, I.F. Electrochemical modification of a pyrolytic graphite sheet for improved negative electrode performance in the vanadium redox flow battery. *J. Power Sources* **2017**, *342*, 31–37. [CrossRef]
322. Wang, W.; Wei, Z.; Su, W.; Fan, X.; Liu, J.; Yan, C.; Zeng, C. Kinetic investigation of vanadium (V)/(IV) redox couple on electrochemically oxidized graphite electrodes. *Electrochim. Acta* **2016**, *205*, 102–112. [CrossRef]
323. Cao, L.; Skyllas-Kazacos, M.; Wang, D.-W. Effects of Surface Pretreatment of Glassy Carbon on the Electrochemical Behavior of V(IV)/V(V) Redox Reaction. *J. Electrochem. Soc.* **2016**, *163*, A1164–A1174. [CrossRef]
324. Bourke, A.; Miller, M.A.; Lynch, R.P.; Gao, X.; Landon, J.; Wainright, J.S.; Savinell, R.F.; Buckley, D.N. Electrode Kinetics of Vanadium Flow Batteries: Contrasting Responses of V-II-V-III and V-IV-V-V to Electrochemical Pretreatment of Carbon. *J. Electrochem. Soc.* **2016**, *163*, A5097–A5105. [CrossRef]
325. Miller, M.A.; Bourke, A.; Quill, N.; Wainright, J.S.; Lynch, R.P.; Buckley, D.N.; Savinell, R.F. Kinetic Study of Electrochemical Treatment of Carbon Fiber Microelectrodes Leading to In Situ Enhancement of Vanadium Flow Battery Efficiency. *J. Electrochem. Soc.* **2016**, *163*, A2095–A2102. [CrossRef]
326. Bourke, A.; Miller, M.A.; Lynch, R.P.; Wainright, J.S.; Savinell, R.F.; Buckley, D.N. Effect of Cathodic and Anodic Treatments of Carbon on the Electrode Kinetics of V-IV/V-V Oxidation-Reduction. *J. Electrochem. Soc.* **2015**, *162*, A1547–A1555. [CrossRef]
327. Bourke, A.; Lynch, R.P.; Buckley, D.N. Effect of Electrode Pretreatment on the Cyclic Voltammetry of $\text{VO}^{2+}/\text{VO}_2^+$ at a Glassy Carbon Electrode. *ECS Trans.* **2013**, *53*, 59–67. [CrossRef]
328. Liu, H.; Yang, L.; Xu, Q.; Yan, C. An electrochemically activated graphite electrode with excellent kinetics for electrode processes of V(II)/V(III) and V(IV)/V(V) couples in a vanadium redox flow battery. *RSC Adv.* **2014**, *4*, 55666–55670. [CrossRef]
329. Li, X.-G.; Huang, K.-L.; Tan, N.; Liu, S.-Q.; Chen, L.-Q. Electrochemical modification of graphite felt electrode for vanadium redox flow battery. *J. Inorg. Mater.* **2006**, *21*, 1114–1120. [CrossRef]

330. Tan, N.; Huang, K.L.; Liu, S.Q.; Li, X.G.; Chang, Z.F. Activation mechanism study of electrochemical treated graphite felt for vanadium redox cell by electrochemical impedance spectrum. *Acta Chim. Sin.* **2006**, *64*, 584–588.
331. Xi, J.; Zhang, W.; Li, Z.; Zhou, H.; Liu, H.; Wu, Z.; Qiu, X. Effect of Electro-Oxidation Current Density on Performance of Graphite Felt Electrode for Vanadium Redox Flow Battery. *Int. J. Electrochem. Sci.* **2013**, *8*, 4700–4711.
332. Men, Y.; Sun, T. Carbon felts electrode treated in different weak acid solutions through electrochemical oxidation method for all vanadium redox flow battery. *Int. J. Electrochem. Sci.* **2012**, *7*, 3482–3488.
333. He, Z.; Jiang, Y.; Zhou, H.; Cheng, G.; Meng, W.; Wang, L.; Dai, L. Graphite felt electrode modified by square wave potential pulse for vanadium redox flow battery. *Int. J. Energy Res.* **2017**, *41*, 439–447. [CrossRef]
334. Buckley, D.N.; Bourke, A.; Lynch, R.P.; Quill, N.; Miller, M.A.; Wainright, J.S.; Savinell, R.F. Influence of Pretreatment on Kinetics at Carbon Electrodes and Consequences for Flow Battery Performance. *MRS Adv.* **2017**, *2*, 1131–1142. [CrossRef]
335. Raj, S.C.; Skyllas-Kazacos, M. Electrochemical studies on wettability of sintered TiB₂ electrodes in aluminum electrolysis. *Electrochim. Acta* **1992**, *37*, 1395–1401. [CrossRef]
336. Li, X.-G.; Huang, K.-L.; Liu, S.-Q.; Chen, L.-Q. Electrochemical behavior of diverse vanadium ions at modified graphite felt electrode in sulphuric solution. *J. Cent. South Univ. Technol.* **2007**, *14*, 51–56. [CrossRef]
337. Liu, S.-Q.; Shi, X.-H.; Huang, K.-L.; Li, X.-G.; Li, Y.-J.; Wu, X.-W. Characteristics of carbon paper as electrode for vanadium redox flow battery. *Chin. J. Inorg. Chem.* **2008**, *24*, 1079–1083.
338. Yue, L.; Li, W.; Sun, F.; Zhao, L.; Xing, L. Highly hydroxylated carbon fibres as electrode materials of all-vanadium redox flow battery. *Carbon* **2010**, *48*, 3079–3090. [CrossRef]
339. Kim, K.J.; Lee, H.S.; Kim, J.; Park, M.-S.; Kim, J.H.; Kim, Y.-J.; Skyllas-Kazacos, M. Superior Electrocatalytic Activity of a Robust Carbon-Felt Electrode with Oxygen-Rich Phosphate Groups for All-Vanadium Redox Flow Batteries. *ChemSusChem* **2016**, *9*, 1329–1338. [CrossRef] [PubMed]
340. Kil, D.; Lee, H.J.; Park, S.; Kim, S.; Kim, H. Synthesis of Activated Graphite Felts Using Short-Term Ozone/Heat Treatment for Vanadium Redox Flow Batteries. *J. Electrochem. Soc.* **2017**, *164*, A3011–A3017. [CrossRef]
341. Dixon, D.; Babu, D.J.; Langner, J.; Bruns, M.; Pfaffmann, L.; Bhaskar, A.; Schneider, J.J.; Scheiba, F.; Ehrenberg, H. Effect of oxygen plasma treatment on the electrochemical performance of the rayon and polyacrylonitrile based carbon felt for the vanadium redox flow battery application. *J. Power Sources* **2016**, *332*, 240–248. [CrossRef]
342. Estevez, L.; Reed, D.; Nie, Z.; Schwarz, A.M.; Nandasiri, M.I.; Kizewski, J.P.; Wang, W.; Thomsen, E.; Liu, J.; Zhang, J.-G.; et al. Tunable Oxygen Functional Groups as Electrocatalysts on Graphite Felt Surfaces for All-Vanadium Flow Batteries. *ChemSusChem* **2016**, *9*, 1455–1461. [CrossRef] [PubMed]
343. Kim, K.J.; Lee, S.-W.; Yim, T.; Kim, J.-G.; Choi, J.W.; Kim, J.H.; Park, M.-S.; Kim, Y.-J. A new strategy for integrating abundant oxygen functional groups into carbon felt electrode for vanadium redox flow batteries. *Sci. Rep.* **2014**, *4*, 6906. [CrossRef] [PubMed]
344. Su, A.-Q.; Wang, N.-F.; Liu, S.-Q.; Wu, T.; Peng, S. Modification of Carbon Paper Electrode via Hydrothermal Oxidation Applied in the Vanadium Redox Battery. *Act. Phys.-Chim. Sin.* **2012**, *28*, 1387–1392.
345. Taylor, S.M.; Patru, A.; Fabbri, E.; Schmidt, T.J. Influence of surface oxygen groups on V(II) oxidation reaction kinetics. *Electrochim. Commun.* **2017**, *75*, 13–16. [CrossRef]
346. Chen, J.-Z.; Liao, W.-Y.; Hsieh, W.-Y.; Hsu, C.-C.; Chen, Y.-S. All-vanadium redox flow batteries with graphite felt electrodes treated by atmospheric pressure plasma jets. *J. Power Sources* **2015**, *274*, 894–898. [CrossRef]
347. Chang, Y.-C.; Chen, J.-Y.; Kabtamu, D.M.; Lin, G.-Y.; Hsu, N.-Y.; Chou, Y.-S.; Wei, H.-J.; Wang, C.-H. High efficiency of CO₂-activated graphite felt as electrode for vanadium redox flow battery. *J. Power Sources* **2017**, *364*, 1–8. [CrossRef]
348. Li, C.; Xie, B.; Chen, J.; He, J.; He, Z. Enhancement of nitrogen and sulfur co-doping on the electrocatalytic properties of carbon nanotubes for VO²⁺/VO₂⁺(+) redox reaction. *RSC Adv.* **2017**, *7*, 13184–13190. [CrossRef]
349. Gursu, H.; Gencen, M.; Sahin, Y. Novel chlorine doped graphene electrodes for positive electrodes of a vanadium redox flow battery. *Int. J. Energy Res.* **2018**, *42*, 3303–3314. [CrossRef]
350. He, Z.; Jiang, Y.; Meng, W.; Jiang, F.; Zhou, H.; Li, Y.; Zhu, J.; Wang, L.; Dai, L. HF/H₂O₂ treated graphite felt as the positive electrode for vanadium redox flow battery. *Appl. Surf. Sci.* **2017**, *423*, 111–118. [CrossRef]

351. Park, J.J.; Park, J.H.; Park, O.O.; Yang, J.H. Highly porous graphenated graphite felt electrodes with catalytic defects for high-performance vanadium redox flow batteries produced via NiO/Ni redox reactions. *Carbon* **2016**, *110*, 17–26. [[CrossRef](#)]
352. Aoki, K.; Kaneko, H.; Nozaki, K. Estimation of charge transfer kinetic parameters from irreversible cyclic voltammograms at carbon fibre. *J. Electroanal. Chem.* **1988**, *247*, 29–36. [[CrossRef](#)]
353. Warburg, O.; Brefeld, W. Über die Aktivierung stickstoffhaltiger Kohlen durch Eisen. *Biochem. Z.* **1924**, *145*, 461–480.
354. Shao, Y.; Zhang, S.; Engelhard, M.H.; Li, G.; Shao, G.; Wang, Y.; Liu, J.; Aksay, I.A.; Lin, Y. Nitrogen-doped graphene and its electrochemical applications. *J. Mater. Chem.* **2010**, *20*, 7491–7496. [[CrossRef](#)]
355. He, Z.-X.; Liu, J.-L.; He, Z.; Liu, S.-Q. Nitrogen-doped Carbon Paper as Electrodes for Vanadium Redox Flow Batteries. *J. Inorg. Mater.* **2015**, *30*, 779–784.
356. Shao, Y.Y.; Wang, X.D.; Engelhard, M.; Wang, C.M.; Dai, S.; Liu, J.; Yang, Z.G.; Lin, Y.H. Nitrogen-doped mesoporous carbon for energy storage in vanadium redox flow batteries. *J. Power Sources* **2010**, *195*, 4375–4379. [[CrossRef](#)]
357. Liu, M.-Y.; Xiang, Z.-P.; Piao, J.-H.; Shi, J.-Y.; Liang, Z.-X. Electrochemistry of vanadium redox couples on nitrogen-doped carbon. *Electrochim. Acta* **2018**, *259*, 687–693. [[CrossRef](#)]
358. Kim, D.S.; Chung, D.J.; Park, H.-I.; Ansari, M.Z.; Song, T.; Kim, H. Direct Nitradated Graphite Felt as an Electrode Material for the Vanadium Redox Flow Battery. *Bull. Korean Chem. Soc.* **2018**, *39*, 281–286. [[CrossRef](#)]
359. Lee, H.J.; Kil, D.; Kim, H. Synthesis of Activated Graphite Felt Using Consecutive Post-Treatments for Vanadium Redox Flow Batteries. *J. Electrochem. Soc.* **2016**, *163*, A2586–A2591. [[CrossRef](#)]
360. He, Z.; Shi, L.; Shen, J.; He, Z.; Liu, S. Effects of nitrogen doping on the electrochemical performance of graphite felts for vanadium redox flow batteries. *Int. J. Energy Res.* **2015**, *39*, 709–716. [[CrossRef](#)]
361. Kim, J.; Lim, H.; Jyoung, J.-Y.; Lee, E.-S.; Yi, J.S.; Lee, D. Effects of Doping Methods and Kinetic Relevance of N and O Atomic Co-Functionalization on Carbon Electrode for V(IV)/V(V) Redox Reactions in Vanadium Redox Flow Battery. *Electrochim. Acta* **2017**, *245*, 724–733. [[CrossRef](#)]
362. Wu, T.; Huang, K.; Liu, S.; Zhuang, S.; Fang, D.; Li, S.; Lu, D.; Su, A. Hydrothermal ammoniated treatment of PAN-graphite felt for vanadium redox flow battery. *J. Solid State Electrochem.* **2012**, *16*, 579–585. [[CrossRef](#)]
363. He, Z.; Chen, Z.; Meng, W.; Jiang, Y.; Cheng, G.; Dai, L.; Wang, L. Modified carbon cloth as positive electrode with high electrochemical performance for vanadium redox flow batteries. *J. Energy Chem.* **2016**, *25*, 720–725. [[CrossRef](#)]
364. He, Z.; Su, A.; Gao, C.; Zhou, Z.; Pan, C.; Liu, S. Carbon paper modified by hydrothermal ammoniated treatment for vanadium redox battery. *Ionis* **2013**, *19*, 1021–1026. [[CrossRef](#)]
365. Jin, J.; Fu, X.; Liu, Q.; Liu, Y.; Wei, Z.; Niu, K.; Zhang, J. Identifying the Active Site in Nitrogen-Doped Graphene for the $\text{VO}^{2+}/\text{VO}_2^+$ Redox Reaction. *ACS Nano* **2013**, *7*, 4764–4773. [[CrossRef](#)] [[PubMed](#)]
366. Huang, Y.; Deng, Q.; Wu, X.; Wang, S. N, O Co-doped carbon felt for high-performance all-vanadium redox flow battery. *Int. J. Hydrogen Energy* **2017**, *42*, 7177–7185. [[CrossRef](#)]
367. Kim, J.; Lim, H.; Jyoung, J.-Y.; Lee, E.-S.; Yi, J.S.; Lee, D. High electrocatalytic performance of N and O atomic co-functionalized carbon electrodes for vanadium redox flow battery. *Carbon* **2017**, *111*, 592–601. [[CrossRef](#)]
368. Lee, H.J.; Kim, H. Graphite Felt Coated with Dopamine-Derived Nitrogen-Doped Carbon as a Positive Electrode for a Vanadium Redox Flow Battery. *J. Electrochem. Soc.* **2015**, *162*, A1675–A1681. [[CrossRef](#)]
369. Flox, C.; Skoumal, M.; Rubio-Garcia, J.; Andreu, T.; Morante, J.R. Strategies for enhancing electrochemical activity of carbon-based electrodes for all-vanadium redox flow batteries. *Appl. Energy* **2013**, *109*, 344–351. [[CrossRef](#)]
370. Kabtamu, D.M.; Chen, J.-Y.; Chang, Y.-C.; Wang, C.-H. Water-activated graphite felt as a high-performance electrode for vanadium redox flow batteries. *J. Power Sources* **2017**, *341*, 270–279. [[CrossRef](#)]
371. Mrha, J. Katalysatoren für die Elektroden der Brennstoffelemente II. Aktivkohle als Katalysator der Elektroreduktion des Sauerstoffes. *Collect. Czechoslov. Chem. Commun.* **1966**, *31*, 715–733. [[CrossRef](#)]
372. Mrha, J. Study of catalysts for fuel cell electrodes. IV. Active carbon electrodes for oxygen in alkaline electrolyte. *Collect. Czechoslov. Chem. Commun.* **1967**, *32*, 708–719. [[CrossRef](#)]
373. Hollax, E.; Cheng, D.S. The Influence of Oxidative Pretreatment of Graphite-Electrodes on the Catalysis of the $\text{Cr}^{3+}/\text{Cr}^{2+}$ and $\text{Fe}^{3+}/\text{Fe}^{2+}$ Redox Reactions. *Carbon* **1985**, *23*, 655–664. [[CrossRef](#)]

374. Lee, M.E.; Jin, H.-J.; Yun, Y.S. Synergistic catalytic effects of oxygen and nitrogen functional groups on active carbon electrodes for all-vanadium redox flow batteries. *RSC Adv.* **2017**, *7*, 43227–43232. [[CrossRef](#)]
375. Walling, C. Fenton’s Reagent Revisited. *Acc. Chem. Res.* **1975**, *8*, 125–131. [[CrossRef](#)]
376. Brillas, E.; Sires, I.; Oturan, M.A. Electro-Fenton Process and Related Electrochemical Technologies Based on Fenton’s Reaction Chemistry. *Chem. Rev.* **2009**, *109*, 6570–6631. [[CrossRef](#)] [[PubMed](#)]
377. Gao, C.; Wang, N.F.; Peng, S.; Lin, S.Q.; Lei, Y.; Liang, X.X.; Zeng, S.S.; Zi, H.F. Influence of Fenton’s reagent treatment on electrochemical properties of graphite felt for all vanadium redox flow battery. *Electrochim. Acta* **2013**, *88*, 193–202. [[CrossRef](#)]
378. He, Z.; Jiang, Y.; Li, Y.; Wang, L.; Dai, L. Boosting the electrocatalytic performance of carbon nanotubes toward V(V)/V(IV) reaction by sulfonation treatment. *Int. J. Energy Res.* **2018**, *42*, 1625–1634. [[CrossRef](#)]
379. Huang, P.; Ling, W.; Sheng, H.; Zhou, Y.; Wu, X.; Zeng, X.-X.; Wu, X.; Guo, Y.-G. Heteroatom-doped electrodes for all-vanadium redox flow batteries with ultralong lifespan. *J. Mater. Chem.* **2018**, *A6*, 41–44. [[CrossRef](#)]
380. Ge, Z.; Wang, L.; He, Z.; Li, Y.; Jiang, Y.; Meng, W.; Dai, L. Electrocatalytic activity of cobalt phosphide-modified graphite felt toward $\text{VO}^{2+}/\text{VO}_2^+$ redox reaction. *Appl. Surf. Sci.* **2018**, *436*, 1030–1037. [[CrossRef](#)]
381. Maruyama, J.; Hasegawa, T.; Iwasaki, S.; Fukuhara, T.; Orikasa, Y.; Uchimoto, Y. Catalysis of Vanadium Ion Redox Reactions on Carbonaceous Material with Metal-N-4 Sites. *ChemCatChem* **2015**, *7*, 2305–2308. [[CrossRef](#)]
382. Maruyama, J.; Hasegawa, T.; Iwasaki, S.; Fukuhara, T.; Orikasa, Y.; Uchimoto, Y. Carbonaceous thin film coating with Fe-N-4 site for enhancement of dioxovanadium ion reduction. *J. Power Sources* **2016**, *324*, 521–527. [[CrossRef](#)]
383. Maruyama, J.; Shinagawa, T. Catalyst Layer Structures for Enhancement of Redox Reactions of V(IV/V) Ions. *Electrochim. Acta* **2016**, *210*, 854–861. [[CrossRef](#)]
384. Chou, Y.-S.; Jeng, K.-T.; Yen, S.-C. Characterization and electrochemical properties of graphite felt-based electrode modified using an ionomer impregnation approach for vanadium redox flow battery. *Electrochim. Acta* **2017**, *251*, 109–118. [[CrossRef](#)]
385. Pupkevich, V.; Glibin, V.; Karamanov, D. The effect of activation on the electrochemical behaviour of graphite felt towards the $\text{Fe}^{3+}/\text{Fe}^{2+}$ redox electrode reaction. *Electrochim. Commun.* **2007**, *9*, 1924–1930. [[CrossRef](#)]
386. Kokkinidis, G. Underpotential deposition and electrocatalysis. *J. Electroanal. Chem.* **1986**, *201*, 217–236. [[CrossRef](#)]
387. Trasatti, S. Electrocatalysis of Hydrogen Evolution: Progress in Cathode Activation. In *Advances in Electrochemical Science and Engineering*; Gerischer, H., Tobias, C.W., Eds.; VCH: Weinheim, Germany, 1990; Volume 2, pp. 1–85.
388. Ross, P.N. The Science of Catalysis on Bimetallic Surfaces. In *Electrocatalysis*; Lipkowski, J., Ross, P.N., Eds.; Wiley-VCH: New York, NY, USA, 1998; pp. 43–74.
389. Dapperheld, S. Elektrokatalytisches Verfahren zur Aufbereitung von Mutterlaugen aus der Chloressigsäure-Produktion. In *DECHEMA-Monographie*; VCH Verlagsgesellschaft: Weinheim, Germany, 1988; Volume 112, pp. 317–324.
390. Holze, R.; Fette, U. The Electrocatalysis of Dichloroacetic Acid Reduction at Lead-Modified Carbon Electrodes. *J. Electroanal. Chem.* **1992**, *339*, 247–253. [[CrossRef](#)]
391. Holze, R.; Fette, U. Zur Elektrokatalyse der Dichloressigsäurereduktion. In *DECHEMA-Monographie*; VCH Verlagsgesellschaft: Weinheim, Germany, 1992; Volume 125, pp. 769–775.
392. Wang, W.; Wang, X. Study of the electrochemical properties of a transition metallic ions modified electrode in acidic VOSO_4 solution. *Rare Met.* **2007**, *26*, 131–135. [[CrossRef](#)]
393. Sun, B.T.; Skyllas-Kazacos, M. Chemical modification and electrochemical behaviour of graphite fibre in acidic vanadium solution. *Electrochim. Acta* **1991**, *36*, 513–517. [[CrossRef](#)]
394. Mehboob, S.; Mehmood, A.; Lee, J.-Y.; Shin, H.-J.; Hwang, J.; Abbas, S.; Ha, H.Y. Excellent electrocatalytic effects of tin through in situ electrodeposition on the performance of all-vanadium redox flow batteries. *J. Mater. Chem.* **2017**, *A5*, 17388–17400. [[CrossRef](#)]
395. Xiang, Y.; Daoud, W.A. Electrochemical Enhancement of Carbon Paper by Indium Modification for the Positive Side of Vanadium Redox Flow Battery. *J. Electrochem. Soc.* **2017**, *164*, A2256–A2261. [[CrossRef](#)]

396. Suarez, D.J.; Gonzalez, Z.; Blanco, C.; Granda, M.; Menendez, R.; Santamaria, R. Graphite Felt Modified with Bismuth Nanoparticles as Negative Electrode in a Vanadium Redox Flow Battery. *ChemSusChem* **2014**, *7*, 914–918. [CrossRef] [PubMed]
397. Liu, T.; Li, X.; Nie, H.; Xu, C.; Zhang, H. Investigation on the effect of catalyst on the electrochemical performance of carbon felt and graphite felt for vanadium flow batteries. *J. Power Sources* **2015**, *286*, 73–81. [CrossRef]
398. Li, B.; Gu, M.; Nie, Z.; Shao, Y.; Luo, Q.; Wei, X.; Li, X.; Xiao, J.; Wang, C.; Sprengle, V.; et al. Bismuth Nanoparticle Decorating Graphite Felt as a High-Performance Electrode for an All-Vanadium Redox Flow Battery. *Nano Lett.* **2013**, *13*, 1330–1335. [CrossRef] [PubMed]
399. Yang, X.; Liu, T.; Xu, C.; Zhang, H.; Li, X.; Zhang, H. The catalytic effect of bismuth for $\text{VO}^{2+}/\text{VO}_2^+$ and $\text{V}^{3+}/\text{V}^{2+}$ redox couples in vanadium flow batteries. *J. Energy Chem.* **2017**, *26*, 1–7. [CrossRef]
400. Lv, Y.; Zhang, J.; Lv, Z.; Wu, C.; Liu, Y.; Wang, H.; Lu, S.; Xiang, Y. Enhanced electrochemical activity of carbon felt for $\text{V}^{3+}/\text{V}^{2+}$ redox reaction via combining KOH-etched pretreatment with uniform deposition of Bi nanoparticles. *Electrochim. Acta* **2017**, *253*, 78–84. [CrossRef]
401. Shen, J.; Liu, S.; He, Z.; Shi, L. Influence of antimony ions in negative electrolyte on the electrochemical performance of vanadium redox flow batteries. *Electrochim. Acta* **2015**, *151*, 297–305. [CrossRef]
402. Flox, C.; Rubio-Garcia, J.; Nafria, R.; Zamani, R.; Skoumal, M.; Andreu, T.; Arbiol, J.; Cabot, A.; Morante, J.R. Active nano-CuPt₃ electrocatalyst supported on graphene for enhancing reactions at the cathode in all-Vanadium redox flow batteries. *Carbon* **2012**, *50*, 2372–2374. [CrossRef]
403. Wei, L.; Zhao, T.S.; Zeng, L.; Zhou, X.L.; Zeng, Y.K. Copper nanoparticle-deposited graphite felt electrodes for all vanadium redox flow batteries. *Appl. Energy* **2016**, *180*, 386–391. [CrossRef]
404. Han, P.; Wang, X.; Zhang, L.; Wang, T.; Yao, J.; Huang, C.; Gu, L.; Cui, G. RuSe/reduced graphene oxide: An efficient electrocatalyst for $\text{VO}^{2+}/\text{VO}_2^+$ redox couples in vanadium redox flow batteries. *RSC Adv.* **2014**, *4*, 20379–20381. [CrossRef]
405. Huang, R.-H.; Sun, C.-H.; Tseng, T.-M.; Chao, W.-K.; Hsueh, K.-L.; Shieh, F.-S. Investigation of Active Electrodes Modified with Platinum/Multiwalled Carbon Nanotube for Vanadium Redox Flow Battery. *J. Electrochem. Soc.* **2012**, *159*, A1579–A1586. [CrossRef]
406. Tseng, T.-M.; Huang, R.-H.; Huang, C.-Y.; Hsueh, K.-L.; Shieh, F.-S. A Kinetic Study of the Platinum/Carbon Anode Catalyst for Vanadium Redox Flow Battery. *J. Electrochem. Soc.* **2013**, *160*, A690–A696. [CrossRef]
407. Tsai, H.-M.; Yang, S.-J.; Ma, C.-C.M.; Xie, X. Preparation and electrochemical activities of iridium-decorated graphene as the electrode for all-vanadium redox flow batteries. *Electrochim. Acta* **2012**, *77*, 232–236. [CrossRef]
408. Chang, C.H.; Yuen, T.S.; Nagao, Y.; Yugami, H. Electrocatalytic activity of iridium oxide nanoparticles coated on carbon for oxygen reduction as cathode catalyst in polymer electrolyte fuel cell. *J. Power Sources* **2010**, *195*, 5938–5941. [CrossRef]
409. Wang, W.H.; Wang, X.D. Investigation of Ir-modified carbon felt as the positive electrode of an all-vanadium redox flow battery. *Electrochim. Acta* **2007**, *52*, 6755–6762. [CrossRef]
410. Fuh, Y.-K.; Chang, T.-C.; Zhang, J.-P. Electroless Plating on Porous Carbon Felts in Redox Flow Batteries and Thickness Effect on the Electrical and Mechanical Properties. *Int. J. Electrochem. Sci.* **2013**, *8*, 8989–8999.
411. Ma, Q.; Deng, Q.; Sheng, H.; Ling, W.; Wang, H.R.; Jiao, H.W.; Wu, X.W.; Zhou, W.X.; Zeng, X.X.; Yin, Y.X.; et al. High electro-catalytic graphite felt/MnO₂ composite electrodes for vanadium redox flow batteries. *Sci. China Chem.* **2018**, *48*, 1–7. [CrossRef]
412. He, Z.; Dai, L.; Liu, S.; Wang, L.; Li, C. Mn₃O₄ anchored on carbon nanotubes as an electrode reaction catalyst of V(IV)/V(V) couple for vanadium redox flow batteries. *Electrochim. Acta* **2015**, *176*, 1434–1440. [CrossRef]
413. Ejigu, A.; Edwards, M.; Walsh, D.A. Synergistic Catalyst-Support Interactions in a Graphene-Mn₃O₄ Electrocatalyst for Vanadium Redox Flow Batteries. *ACS Catal.* **2015**, *5*, 7122–7130. [CrossRef]
414. Wu, X.; Xu, H.; Lu, L.; Zhao, H.; Fu, J.; Shen, Y.; Xu, P.; Dong, Y. PbO₂-modified graphite felt as the positive electrode for an all-vanadium redox flow battery. *J. Power Sources* **2014**, *250*, 274–278. [CrossRef]
415. Yao, C.; Zhang, H.; Liu, T.; Li, X.; Liu, Z. Carbon paper coated with supported tungsten trioxide as novel electrode for all-vanadium flow battery. *J. Power Sources* **2012**, *218*, 455–461. [CrossRef]
416. Faraji, M.; Hassanzadeh, A.; Mohseni, M. Interlaced WO₃-carbon nanotube nanocomposite electrodeposited on graphite as a positive electrode in vanadium redox flow battery. *Thin Solid Films* **2017**, *642*, 188–194. [CrossRef]

417. Shen, Y.; Xu, H.; Xu, P.; Wu, X.; Dong, Y.; Lu, L. Electrochemical catalytic activity of tungsten trioxide-modified graphite felt toward $\text{VO}^{2+}/\text{VO}_2^+$ redox reaction. *Electrochim. Acta* **2014**, *132*, 37–41. [CrossRef]
418. Zhou, H.; Shen, Y.; Xi, J.; Qiu, X.; Chen, L. ZrO_2 -Nanoparticle-Modified Graphite Felt: Bifunctional Effects on Vanadium Flow Batteries. *ACS Appl. Mater. Interf.* **2016**, *8*, 15369–15378. [CrossRef] [PubMed]
419. Kabtamu, D.M.; Chen, J.-Y.; Chang, Y.-C.; Wang, C.-H. Electrocatalytic activity of Nb-doped hexagonal WO_3 nanowire-modified graphite felt as a positive electrode for vanadium redox flow batteries. *J. Mater. Chem.* **2016**, *A4*, 11472–11480. [CrossRef]
420. Hosseini, M.G.; Mousavishahemi, S.; Murcia-Lopez, S.; Flox, C.; Andreu, T.; Morante, J.R. High-power positive electrode based on synergistic effect of N- and WO_3 -decorated carbon felt for vanadium redox flow batteries. *Carbon* **2018**, *136*, 444–453. [CrossRef]
421. Cao, L.; Skyllas-Kazacos, M.; Wang, D.-W. Modification Based on MoO_3 as Electrocatalysts for High Power Density Vanadium Redox Flow Batteries. *ChemElectroChem* **2017**, *4*, 1836–1839. [CrossRef]
422. Pham, H.T.T.; Jo, C.; Lee, J.; Kwon, Y. MoO_2 nanocrystals interconnected on mesocellular carbon foam as a powerful catalyst for vanadium redox flow battery. *RSC Adv.* **2016**, *6*, 17574–17582. [CrossRef]
423. Vazquez-Galvan, J.; Flox, C.; Fàbrega, C.; Ventosa, E.; Parra, A.; Andreu, T.; Morante, J.R. Hydrogen-Treated Rutile TiO_2 Shell in Graphite-Core Structure as a Negative Electrode for High-Performance Vanadium Redox Flow Batteries. *ChemSusChem* **2017**, *10*, 2089–2098. [CrossRef] [PubMed]
424. Tseng, T.-M.; Huang, R.-H.; Huang, C.-Y.; Hsueh, K.-L.; Shieu, F.-S. Improvement of Titanium Dioxide Addition on Carbon Black Composite for Negative Electrode in Vanadium Redox Flow Battery. *J. Electrochem. Soc.* **2013**, *160*, A1269–A1275. [CrossRef]
425. Tseng, T.-M.; Huang, R.-H.; Huang, C.-Y.; Liu, C.-C.; Hsueh, K.-L.; Shieu, F.-S. Carbon Felt Coated with Titanium Dioxide/Carbon Black Composite as Negative Electrode for Vanadium Redox Flow Battery. *J. Electrochem. Soc.* **2014**, *161*, A1132–A1138. [CrossRef]
426. He, Z.; Li, M.; Li, Y.; Zhu, J.; Jiang, Y.; Meng, W.; Zhou, H.; Wang, L.; Dai, L. Flexible electrospun carbon nanofiber embedded with TiO_2 as excellent negative electrode for vanadium redox flow battery. *Electrochim. Acta* **2018**, *281*, 601–610. [CrossRef]
427. Bayeh, A.W.; Kabtamu, D.M.; Chang, Y.-C.; Chen, G.-C.; Chen, H.-Y.; Lin, G.-Y.; Liu, T.-R.; Wondimu, T.H.; Wang, K.-C.; Wang, C.-H. Ta_2O_5 -Nanoparticle-Modified Graphite Felt As a High-Performance Electrode for a Vanadium Redox Flow Battery. *ACS Sustain. Chem. Eng.* **2018**, *6*, 3019–3028. [CrossRef]
428. Fetyan, A.; El-Nagar, G.A.; Derr, I.; Kubella, P.; Dau, H.; Roth, C. A neodymium oxide nanoparticle-doped carbon felt as promising electrode for vanadium redox flow batteries. *Electrochim. Acta* **2018**, *268*, 59–65. [CrossRef]
429. Li, B.; Gu, M.; Nie, Z.; Wie, X.; Wang, C.; Sprenkle, V.; Wang, W. Nanorod Niobium Oxide as Powerful Catalysts for an All Vanadium Redox Flow Battery. *Nano Lett.* **2014**, *14*, 158–165. [CrossRef] [PubMed]
430. Yan, L.; Rui, X.; Chen, G.; Xu, W.; Zou, G.; Luo, H. Recent advances in nanostructured Nb-based oxides for electrochemical energy storage. *Nanoscale* **2016**, *8*, 8443–8465. [CrossRef] [PubMed]
431. Gobal, F.; Faraji, M. $\text{RuO}_2/\text{MWCNT}$ /stainless steel mesh as a novel positive electrode in vanadium redox flow batteries. *RSC Adv.* **2015**, *5*, 68378–68384. [CrossRef]
432. Zhou, H.; Xi, J.; Li, Z.; Zhang, Z.; Yu, L.; Liu, L.; Qiu, X.; Chen, L. CeO_2 decorated graphite felt as a high-performance electrode for vanadium redox flow batteries. *RSC Adv.* **2014**, *4*, 61912–61918. [CrossRef]
433. Holze, R. Carbon as Electrocatalyst for Applications in Electrochemical Energy Conversion—An Overview. In Proceedings of the 4th International Carbon Conference (Carbon'86), Baden-Baden, Germany, 30 June–4 July 1986; pp. 361–363.
434. Krüger, A. *Neue Kohlenstoffmaterialien*; Teubner-Verlag: Wiesbaden, Germany, 2007.
435. Haddadi-Asl, V.; Kazacos, M.; Skyllas-Kazacos, M. Carbon-Polymer Composite Electrodes for Redox Cells. *J. Appl. Polym. Sci.* **1995**, *57*, 1455–1463. [CrossRef]
436. Haddadi-Asl, V.; Kazacos, M.; Skyllas-Kazacos, M. Conductive carbon-polypropylene composite electrodes for vanadium redox battery. *J. Appl. Electrochem.* **1995**, *25*, 29–33. [CrossRef]
437. Zhang, Y.-M.; Huang, Q.-M.; Li, W.-S.; Peng, H.-Y.; Hu, S.-J. Graphite-acetylene black composite electrodes for all vanadium redox flow battery. *J. Inorg. Mater.* **2007**, *22*, 1051–1055.
438. Tsai, H.-M.; Yang, S.-Y.; Ma, C.-C.M.; Xie, X. Preparation and Electrochemical Properties of Graphene-Modified Electrodes for All-Vanadium Redox Flow Batteries. *Electroanalysis* **2011**, *23*, 2139–2143. [CrossRef]

439. Ji, Y.; Li, J.L.; Li, S.F.Y. Synergistic effect of the bifunctional polydopamine-Mn₃O₄ composite electrocatalyst for vanadium redox flow batteries. *J. Mater. Chem.* **2017**, *A5*, 15154–15166. [[CrossRef](#)]
440. Kabtamu, D.M.; Chang, Y.-C.; Lin, G.-Y.; Bayeh, A.W.; Chen, J.-Y.; Wondimu, T.H.; Wang, C.-H. Three-dimensional annealed WO₃ nanowire/graphene foam as an electrocatalytic material for all vanadium redox flow batteries. *Sustain. Energy Fuels* **2017**, *1*, 2091–2100. [[CrossRef](#)]
441. Bayeh, A.W.; Kabtamu, D.M.; Chang, Y.-C.; Chen, G.-C.; Chen, H.-Y.; Lin, G.-Y.; Liu, T.-R.; Wondimu, T.H.; Wang, K.-C.; Wang, C.-H. Synergistic effects of a TiNb₂O₇-reduced graphene oxide nanocomposite electrocatalyst for highperformance all-vanadium redox flow batteries. *J. Mater. Chem. A* **2018**, *6*, 13908–13917. [[CrossRef](#)]
442. Patil, J.V.; Mali, S.S.; Kamble, A.S.; Hong, C.K.; Kim, J.H.; Patil, P.S. Electrospinning: A versatile technique for making of 1D growth of nanostructured nanofibers and its applications: An experimental approach. *Appl. Surf. Sci.* **2017**, *423*, 641–674. [[CrossRef](#)]
443. Fetyan, A.; Derr, I.; Kayarkatte, M.K.; Langner, J.; Bernsmeier, D.; Krahnert, R.; Roth, C. Electrospun Carbon Nanofibers as Alternative Electrode Materials for Vanadium Redox Flow Batteries. *ChemElectroChem* **2015**, *2*, 2055–2060. [[CrossRef](#)]
444. Flox, C.; Fabrega, C.; Andreu, T.; Morata, A.; Skoumal, M.; Rubio-Garcia, J.; Morante, J.R. Highly electrocatalytic flexible nanofiber for improved vanadium-based redox flow battery cathode electrodes. *RSC Adv.* **2013**, *3*, 12056–12059. [[CrossRef](#)]
445. Wei, G.; Su, W.; Wei, Z.; Jing, M.; Fan, X.; Liu, J.; Yan, C. Effect of the graphitization degree for electrospun carbon nanofibers on their electrochemical activity towards VO²⁺/VO₂⁺ redox couple. *Electrochim. Acta* **2016**, *199*, 147–153. [[CrossRef](#)]
446. Etesami, M.; Abouzari-Loff, E.; Sha'rani, S.S.; Miyake, M.; Nia, P.M.; Ripin, A.; Ahmad, A. Self-assembled heteropolyacid on nitrogen-enriched carbon nanofiber for vanadium flow batteries. *Nanoscale* **2018**, *10*, 13212–13222. [[CrossRef](#)] [[PubMed](#)]
447. Jing, M.; Zhang, X.; Fan, X.; Zhao, L.; Liu, J.; Yan, C. CeO₂ embedded electrospun carbon nanofibers as the advanced electrode with high effective surface area for vanadium flow battery. *Electrochim. Acta* **2016**, *215*, 57–65. [[CrossRef](#)]
448. Xu, C.; Yang, X.; Li, X.; Liu, T.; Zhang, H. Ultrathin free-standing electrospun carbon nanofibers web as the electrode of the vanadium flow batteries. *J. Energy Chem.* **2017**, *26*, 730–737. [[CrossRef](#)]
449. Wei, G.; Liu, J.; Zhao, H.; Yan, C. Electrospun carbon nanofibres as electrode materials toward VO²⁺/VO₂⁺ redox couple for vanadium flow battery. *J. Power Sources* **2013**, *241*, 709–717. [[CrossRef](#)]
450. Wei, G.; Gao, Z.; Wei, Z.; Fan, X.; Liu, J.; Yan, C. Coupling effect between the structure and surface characteristics of electrospun carbon nanofibres on the electrochemical activity towards the VO²⁺/VO₂⁺ redox couple. *Phys. Chem. Chem. Phys.* **2015**, *17*, 20368–20375. [[CrossRef](#)] [[PubMed](#)]
451. Wei, G.; Fan, X.; Liu, J.; Yan, C. Investigation of the electrospun carbon web as the catalyst layer for vanadium redox flow battery. *J. Power Sources* **2014**, *270*, 634–645. [[CrossRef](#)]
452. Shi, L.; Liu, S.; He, Z.; Yuan, H.; Shen, J. Synthesis of boron and nitrogen co-doped carbon nanofiber as efficient metal-free electrocatalyst for the Redox Reaction. *Electrochim. Acta* **2015**, *178*, 748–757. [[CrossRef](#)]
453. Busacca, C.; Di Blasi, O.; Briguglio, N.; Ferraro, M.; Antonucci, V.; Di Blasi, A. Electrochemical performance investigation of electrospun urchin-like V₂O₃-CNF composite nanostructure for vanadium redox flow battery. *Electrochim. Acta* **2017**, *230*, 174–180. [[CrossRef](#)]
454. Di Blasi, A.; Busacca, C.; Di Blasia, O.; Briguglio, N.; Squadrito, G.; Antonuccia, V. Synthesis of flexible electrodes based on electrospun carbon nanofibers with Mn₃O₄ nanoparticles for vanadium redox flow battery application. *Appl. Energy* **2017**, *190*, 165–171. [[CrossRef](#)]
455. Wei, G.; Fan, X.; Liu, J.; Yan, C. Electrospun carbon nanofibers/electrocatalyst hybrids as asymmetric electrodes for vanadium redox flow battery. *J. Power Sources* **2015**, *281*, 1–6. [[CrossRef](#)]
456. Han, J.; Yoo, H.; Kim, M.; Lee, G.; Choi, J. High-performance bipolar plate of thin IrO_x-coated TiO₂ nanotubes in vanadium redox flow batteries. *Catal. Today* **2017**, *295*, 132–139. [[CrossRef](#)]
457. Wei, L.; Zhao, T.S.; Zeng, L.; Zeng, Y.K.; Jiang, H.R. Highly catalytic and stabilized titanium nitride nanowire array-decorated graphite felt electrodes for all vanadium redox flow batteries. *J. Power Sources* **2017**, *341*, 318–326. [[CrossRef](#)]

458. Zhao, F.-M.; Wen, G.; Kong, L.-Y.; Chu, Y.-Q.; Ma, C.-A. Structure Characteristic of Titanium Nitride Nanowires and Its Electrode Processes for V(II)/V(III) Redox Couple. *Acta Phys. Chim. Sin.* **2017**, *33*, 1181–1188.
459. Zhao, F.-M.; Wen, G.; Kong, L.-Y.; Chu, C.-Q.; Ma, C.-A. Electrochemical Performance of Titanium Nitride Nanotubes as Negative Electrode in a Static Vanadium Battery Towards V(II)/V(III) Redox Couple. *Chin. J. Inorg. Chem.* **2017**, *33*, 501–508.
460. Wei, L.; Zhao, T.; Zeng, L.; Zhou, X.; Zeng, Y. Titanium Carbide Nanoparticle-Decorated Electrode Enables Significant Enhancement in Performance of All-Vanadium Redox Flow Batteries. *Energy Technol.* **2016**, *4*, 990–996. [CrossRef]
461. Yang, C.; Wang, H.; Lu, S.; Wu, C.; Liu, Y.; Tan, Q.; Liang, D.; Xiang, Y. Titanium nitride as an electrocatalyst for V(II)/V(III) redox couples in all-vanadium redox flow batteries. *Electrochim. Acta* **2015**, *182*, 834–840. [CrossRef]
462. Huang, Y.; Huo, J.; Dou, S.; Hu, K.; Wang, S. Graphitic C₃N₄ as a powerful catalyst for all-vanadium redox flow batteries. *RSC Adv.* **2016**, *6*, 66368–66372. [CrossRef]
463. Su, J.; Zhao, Y.; Xi, J. Phosphorus-doped carbon nitride as powerful electrocatalyst for highpower vanadium flow battery. *Electrochim. Acta* **2018**, *286*, 22–28. [CrossRef]
464. Liu, H.; Cai, T.; Song, Q.; Yang, L.; Xu, Q.; Yan, C. Electrochemical Behavior of the Titanium Plate with Carbon Films in a Vanadium Sulfate Solution. *Int. J. Electrochem. Sci.* **2013**, *8*, 2515–2523.
465. Chandrabose Raghu, S.; Ulaganathan, M.; Lim, T.M.; Skyllas-Kazacos, M. Electrochemical behaviour of titanium/iridium(IV) oxide: Tantalum pentoxide and graphite for application in vanadium redox flow battery. *J. Power Sources* **2013**, *238*, 103–108. [CrossRef]
466. Lee, W.; Jo, C.; Youk, S.; Shin, H.Y.; Lee, J.; Chung, Y.; Kwon, Y. Mesoporous tungsten oxynitride as electrocatalyst for promoting redox reactions of vanadium redox couple and performance of vanadium redox flow battery. *Appl. Surf. Sci.* **2018**, *429*, 187–195. [CrossRef]
467. Flox, C.; Murcia-Lopez, S.; Carretero, N.M.; Ros, C.; Morante, J.R.; Andreu, T. Role of Bismuth in the Electrokinetics of Silicon Photocathodes for Solar Rechargeable Vanadium Redox Flow Batteries. *ChemSusChem* **2018**, *11*, 125–129. [CrossRef] [PubMed]
468. He, Z.; Chen, L.; He, Y.; Chen, C.; Jiang, Y.; He, Z.; Liu, S. Effect of In³⁺ ions on the electrochemical performance of the positive electrolyte for vanadium redox flow batteries. *Ionics* **2013**, *19*, 1915–1920. [CrossRef]
469. Huang, F.; Zhang, Q.; Luo, C.-H.; Wang, G.X.; Yan, K.P.; Luo, D.M. Influence of Cr³⁺ concentration on the electrochemical behavior of the anolyte for vanadium redox flow batteries. *Chin. Sci. Bull.* **2012**, *57*, 4237–4243. [CrossRef]
470. Huang, F.; Wang, G.-X.; Yan, K.-P.; Luo, D.-M. Influence of Mn²⁺ Concentration on the Electrochemical Behavior of the Anolyte for Vanadium Redox Flow Batteries. *Chin. J. Inorg. Chem.* **2012**, *28*, 898–904.
471. Kim, M.; Yoo, H.; Lee, G.; Choi, J. Enhanced VRB electrochemical performance using tungsten as an electrolyte additive. *Electrochim. Acta* **2017**, *246*, 190–196. [CrossRef]
472. Li, S.; Huang, K.; Lu, S.; Fang, D.; Wu, X.; Lu, D.; Wu, T. Effect of organic additives on positive electrolyte for vanadium redox battery. *Electrochim. Acta* **2011**, *56*, 5483–5487. [CrossRef]
473. Kazacos, M.; Skyllas-Kazacos, M. High Energy Density Vanadium Electrolyte Solutions. WO Patent 96/35239, 7 November 1996.
474. Skyllas-Kazacos, M.; Kazacos, M. Stabilised Electrolyte Solutions, Methods of Preparation Thereof and Redox Cells and Batteries Containing Stabilised Electrolyte Solutions. U.S. Patent 6,143,443, 7 November 2000.
475. Samad, M.; Kazacos, M.; Skyllas-Kazacos, M. Stabilised Electrolyte Solutions. WO Patent 95/12219, 4 May 1992.
476. Hwang, J.; Kim, B.-M.; Moon, J.; Mehmood, A.; Ha, H.Y. A highly efficient and stable organic additive for the positive electrolyte in vanadium redox flow batteries: Taurine biomolecules containing -NH₂ and -SO₃H functional groups. *J. Mater. Chem.* **2018**, *A6*, 4695–4705. [CrossRef]
477. Yang, Y.; Zhang, Y.; Liu, T.; Huang, J. Improved properties of positive electrolyte for a vanadium redox flow battery by adding taurine. *Res. Chem. Intermed.* **2018**, *44*, 769–786. [CrossRef]
478. Jia, Z.; Wang, B.; Song, S.; Chen, X. Effect of Polyhydroxy-Alcohol on the Electrochemical Behavior of the Positive Electrolyte for Vanadium Redox Flow Batteries. *J. Electrochem. Soc.* **2012**, *159*, A843–A847. [CrossRef]

479. Wu, X.; Liu, S.; Wang, N.; Peng, S.; He, Z. Influence of organic additives on electrochemical properties of the positive electrolyte for all-vanadium redox flow battery. *Electrochim. Acta* **2012**, *78*, 475–482. [[CrossRef](#)]
480. Han, H.; He, Z.; Liu, J.; Chen, Y.; Liu, S. Effects of pyridine carboxylic acid on the positive electrolyte for vanadium redox flow battery. *Ionics* **2015**, *21*, 167–174. [[CrossRef](#)]
481. Wang, G.; Chen, J.; Xu, Y.; Yan, B.; Wang, X.; Zhu, X.; Zhang, Y.; Liu, X.; Wang, R. Several ionic organic compounds as positive electrolyte additives for a vanadium redox flow battery. *RSC Adv.* **2014**, *4*, 63025–63035. [[CrossRef](#)]
482. Wu, X.-W.; Liu, S.-Q.; Huang, R.-L. Characteristics of CTAB as Electrolyte Additive for Vanadium Redox Flow Battery. *J. Inorg. Mater.* **2010**, *25*, 641–646. [[CrossRef](#)]
483. Wang, G.; Zhang, J.; Zhang, J.; Chen, J.; Zhu, S.; Liu, X.; Wang, R. Effect of different additives with $-\text{NH}_2$ or $-\text{NH}_4^+$ functional groups on V(V) electrolytes for a vanadium redox flow battery. *J. Electroanal. Chem.* **2016**, *768*, 62–71. [[CrossRef](#)]
484. Wang, G.; Chen, J.; Wang, X.; Tian, J.; Kang, H.; Zhu, X.; Zhang, Y.; Liu, X.; Wang, R. Influence of several additives on stability and electrochemical behavior of V(V) electrolyte for vanadium redox flow battery. *J. Electroanal. Chem.* **2013**, *709*, 31–38. [[CrossRef](#)]
485. Liu, J.; Liu, S.; He, Z.; Han, H.; Chen, Y. Effects of organic additives with oxygen- and nitrogen-containing functional groups on the negative electrolyte of vanadium redox flow battery. *Electrochim. Acta* **2014**, *130*, 314–321. [[CrossRef](#)]
486. Liang, X.; Peng, S.; Lei, Y.; Gao, C.; Wang, N.; Liu, S.; Fang, D. Effect of l-glutamic acid on the positive electrolyte for all-vanadium redox flow battery. *Electrochim. Acta* **2013**, *95*, 80–86. [[CrossRef](#)]
487. He, Z.; Liu, J.; Han, H.; Chen, Y.; Zhou, Z.; Zheng, S.; Lu, W.; Liu, S.; He, Z. Effects of organic additives containing $-\text{NH}_2$ and $-\text{SO}_3\text{H}$ on electrochemical properties of vanadium redox flow battery. *Electrochim. Acta* **2013**, *106*, 556–562. [[CrossRef](#)]
488. Chang, F.; Hu, C.; Liu, X.; Liu, L.; Zhang, J. Coulter dispersant as positive electrolyte additive for the vanadium redox flow battery. *Electrochim. Acta* **2012**, *60*, 334–338. [[CrossRef](#)]
489. Nguyen, T.D.; Whitehead, A.; Scherer, G.G.; Wai, N.; Oo, M.O.; Bhattacharai, A.; Chandra, G.P.; Xu, Z.J. The oxidation of organic additives in the positive vanadium electrolyte and its effect on the performance of vanadium redox flow battery. *J. Power Sources* **2016**, *334*, 94–103. [[CrossRef](#)]
490. Li, L.Y.; Kim, S.; Wang, W.; Vijayakumar, M.; Nie, Z.M.; Chen, B.W.; Zhang, J.L.; Xia, G.G.; Hu, J.Z.; Graff, G.; et al. A Stable Vanadium Redox-Flow Battery with High Energy Density for Energy Storage. *Adv. Energy Mater.* **2011**, *1*, 394–400. [[CrossRef](#)]
491. Roe, S.; Menictas, C.; Skyllas-Kazacos, M. A High Energy Density Vanadium Redox Flow Battery with 3 M Vanadium Electrolyte. *J. Electrochem. Soc.* **2016**, *163*, A5023–A5028. [[CrossRef](#)]
492. Skyllas-Kazacos, M.; Peng, C.; Cheng, M. Evaluation of precipitation inhibitors for supersaturated vanadyl electrolytes for the vanadium redox battery. *Electrochim. Solid State Lett.* **1999**, *2*, 121–122. [[CrossRef](#)]
493. Mousa, A.; Skyllas-Kazacos, M. Effect of Additives on the Low-Temperature Stability of Vanadium Redox Flow Battery Negative Half-Cell Electrolyte. *ChemElectroChem* **2015**, *2*, 1742–1751. [[CrossRef](#)]
494. Kausar, N.; Mousa, A.; Skyllas-Kazacos, M. The Effect of Additives on the High-Temperature Stability of the Vanadium Redox Flow Battery Positive Electrolytes. *ChemElectroChem* **2016**, *3*, 276–282. [[CrossRef](#)]
495. Rahman, F.; Skyllas-Kazacos, M. Evaluation of additive formulations to inhibit precipitation of positive electrolyte in vanadium battery. *J. Power Sources* **2017**, *340*, 139–149. [[CrossRef](#)]
496. Park, S.-K.; Shim, J.; Yang, J.H.; Jin, C.-S.; Lee, B.S.; Lee, Y.-S.; Shin, K.-H.; Jeon, J.-D. Effect of inorganic additive sodium pyrophosphate tetrabasic on positive electrolytes for a vanadium redox flow battery. *Electrochim. Acta* **2014**, *121*, 321–327. [[CrossRef](#)]
497. Ding, C.; Ni, X.; Li, X.; Xi, X.; Han, X.; Bao, X.; Zhang, H. Effects of phosphate additives on the stability of positive electrolytes for vanadium flow batteries. *Electrochim. Acta* **2015**, *164*, 307–314. [[CrossRef](#)]
498. Peng, S.; Wang, N.; Gao, C.; Lei, Y.; Liang, X.; Liu, S.; Liu, Y. Influence of trishydroxymethyl aminomethane as a positive electrolyte additive on performance of vanadium redox flow battery. *Int. J. Electrochem. Sci.* **2012**, *7*, 4314–4321.
499. Peng, S.; Wang, N.; Gao, C.; Lei, Y.; Liang, X.; Liu, S.; Liu, Y. Influence of trishydroxymethyl aminomethane as a positive electrolyte additive on performance of vanadium redox flow battery. *Int. J. Electrochem. Sci.* **2012**, *7*, 2440–2447.

500. Kim, D.; Jeon, J. An electrolyte with high thermal stability for the vanadium redox flow battery. In *Advanced Materials, Mechanical and Structural Engineering*; Hong, S.H., Seo, J., Moon, K., Eds.; CRC Press: Boca Raton, FL, USA, 2016; pp. 371–375.
501. Flox, C.; Rubio-Garcia, J.; Skoumal, M.; Vazquez-Galvan, J.; Ventosa, E.; Ramon, J. Morante Thermally Stable Positive Electrolytes with a Superior Performance in All-Vanadium Redox Flow Batteries. *ChemPlusChem* **2015**, *80*, 354–358. [[CrossRef](#)]
502. Lei, Y.; Liu, S.-Q.; Gao, C.; Liang, X.-X.; He, Z.-X.; Deng, Y.-H.; He, Z. Effect of Amino Acid Additives on the Positive Electrolyte of Vanadium Redox Flow Batteries. *J. Electrochem. Soc.* **2013**, *160*, A722–A727. [[CrossRef](#)]
503. Lim, J.W.; Lee, D.G. Carbon fiber/polyethylene bipolar plate-carbon felt electrode assembly for vanadium redox flow batteries (VRFB). *Compos. Struct.* **2015**, *134*, 483–492. [[CrossRef](#)]
504. Qian, P.; Zhang, H.; Chen, J.; Wen, Y.; Luo, Q.; Liu, Z.; You, D.; Yi, B. A novel electrode-bipolar plate assembly for vanadium redox flow battery applications. *J. Power Sources* **2008**, *175*, 613–620. [[CrossRef](#)]
505. Zhong, S.; Skyllas-Kazacos, M. Electrochemical behaviour of vanadium(V)/vanadium(IV) redox couple at graphite electrodes. *J. Power Sources* **1992**, *39*, 1–9. [[CrossRef](#)]
506. Herrmann, J. Entwicklung und Anwendung einer elektrochemischen Methode zur Untersuchung schneller zwischengelagerter Reaktionen an Ringelektroden in turbulenter Rohrströmung. Ph.D. Thesis, Bonn University, Bonn, Germany, 1983.
507. Herrmann, J.; Schmidt, H.; Vielstich, W. Electrochemical Investigations of a Fast Chemical Step between two Charge Transfer Reactions. *Z. Phys. Chem. NF* **1984**, *139*, 83–96. [[CrossRef](#)]



© 2018 by the authors. Licensee MDPI, Basel, Switzerland. This article is an open access article distributed under the terms and conditions of the Creative Commons Attribution (CC BY) license (<http://creativecommons.org/licenses/by/4.0/>).